SUMMARY REPORT
RESEARCH AND DEVELOPMENT ON THE PULSED PLASMA ACCELERATOR (REPPAC)

by

B. Gorowitz, T. Karras, C. Cook, and P. Gloersen

prepared for

NATIONAL AERONAUTICS AND SPACE ADMINISTRATION

contract NAS3-8906

SPACE SCIENCES LABORATORY

GENERAL ELECTRIC

MISSILE AND SPACE DIVISION

CR 72271

SUMMARY REPORT

RESEARCH AND DEVELOPMENT ON THE PULSED PLASMA ACCELERATOR (REPPAC)

by

B. Gorowitz, T. Karras, C. Cook and P. Gloersen

Prepared for

NATIONAL AERONAUTICS AND SPACE ADMINISTRATION

April 25, 1967

CONTRACT NAS3-8906

Project Manager
NASA Lewis Research Center
Cleveland, Ohio
Spacecraft Technology Division
Mr. Peter Ramins

GENERAL ELECTRIC COMPANY
SPACE SCIENCES LABORATORY
MISSILE AND SPACE DIVISION
P. O. Box 8555
PHILADELPHIA, PA. 19101

ABSTRACT

This report describes laboratory programs aimed at the improvement of the performance of a repetitively pulsed, xenon propellant, plasma accelerator, and the development of a reliable, metal vapor propellant injector for the accelerator. Although early results indicated reasonably high efficiencies (67% at 5000 sec I_{sp}) for the accelerator, it was later found that level of performance could no longer be obtained and that the most consistently obtainable efficiency was ~ 28% at 5000 sec I_{sp}. The possible causes for this change and the results of unsuccessful attempts to restore the original performance of the accelerators are discussed.

A means of injecting small quantities of metal vapor into a plasma accelerator has been developed. This system which repetitively vaporizes a self replenishing capillary of liquid metal eliminates the need for mechanical valves or boilers and has a potential for high reliability and long life.

TABLE OF CONTENTS

LIST OF FIGURES

I. 1 SUMMARY

Efforts made to improve the performance of a repetitively pulsed, xenon propellant, plasma accelerator have produced inconclusive results. Although early results indicated reasonably high efficiencies (67% at 5000 sec I_{sp}) for the accelerator, it was later found that level of performance could no longer be obtained and that the most consistently obtainable efficiency was $\sim$ 28% at 5000 sec I_{sp}.

Detailed diagnostics of the accelerator exhaust disclosed that the magnetic field and ion density distributions were, on average, different from those observed previously,[1] and exhibited a degree of non-reproducibility not previously seen. The effects of changes in the operation of various accelerator components were examined. In addition, environmental effects or possible flaws in the measurement technique were investigated. As a result of these efforts, it has not been possible either to disprove the earlier data or to improve the performance so that it would remain consistently above the lower value quoted.

Another portion of the experimental program was devoted to the development of a means for injecting small quantities of metal vapor into a plasma accelerator. Studies were made on a system which repetitively vaporizes a self replenishing capillary of liquid metal (ELM). This system was developed to a point where one injector unit could serve as a working prototype for a total of six identical units which would consitutue a full scale accelerator propellant feed.

I. 2 INTRODUCTION

The work described in this report consisted of two parallel efforts which may be summarized as follows:

1. The experimental study of the performance of a repetitively pulsed, gaseous propellant, coaxial plasma accelerator with a goal of maximizing its overall efficiency in the 2000-5000 sec specific impulse range.
2. The design, fabrication and testing of a metal vapor propellant feed system with a goal of integrating it into a repetitively pulsed coaxial plasma engine.

The gaseous propellant accelerator which is discussed throughout the major portion of this report was similar in design to an engine previously designated the "A-7D".[1] (See Figs. 1 and 2). This engine had been found to operate with an overall efficiency of 63% at a specific impulse of 5000 sec. (Overall efficiency is here defined as $T^2/2\dot{m}P$;* $I_{sp} = T/\dot{m}g$.) Attempts were made to improve this performance primarily through changes in the engine electrode geometry, changes in the propellant distribution and increases in the energy storage bank capacitance - parameters which had previously[1] demonstrated a marked influence on engine efficiency. A relatively slight increase in the overall efficiency ($\eta_o = 67\%$, $I_{sp} = 5000$ sec) resulted from an increase in the angle of divergence of the outer electrode (engine designation - A-7XD). Other changes which were instituted invariably resulted in decreases in efficiency and indicated that for the various parametric combinations investigated during this period, the peak overall efficiency

---

*-The power input, P for all performance data presented in this report is defined as $P = 1/2\ CV_o^2\ (1-1/Q)\ \nu$ where Q is characteristic of the particular capacitors used and was typically 14 at a frequency of 100 KC.

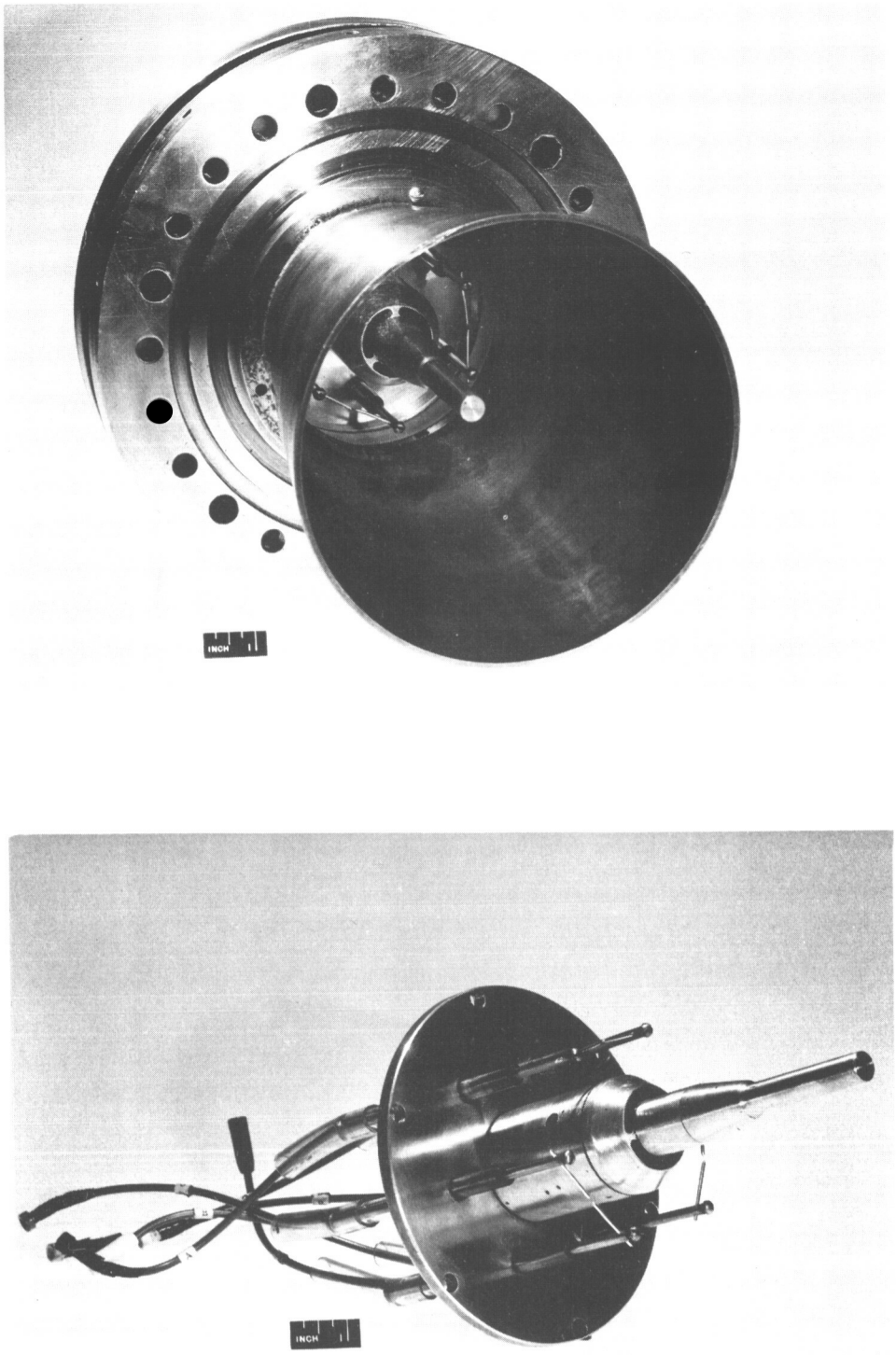

Figure 1. (a) Mod. A-7D Accelerator, (b) Mod. A-7D Center Electrode

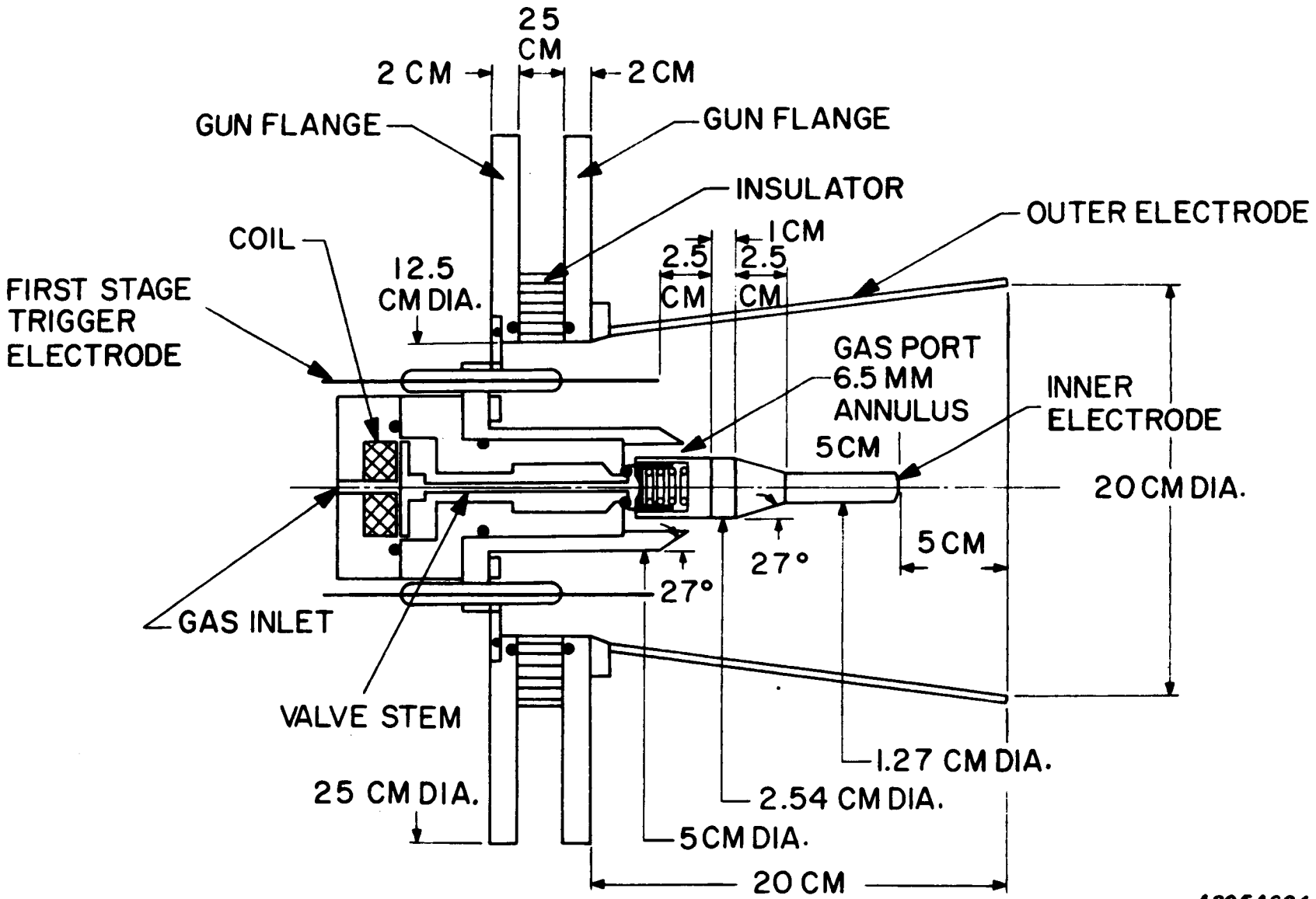

Figure 2. Drawing of Mod A-7D Accelerator

in the 2000-5000 sec specific impulse range was 67% at 5000 sec, as obtained with the A-7XD accelerator. Partial verification of this level of performance was provided by the results of exhaust stream calorimetry, and on-axis gridded probe determinations of ion velocities (the latter of which, after adjustment for the fraction of injected propellant unavailable to the discharge, $\sim$ 10%, yielded an average exhaust velocity and corresponding specific impulse in close agreement with the thrust determined specific impulse).

In the course of additional parametric studies of the A-7XD engine, there occurred an abrupt decrease in its thrust output for a fixed given propellant flow rate and power input. The indicated amount of propellant required to produce a given thrust for a fixed power input increased by over a factor of two, thereby decreasing the efficiency and specific impulse by a like factor.

Accelerator operation had, in the past, been found to be extremely sensitive to changes in the propellant distribution caused by changes in the characteristics of the propellant injection valve. The details of valve operation and the propellant distributions from various injector nozzle configurations were therefore, the first areas investigated in attempts to restore the original performance of the engine. A major portion of the program was also devoted to the examination of electrical, geometrical and environmental factors which might effect accelerator operation. In spite of these efforts the most recently measured level of performance has been $\sim$ 28% at a specific impulse of 5000 sec.

Simultaneous with these studies of the characteristics of a gaseous plasma accelerator, a program for the development of a valveless metal vapor feed for the pulsed plasma engine proceeded. The desirability of such a device and the progress made toward developing it are discussed in section III of this report.

II. PERFORMANCE OF THE GASEOUS PROPELLANT ACCELERATOR

A. Description of the Accelerator

The accelerator in use at the outset of the studies described in this report was similar in design to that shown in Figs. 1 and 2 and described in Ref. 1. This accelerator had been designated "Mod A-7D" in the progression of accelerator development. Its capacitor bank, associated circuitry and electrically triggered mode of operation were the same as those described in Ref. 1. Typical operating parameters for the engine are listed in Table 1. The techniques used for the evaluation of its performance are reviewed in the Appendix.

TABLE 1

A-7D, A-7XD Operating Parameters

Accelerator	Mod A-7D, A-7XD
Capacitance	218 μfd (nominal 225 μfd)
Capacitor Bank Q	14
Voltage	900-1000V
Firing Rate	10 cps
Propellant	Xenon
Propellant Flow Rate	0.3 - 1.0 mg/sec.
Trigger Delay Time	0.6 - 0.8 ms. after valve actuation

The first modification of the Mod A-7D geometry involved an increase in the outer electrode divergence to a shape shown in Fig. 3 and designated the A-7XD.

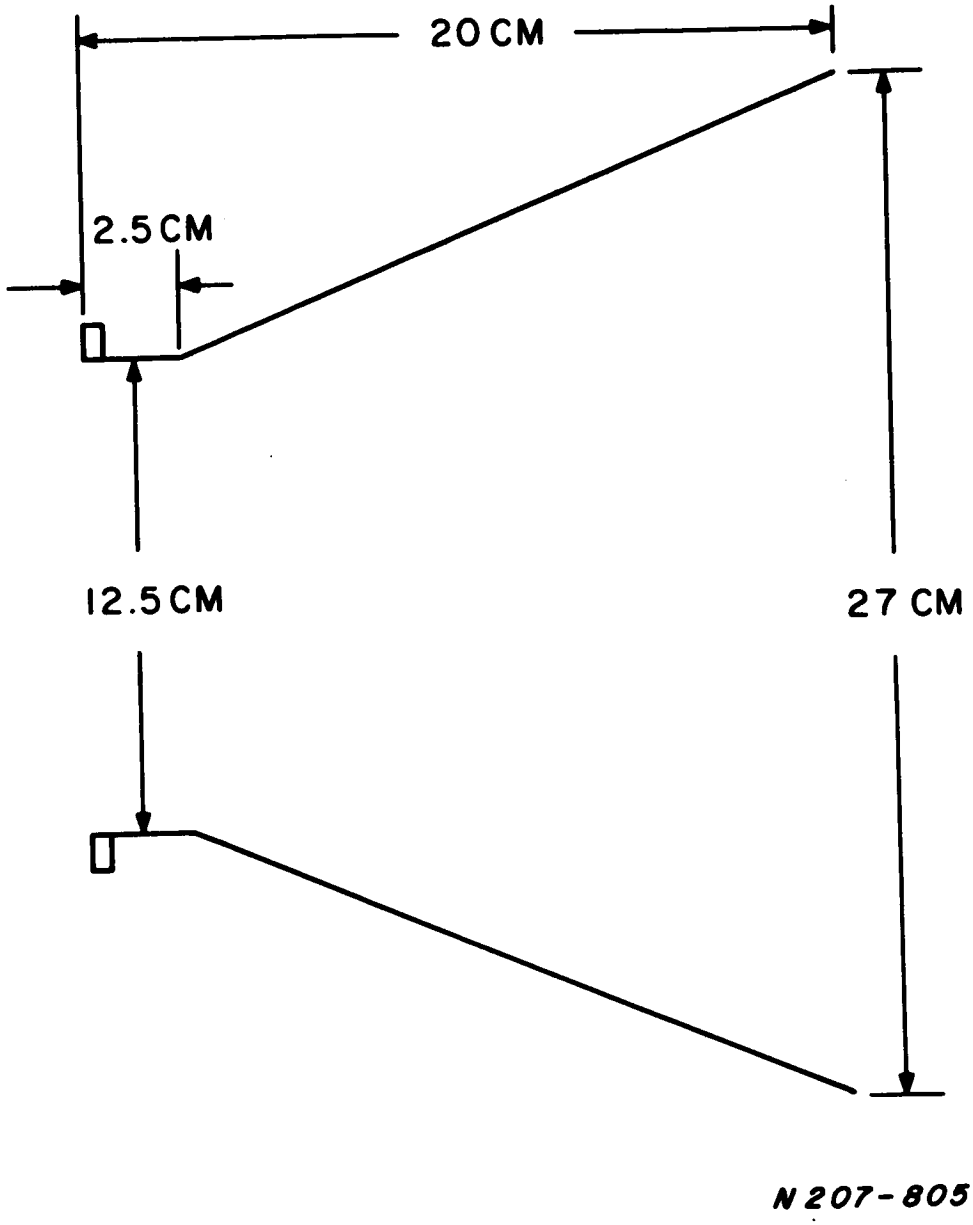

Figure 3. Outer Electrode of Mod A-7XD Accelerator

B. Effects of Increased Outer Electrode Divergence

The substitution of a diverging outer electrode for a straight cylinder had, in the past,[1] resulted in an increase in the overall efficiency of the accelerator. This was attributed to an increase in the inductance per unit length-to-circuit resistance ratio which could increase the efficiency of energy transfer to the plasma, and a decrease in the electrode surface-to-volume ratio which could reduce wall losses. Since it provided a greater volume over which the propellant could spread before it made contact with the outer electrode, the divergent outer electrode was also found to permit the injection of greater amounts of propellant for a given voltage without it resulting in self triggering than could be injected with the straight cylinder. All of these factors motivated a further increase in the outer electrode divergence from a muzzle diameter of 20 cm to a diameter of 27 cm, with the breech diameter remaining at 12.5 cm, as shown in Fig. 3. The performance of the A-7D and the A-7XD accelerators is presented in Fig. 4. The data points used in plotting the performance curve for the A-7XD accelerator are shown in Fig. 5. Many of the points shown represent several runs where identical results were obtained. Several hundred 15 and 30 sec runs at 10 cps were made in the 3000-6000 sec range for various flow rates, voltages and trigger delay times. The spread in the data is associated with the range of trigger delay times used, the cumulative results of fluctuations in mass flow, power input (voltage) and thrust produced and the accuracies of measurement of the various parameters.

A further increase in divergence to a muzzle diameter of 30 cm with the same breech diameter and shape reversed the trend toward higher performance, resulting in an approximate 10% decrease in efficiency in the range of specific impulse from 2000-5000 sec.

C. Effect of Increased Capacitance

The capacitance of the energy storage bank was increased from 218 μfd to 286 μfd using the flexible capacitor arrangement described previously.[1] This change was in line with the earlier observed trend toward increased efficiency with higher capacitance. Initial measurements of thrust, mass flow and power input indicated that the overall efficiency had been increased

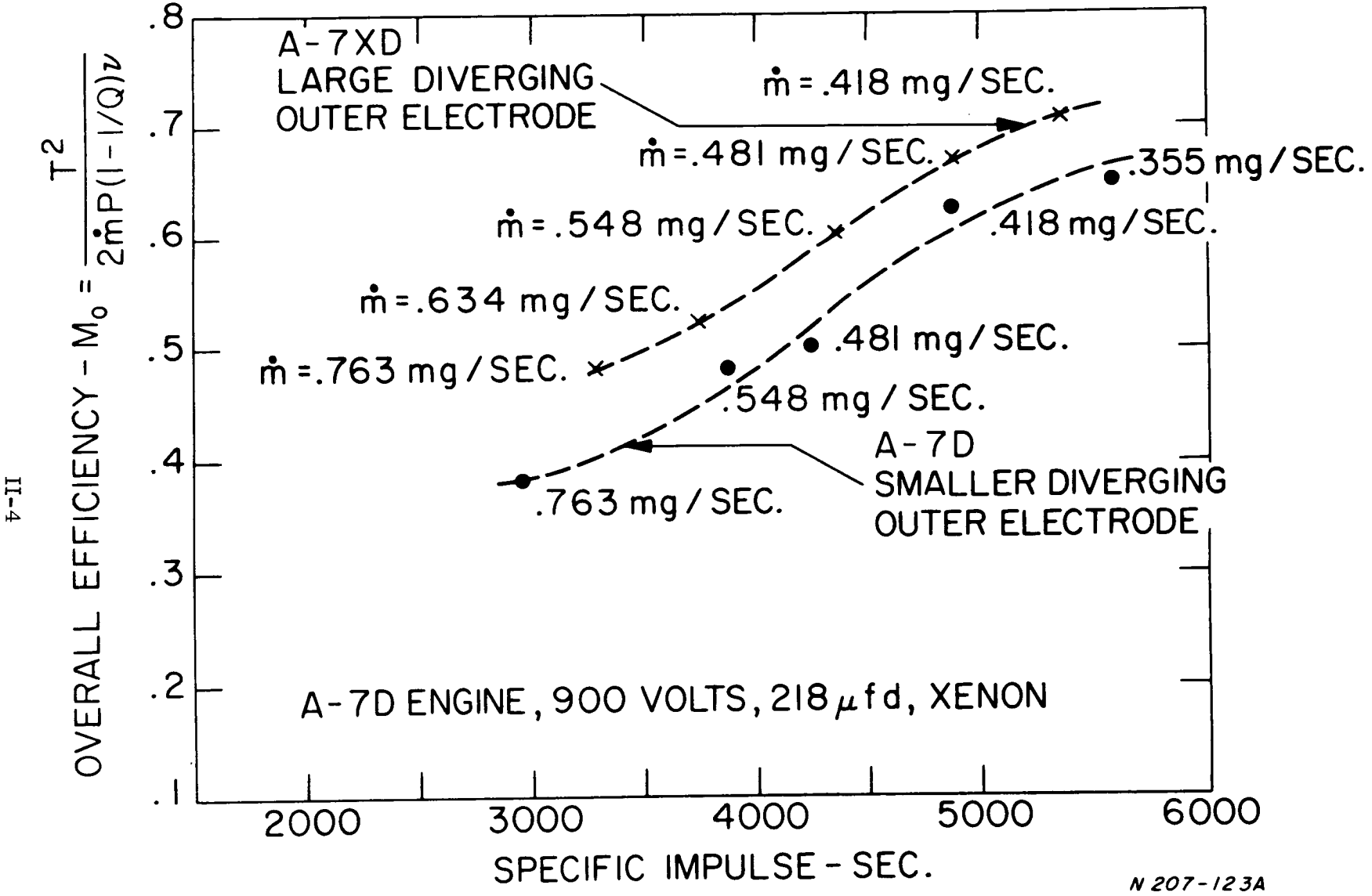

Figure 4. Overall Efficiency vs. Specific Impulse for A-7D and A-7XD Accelerators

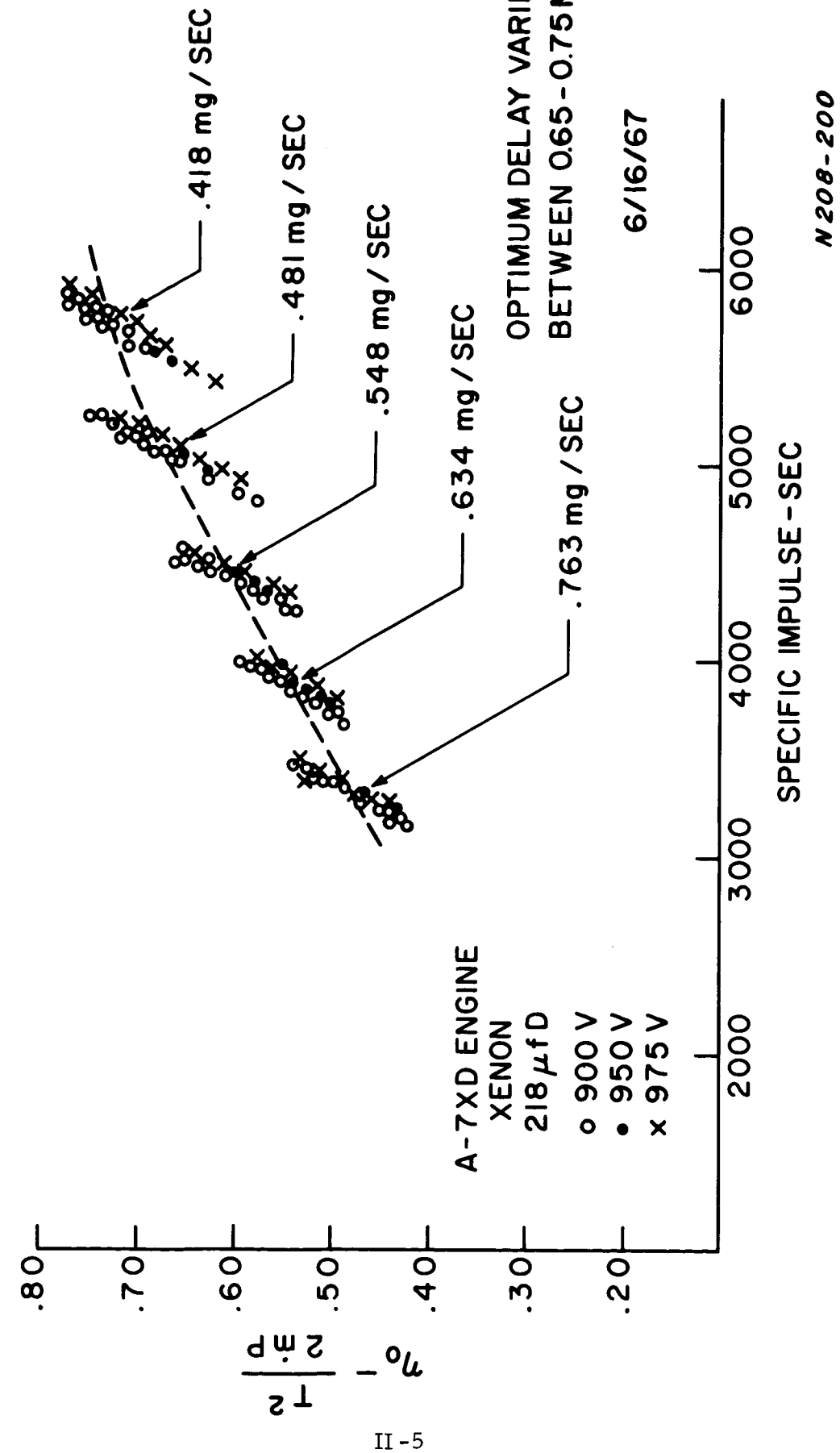

Figure 5. Specific Impulse vs Overall Efficiency A-7XD Accelerator

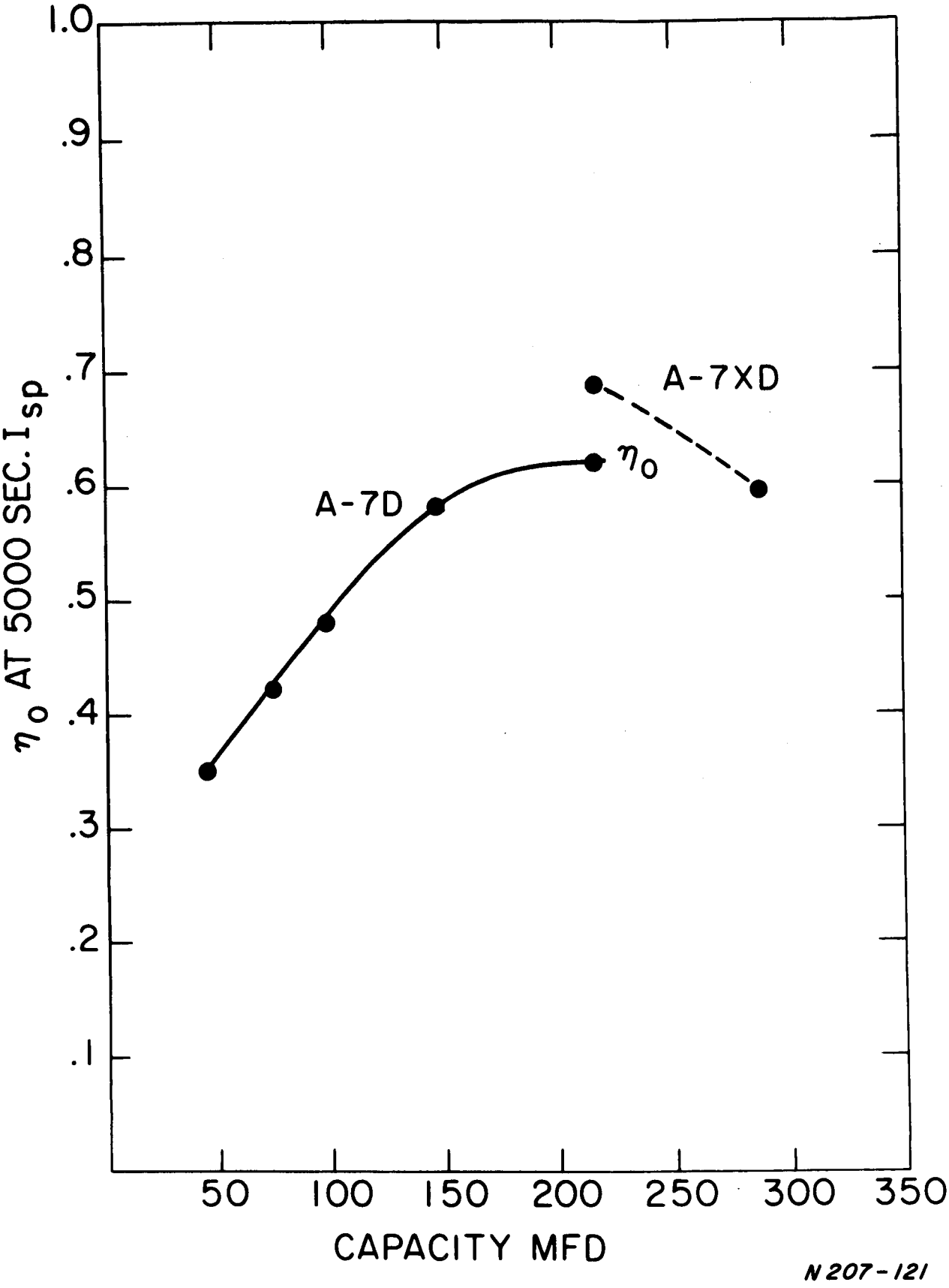

Figure 6. Efficiency vs. Capacitance at a Specific Impulse of 5000 sec., A-7D and A-7XD Accelerators.

to an average of 72% at 5000 sec specific impulse. However, more extensive examination of the performance of the A-7XD accelerator operating with a capacitance of 286 μfd and 900 V potential demonstrated that the early results were spurious. The thrusts produced by the engine were augmented by the apparent entrainment of gas resulting from an increase in the background pressure in the test facility. This increase was, in part, due to a malfunction of the pumping system (depletion of oil in two of three diffusion pumps). The additional propellant input necessary to obtain the desired I_{sp}'s with the increased energy input associated with the higher capacitance and voltage also contributed to the increased background pressure. Confirmation of the effect of gas entrainment at increased pressure was offered by the fact that the thrust produced at a 10 cps repetition rate was disproportionately greater than that produced at a 5 cps repetition rate. In addition, after the vacuum system was repaired, the thrust for otherwise identical conditions of voltage, capacitance, delay time and propellant input decreased by about 20%. Shutting down of the pumps to decrease the pumping speed and hence to increase the background pressure in the system resulted in a return of the spuriously high thrust. The process of alternately decreasing and increasing the pumping speed confirmed that this phenomenon was reproducible.

The overall efficiency of this accelerator operating at a repetition rate of 5 cps into a decreased background pressure and with the operating parameters mentioned above was found to be 47% at a specific impulse of 3800 sec. This specific impulse was corroborated by gridded probe measurements of the exhaust stream, which indicated an average velocity of 3.66×10^4 m/sec. The technique used in making these measurements has been described previously.[1] At 5000 sec the average overall efficiency was 57%. This value indicates that the trend to increased efficiency with capacitance shown in Fig. 6 had apparently reached a peak and was turning downward.

To confirm the validity of the results previously obtained for lower capacitance, the A-7XD engine with 218 μfd capacitance was operated

under various repetition rates and background pressures. Overall efficiency vs specific impulse as shown in Fig. 4 remained unchanged for the conditions examined.

It appears that the combination of higher mass input, higher background pressure, and longer duration of current waveform associated with a capacitance of 286 μfd resulted in conditions where currents extending from the accelerator and entraining background gas may play a significant role in producing thrust.

D. Effects of Modified Center Electrode Geometry

D.1 Electrode Diameter

A modification of the inner electrode geometry which was tested involved the use of an increased breech diameter tapering into the existing geometry in the vicinity of the nozzles, as shown in Fig. 7. The arrangement was similar to that of the Mod A-5 accelerator described in Ref. 1. The purpose of the new electrode shape was to provide a more pronounced change in L' in the gun and a lower initial inductance. In the A-5 accelerator some increase in efficiency had been observed but the geometry was abandoned for the installation of the trigger electrodes. In the modified A-7X D accelerator the trigger electrodes protrude through six holes in the 11 cm diameter breech end. The overall efficiency of this accelerator at 5000 sec was 61% for 1 KV and 214 μfd. Since this value was slightly lower than the performance with the normal inner electrode, the original A-7XD geometry was retained.

D.2 Electrode Length

Although energy efficiency measurements conducted with an earlier model accelerator[1] had led to an apparently optimum center electrode length, it was feasible to repeat the changes in length with the A-7XD accelerator, and to evaluate operation in terms of thrust and overall efficiency.

The results of these measurements indicated that the present electrode length (5 cm between the end of the outer electrode and the tip of the center electrode) provided higher performance (67% at 5000 sec.) than did electrodes

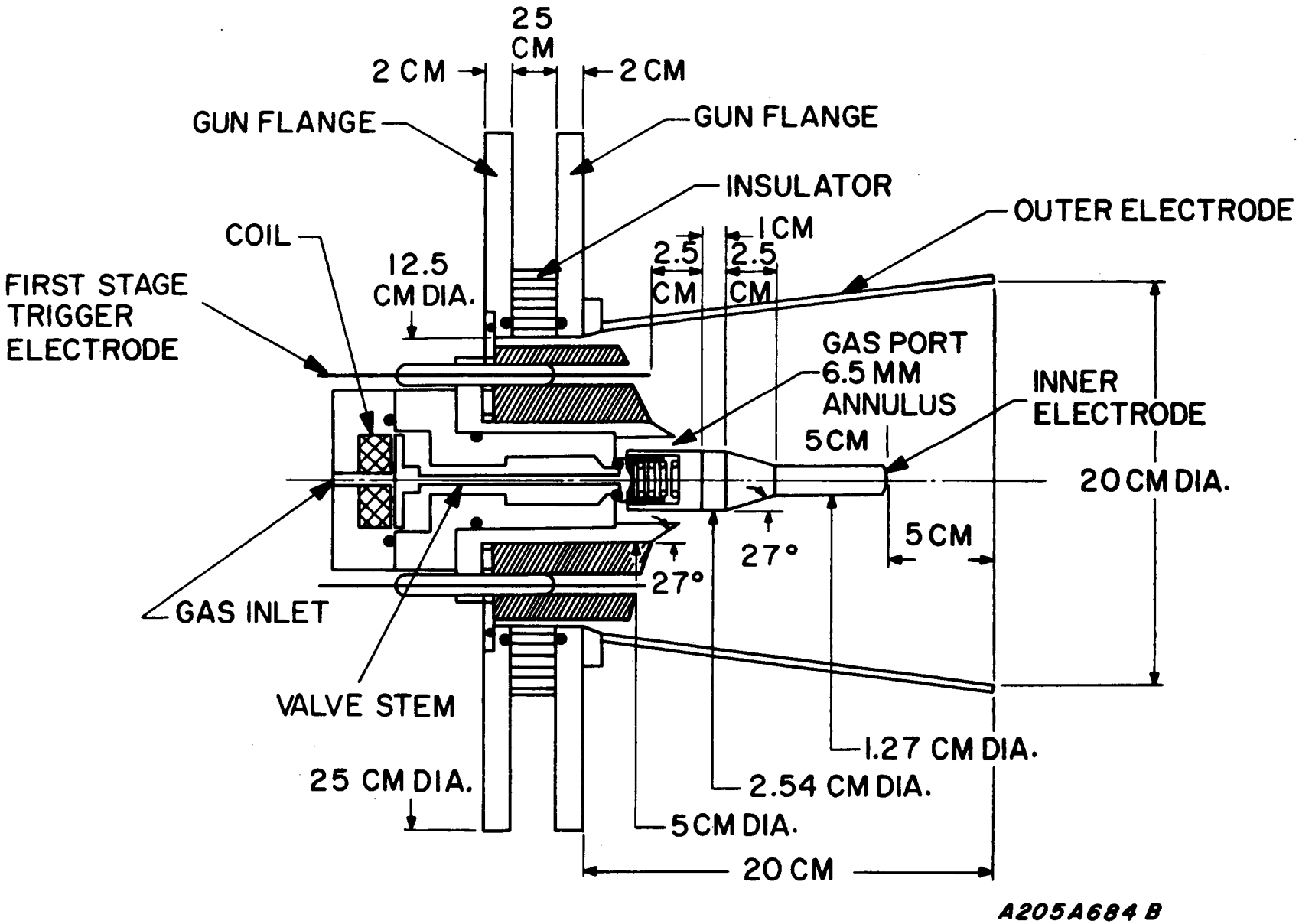

Figure 7. Drawing of Mod A-7D Accelerator with Center Electrode Modified.

either 5 cm shorter or 5 cm longer. For otherwise identical operating conditions, in the case of the shorter electrode, thrusts were an average of 25% lower than those for the intermediate length. In addition, erosion, from visual inspection, was far more marked on the tip of the electrode stub. The longer electrode yielded thrust about 10% lower than that obtained with the intermediate length electrodes, but erosion was much reduced.

E. Deterioration of Engine Performance

In the course of engine runs for the purpose of compiling additional statistics on the operation of the most efficient A-7XD configuration, an abrupt loss of thrust was observed to occur. The thrust decreased to about 70% of its prior level and could not be restored to its original value without an inordinately large increase in the propellant input rate. The change in performance also manifested itself in the current waveform, which, for a given mass flow, decreased in amplitude, increased in period by a factor of two or more, and failed to display the slight ($\sim$5%) reversal which had been associated with efficient operation. Waveforms representative of those observed before and after the deterioration of performance are shown in Fig. 8.

Visual observations of the accelerator exhaust found that the appearance of a plume of about 2 cm diam. extending several cm downstream from the center electrode was also associated with higher efficiency. A relatively diffuse exhaust luminosity with the absence of a plume could be associated with poorer performance. These difficulties were attributed to malfunction of the propellant fast acting valve which had at another time in the past been responsible for a deterioration in performance due to non-uniform distribution of propellant. The valve was dismantled and found to be improperly seated, with frictional wear indicated on one side of the restoring spring and spring retainer. In addition, the teflon "O" ring had shrunk to the extent that it was noticeably loose in its seat whereas it had previously been a press fit into that seat. The defective components were replaced

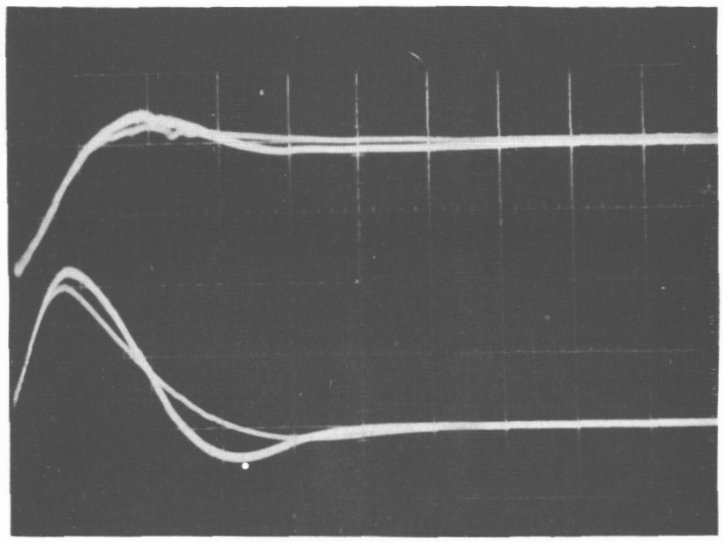

Time Scale - 5 μ sec/cm.

Upper Traces - Voltage - 500 V/cm.
Lower Traces - Current - 22 K amps/cm.

Higher Amplitude Current Signal
Deeper Reversal Voltage Signal - Typical of "High" Efficiency Operation

Lower Amplitude Current Signal
Lower Reversal Voltage Signal - Typical of Waveforms Obtained after loss of high efficiency

Figure 8. Discharge Waveforms for Mod A-7XD Accelerator.

and the valve reassembled and realigned. The performance of the A-7XD accelerator was subsequently restored to its original value. This return to high efficiency was found to be short-lived, however. Once more, the valve was suspect. In order to investigate its behavior measurements were made of the neutral gas density at the nozzles of the center electrode. These measurements, described earlier[1], indicated severe multiple bounce of the valve disc off its teflon seat. The magnitude of these bounces was such that from 30-50% of the propellant injected by the valve was left in the nozzles of the center electrode at the time of discharge initiation. (See Fig. 9)

It seemed apparent that the operation of the valve prior to the deterioration in performance had been free from bounce due to frictional damping of the spring by its retainer. This damping had disappeared due to wear of the retainer wall, resulting not only in valve bounce but in a decrease in the voltage required to open the valve. This latter characteristic was perhaps the best indication that frictional damping had diminished. Some attempts to reintroduce frictional damping were made. Neutral density measurements indicated that the insertion of a close fitting plug into the spring provided sufficient rubbing to eliminate bounce as observed on a single shot basis. Repetitive operation of the engine indicated an average efficiency of 61% at 5000 sec, I_{sp} for about twenty 30 sec duration runs. Longer term repetitive operation however, apparently resulted in wear of the interference fit and renewed onset of bounce.

The use of a spherical seat such as that of the A-8DB[1] accelerator was investigated as a means for eliminating bounce without frictional damping. Neutral density measurements indicated that the valve was indeed bounce free. However, its propellant distribution was found to be unfavorable for peak efficiency in the specific impulse range of interest. A spherical seat more closely approximating in size that of the A-7D valve (using the A-7D "O" ring seat) was installed in the A-7D nozzles. This valve was tested using the neutral density probe and was found to operate satisfactorily only

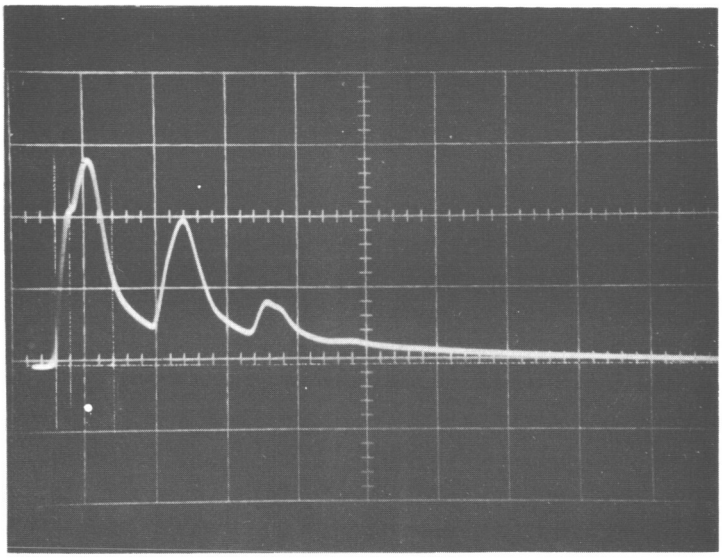

Fig. 9. Neutral Density Probe Trace Showing Valve Bounce

Probe opposite A-7XD nozzles
High Energy Valve
. 2V/cm, 0.5 m sec/cm

in a narrow range of combinations of valve voltage and plenum pressure. This range of valve operating conditions, however, provided quantities of gas about a factor of two in excess of that required for efficient operation at 5000 sec specific impulse with an energy input of about 100 joules per shot. It appeared that relatively small travel of the valve ball away from its seat minimized bounce but increased the possibility of non reproducibility of gas flow and assymetry of distribution. This was found to be the case for relatively low valve voltage (e.g., $\lesssim$ 4600 V) and high plenum pressure (e.g., 7-20 psig). Neutral density measurements indicated shot to shot variation of gas flow at a single position by as much as a factor of three and an asymmetry of distribution of a like factor. At higher valve voltage (e.g., $\gtrsim$ 4600 V) and low plenum pressure (e.g., $\lesssim$ 7 psig) valve bounce and loss of propellant occurred as had been the case with the undamped flat seat valve. The maximum fraction of injected propellant available in the accelerator was found to be about 0.75. However, at 650 μ sec after valve actuation the time at which maximum thrust was observed, the propellant mass fraction was 0.50 - 0.60. This result reinforced the belief that the proper distribution of propellant in the accelerator was as important a requirement as the availability of a high fraction of the injected propellant. For the above case, the average efficiency at 5000 sec specific impulse was 48%.

In order to obtain a more symmetric distribution of propellant while simulating the more radially directed flow of gas from the plate valve into the plenum chamber adjacent to the nozzles, a 3/4" dia. washer was affixed to the base of the hemispherical end of the moving valve member as shown in Fig. 10. The efficiency of the engine with this valve modification decreased to 39% at a specific impulse of 5000 sec. In order to further minimize the possibility of valve bounce by causing the ball end to seat more deeply into the "O" ring, its radius of curvature was decreased from 5/16" to 9/32". The efficiency of the engine was found to increase to 45% at 5000 sec I_{sp}.

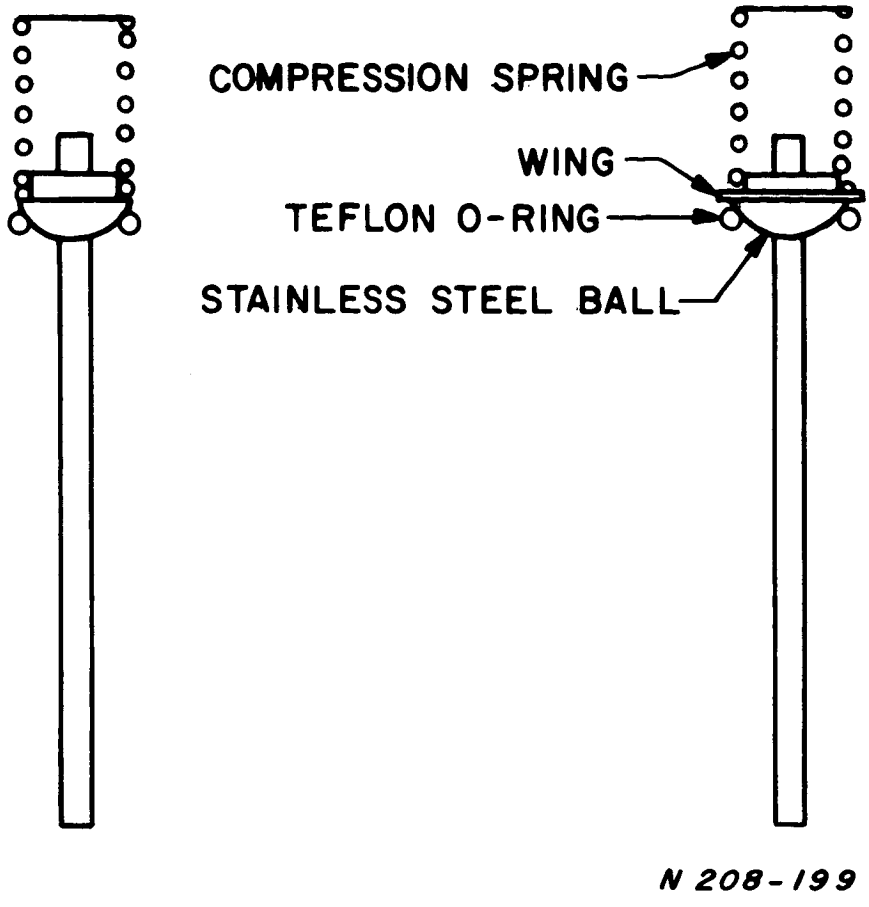

Figure 10. Ball Seat Configurations

In the course of the above mentioned studies, other possible causes of deterioration of performance were investigated. Possible electrical causes included changes in capacitance, voltage and contact resistance. Measurements indicated that no such changes had occurred. Nevertheless, to obviate the possibility that unobserved transients might be responsible, new capacitor modules were inserted in the bank. The most consistently obtainable performance was essentially unchanged from that observed prior to the insertion of the new capacitors. The operation of the trigger electrode system was also checked. Trigger voltages, trigger gap lengths and the shape of trigger electrode tips, were checked and varied systematically. Insulators, both on the trigger electrodes and between the flanges of the accelerator were checked and cleaned. The operation of the thrust stand and readout equipment was also checked and recalibrated. In none of the above cases were there any indications of causes for a change in indicated engine performance. Changes in the behavior of the fast acting valve and the resultant change in propellant distribution remained as the most apparent sources of engine deterioration.

F. Low Energy Valve

In order to optimize the performance of the propellant valve, (while significantly decreasing its energy requirements in anticipation of engine firing rates above 10 cps) a new valve design was implemented. A solenoid type valve was constructed using as a moving armature half of a Ferroxcube cup core to which is attached the valve stem. (See Fig. 11). It was believed that changes in the seating arrangement as well as closer coupling of energy between the electromagnetic driver and the moving valve element could result in greater control over the dynamic valve characteristics. This valve was operated at rates up to 120 cps with the valve coil requiring an average power of less than 38 watts to inject a gas load of the order of that which would be necessary for 10 KW engine operation. Although the initially observed gas pulse width was 500-600 μsec as opposed to a typical pulse width of 300 μsec for the high energy eddy current valve, it was possible to decrease this width to 300 μ sec by increasing the spring rate of the valve return spring and by using a plate seat design as opposed to a ball seat. The ball seat apparently provided a lower conductance path for the gas through the seal than did the flat seat which offered a lower area of surface contact.

In both cases, operation was completely bounce free and exhibited high reproducibility. The shape of gas pulse out of the nozzles of this valve differed from that observed for the high energy valve in that it was more highly structured, as demonstrated in Fig. 12. The significance of this structuring has not been determined. It was found that the overall efficiency of the engine using the low energy valve was approximately 35% at a specific impulse of 5000 sec (vs $\sim$45% @ 5000 sec for the A-7XD engine with a high energy valve). In addition, efficiency was rather insensitive to triggering time for the range of times during which propellant was in the accelerator. This offers additional evidence of the interplay of propellant distribution and propellant availability.

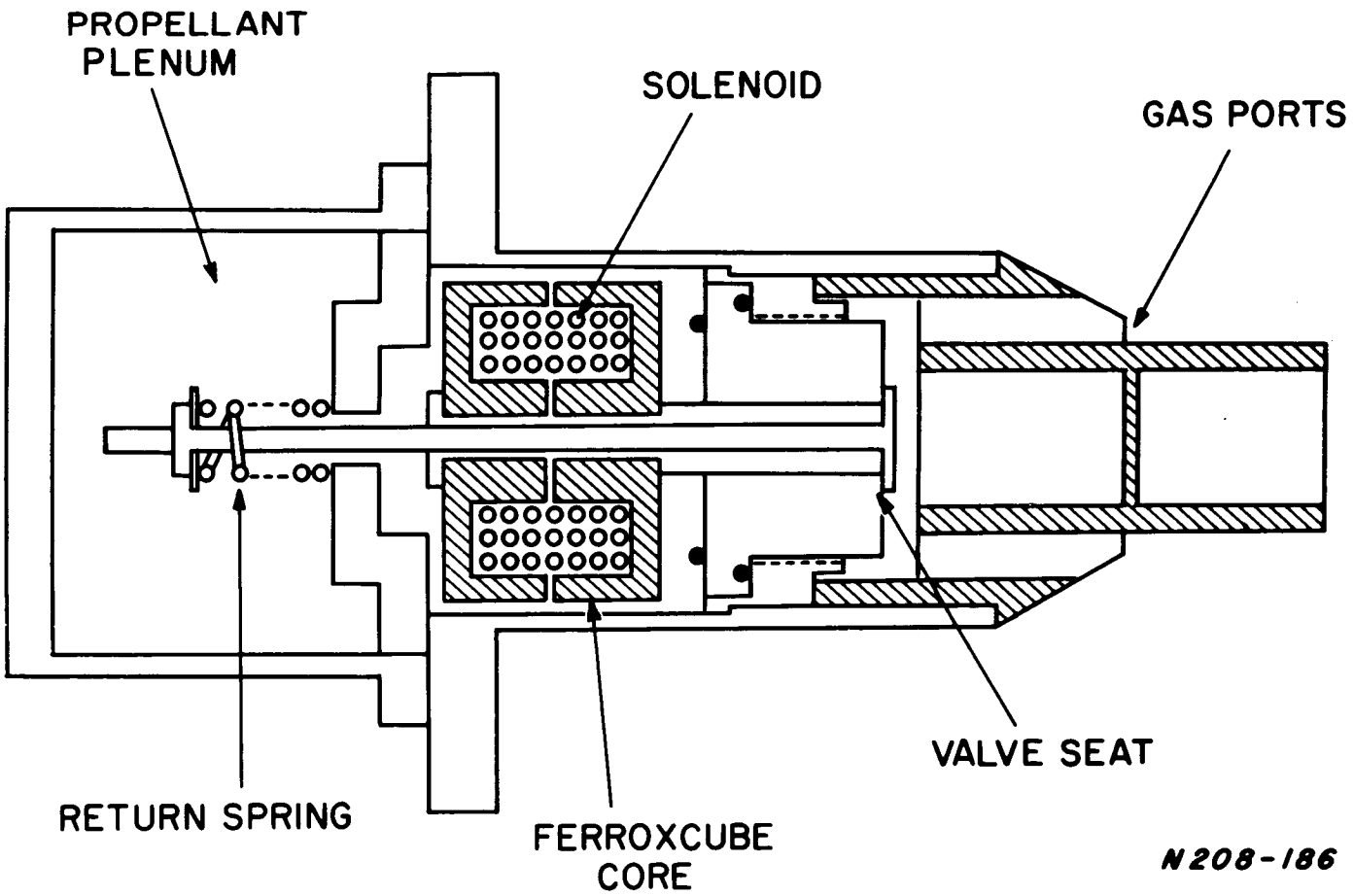

Figure 11. Drawing of Low Energy Valve

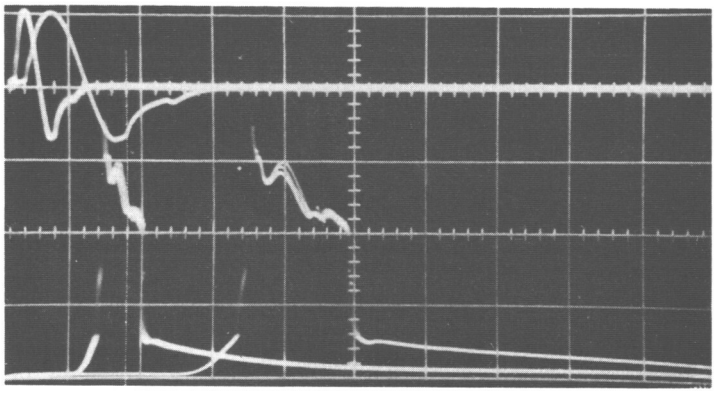

Fig. 12. Neutral Density Probe Trace of Output of Low Energy Valve.

Probe Opposite A-7XD Nozzles

Upper Beam - Valve actuating current pulse, 0.5 and 0.2 msec/cm
Lower Beam - Gas density signal 1.0 V/cm, 0.5 and 0.2 msec/cm

4 traces at each sweep speed.

G. Engine Performance Following Reconstruction of Test Facility

At the conclusion of these initial tests with the low energy valve, the plasma engine test vacuum facility was temporarily dismantled for preventive maintenance of the oil diffusion pumps and the installation of three 32" gate valves and baffles. The presence of diffusion pump oil vapor and droplets or other pumping system associated contaminants, was a factor which had been tolerated in the absence of valve and baffle systems. Commercially available systems would have decreased the backstreaming of such contaminants at the cost of a significant decrease in the pumping speed of the vacuum system. The high conductance, variable geometry, baffle system, designed and built in-house removed the major portion of these contaminants without any observable decrease in pumping speed. The valves and baffles also permitted more rapid access to the facility for modifications and were required in connection with the anticipated use of mercury as a propellant for the accelerator. After reassembly of the facility, the engine, which had otherwise been untouched, was remounted on the thrust balance and runs commenced with the same accelerator and operating conditions as had been used previously. In these tests it was found that the accelerator could be triggered with reasonable reliability only with flow rates greater than 0.6 mg/sec and in a range of triggering times between 700 and 820 μsec. The upper limit of this range was sufficiently sharp that at 840 μ sec the accelerator could be triggered with only sporadic success. The highest level of performance which was measured was 13% at 2500 sec I_{sp}. Neutral density measurements indicated that the maximum propellant mass fraction occurred at about 1100 μ sec. However, the accelerator could not be triggered at that time. Examination of the trigger electrode system indicated no decrease in the trigger transformer output or any trigger insulator breakdown. Several variations of trigger electrode geometry were tested with little success in obtaining reliable triggering. The discharge could be gas triggered, but the flow rate required for triggering was about 2.0 mg/sec, almost twice that previously required. The most apparent possibility was that the propellant

distribution had changed sufficiently to alter the breakdown characteristics of both the triggers and the main discharge. In the case of the triggers, this seemed unlikely, since they could be operated at pressures down to 10^{-6} torr as opposed to the 0.1 - 1 micron pressure which was measured in the region of the triggers by the neutral density probe. Another possibility for the change in breakdown conditions was the removal of diffusion pump oil vapor from the test facility which had been accomplished by the installation of baffles. Reference is made in the literature[2] to the role of electrode contaminants in lowering the breakdown strength of a gap in a vacuum and in effecting electrode current flow.

In order to examine both possibilities on an engine with which the most information was available, the A-7XD center electrode with high energy valve was reinstalled. The same difficulty with triggering was encountered with this configuration, suggesting that a changed propellant distribution was a less likely cause. In the likelihood of effects due to oil vapor, it was obvious that a system which would operate in a clean vacuum environment was required. One approach to this problem involved the insertion of a solid surface across the gap between each trigger electrode pair so that the discharge could track across this surface. Lavite plugs were used in the first attempts and permitted the accelerator discharge to be triggered at flow rate as low as 0.3 mg/sec., about half that previously required for operation of the vacuum gap. The peak efficiency measured for this flow rate and the other conditions of operation stated in Table I was 13% at 2250 sec I_{sp}. At higher flow rates the efficiency was approximately the same with a slight drop in the specific impulse. More reliable triggering, therefore, resulted in no improvement of engine performance. Since it was desirable to further increase the range of usable propellant flow rates, and to improve the trigger system reliability, "Textolite", phenolic resin plugs were substituted for the lavite material. The Textolite provided a charring surface which served as a superior medium for surface tracking. This system was found to be completely reliable, could operate without the presence of any background gas and demonstrated

negligible mass loss in over 10^6 shots. Since reliable triggering merely permitted operation of the engine in the absence of oil vapor without increasing its overall efficiency, the role of oil vapor as an influence in engine performance was investigated. "Convoil-20" diffusion pump oil was rubbed on the electrode surfaces of the accelerator. Thrust runs under these conditions yielded an average efficiency of 20% at 3200 sec I_{sp}. It is worthy of note that in these runs, the efficiency could not be raised significantly even at a higher specific impulse, by decreasing the mass flow as was indicated in Fig. 5, for example. With decreased propellant flow, the thrust dropped sufficiently to limit the efficiency and to limit the specific impulse to $\sim$ 3000 sec. The presence of oil on the electrodes and in the vacuum chamber improved the efficiency by some yet undetermined mechanism which enhanced breakdown and current flow in the plasma. Although this improvement might be attributed to mass addition due to the presence of oil on the electrodes, long term running of the engine without deterioration of the stated level of performance and consideration of the total propellant mass input suggests that this was not a significant factor. It was noted that the initial firings of an oil coated accelerator yielded higher thrusts (by about 25%) than were later measured. After about three 30 second runs of the engine, with apparent blowing off of the oil coating, a steady state level of operation was achieved with a carbonized oil layer remaining on the electrodes. Since the vapor pressure of oil in the system was sufficiently low for a pressure of 10^{-6} torr to be maintained between engine runs, the role of entrained oil vapor in the increasing thrust might also be discounted. One effect which cannot be easily discounted is the possibility that oil droplets rather than vapor, associated with backstreaming would not be detected by a pressure gauge and could contribute unaccounted mass to the discharge. Such an effect could not be simulated by the mere presence of oil in the chamber.

After the numerous changes in operating and environmental conditions mentioned above and which had been believed to offer an apparent ready solution to the problem of restoring or at least accounting for the earlier performances, it was decided that a systematic re-evaluation of areas which could influence either engine operation or measurements of operation was warranted.

G. 1 Effects of Propellant Loading

The propellant distribution of the A-7XD accelerator using the high energy valve was re-examined using the neutral density probe. It was immediately apparent that valve bounce was once more a problem and that only about 40% of the injected propellant was available to the discharge. The width of the primary gas pulse was about 400 μ sec, compared to the typical value of 300 μ sec which had previously been measured. In order to decrease the gas pulse width and to possibly decrease the magnitude of valve bounce, a valve return spring of higher spring rate (135 lb/in vs 50 lb/in) was installed. The result of this change was a 25% decrease in the pulse width to 300 μsec and a reduction in bounce to the extent that at optimum triggering time the propellant mass fraction at a flow of about 0.4 mg/sec was 0.75. The overall efficiency for these conditions was 28% at a specific impulse of 5000 sec.

As an auxiliary experiment, argon, nitrogen and ammonia were substituted for xenon, the propellant most frequently used. Unlike previous results which indicated that xenon was superior for lower specific impulse performance, neither argon nor nitrogen were found to produce any lower performance. In fact, below 5000 sec, the efficiency increased slightly as the atomic weight decreased. At 5000 sec, the efficiencies were essentially the same. With nitrogen used as a propellant, thrust was examined as a function of trigger delay time for constant mass flow. It was found that thrust decreased for trigger times from 400 μ sec to 600 μ sec after valve actuation, and that the engine could not be triggered at 700 μsec. However, it would run at 900 μsec with a thrust level equal to that at 400 μsec. At 1.0 m sec the thrust again decreased, while at later times, the accelerator, once more, would not fire regularly. Gas density measurements indicated that the gas pulse from the nozzles showed an initial peak at 340 μ sec and a bounce at 850 μsec. The relationship between thrust and propellant mass distribution as a function of time is shown in Fig. 13. Apparently, at times $600 \leq t \leq 900$ μ sec

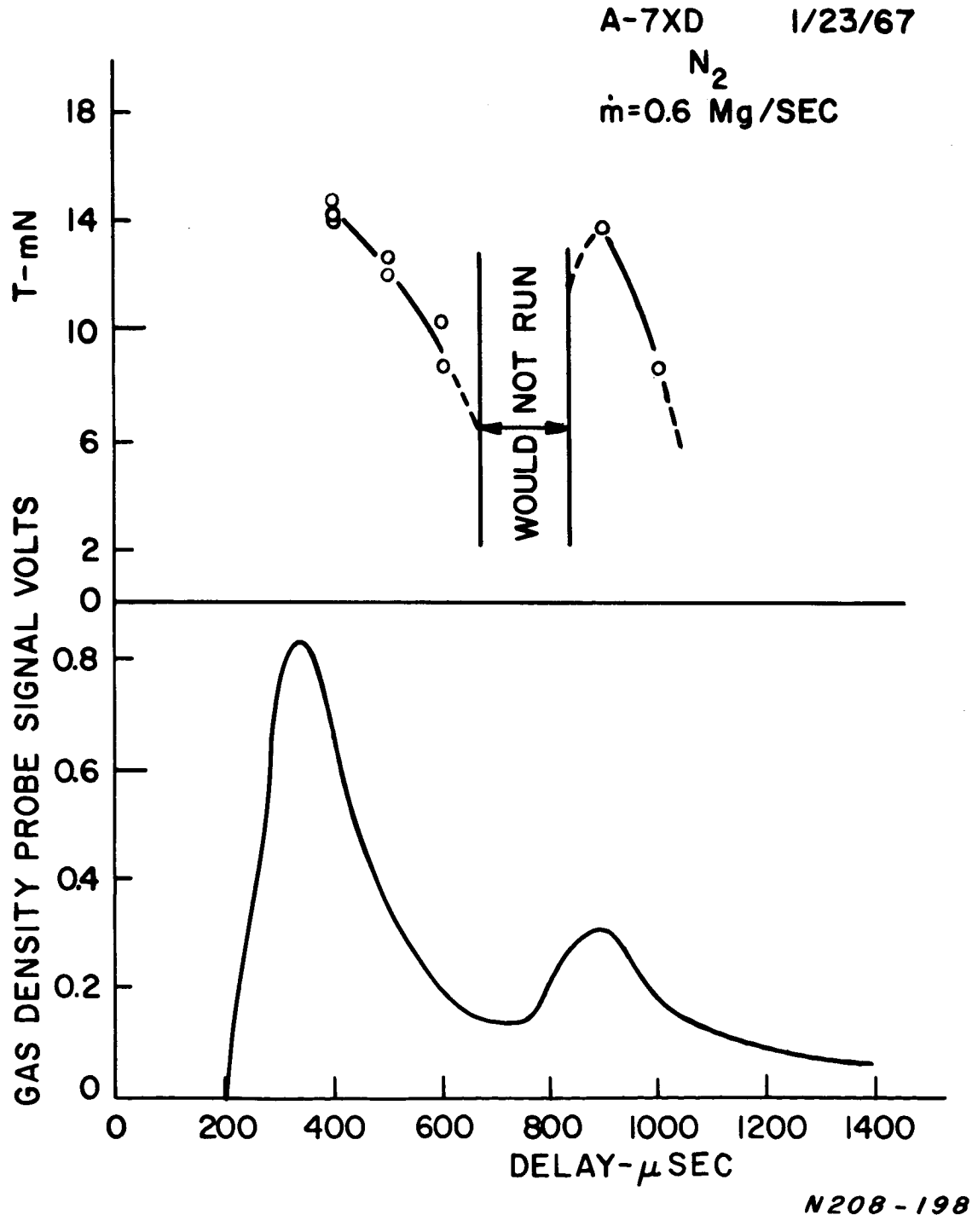

Figure 13. Propellant Density at Nozzles and Thrust vs Trigger Delay Time

insufficient gas in the breech of the accelerator would not allow discharge, while peak efficiency was obtainable at other times corresponding to maximum density in that region. Further examination of the distribution of propellant throughout the accelerator at the time of discharge indicated that the propellant stream from the nozzle was directed at about a 20^{o} angle with respect to the axis of the center electrode. This compares with an angle of 45^{o} observed previously for the A-7 nozzles used with a flat seat, high energy valve. In order to direct the gas more radially, deflecting rings of two different diameters (initially 1/2" and later 1/4") were constructed to slip over the center electrode to a distance of 1/2" in front of the nozzles. Although these rings changed the distribution of propellant, there was no significant change in the gross performance. The discharge current waveform exhibited a shorter period, higher peak current, and higher reversal, indicating a lower inductance change with time, $\dot{L}$. Inspection of these rings disclosed that erosion patterns which were greater than at any other location in the accelerator, with the possible exception of the extreme tip of the center electrode. In order to effect the desired change in propellant distribution without the presence of obstructions or sharp discontinuities in the electrode geometry some additional nozzle designs were investigated.

The A-8 nozzles with shorter and wider ports had been found to provide a more radially directed propellant stream than was possible with the A-7 nozzles. Gas density distribution measurements were again made with these nozzles installed in the accelerator. The propellant mass fraction at the time which was later found to correspond to that of peak thrust was found to be about 0.65. Contrary to what was found previously, the gas stream angle with respect to the center electrode was less than that with the A-7 nozzles. Once more the efficiency vs specific impulse relationship was not significantly different, with an average of 30% measured at 5000 sec I_{sp}.

The A-9 nozzle geometry was an open configuration designed for maximum gaseous conductance. The absence of ports in this design permitted expansion of the propellant in both radial and axial directions out of the valve. Neutral density probe measurements showed a mass fraction of > 0.90 at the time of peak engine thrust. The propellant distribution however, was no more radial than it had been for the A-8 nozzles. In this case, the valve seat design appeared to dictate the distribution to a greater extent than did the nozzle structure. The efficiency of the engine was 22% at a specific impulse of 4500 sec. This result offered further confirmation of the fact that propellant distribution was a more important factor in performance than was the availability of a high fraction of injected propellant.

Having achieved little success (in this series of changes) in effecting the propellant distribution through alterations in the ℓ/d ratio of the ports or changes in the valve plenum pressure, an effort was made to achieve the desired spreading angle ($\sim 45^{\circ}$) by placing the ports at a 45° angle with respect to the center electrode, rather than parallel to it, as had previously been the case. A drawing of this nozzle, designated A-7, 45°, is shown in Fig. 14. With this nozzle, the propellant mass flow required for self triggering decreased by about a factor of two to ~ 11 mg/sec., indicating that a more radial distribution had been obtained. This was confirmed by neutral density distribution measurements, which indicated that the propellant stream following closely the direction of the nozzles; perhaps too closely in view of the relatively low density of gas found along the center electrode.

In order to increase the amount of gas in this region, the inner boundary of the nozzles was machined so that it made an angle of 5° with the center electrode (Nozzle designation A-7XD, $45^{\circ}, 5^{\circ}$).

With this nozzle geometry, the mass flow of propellant for self triggering was found to be ~ 13 mg/sec. indicating that the gas density distribution still had a large radial component. The distribution of xenon in the accelerator at the time of triggering for peak thrust (650 μ sec) is shown in Fig. 15.

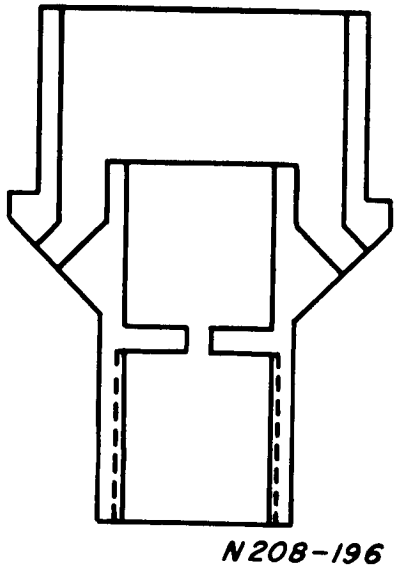

Figure 14. A-7D, 45° Nozzles

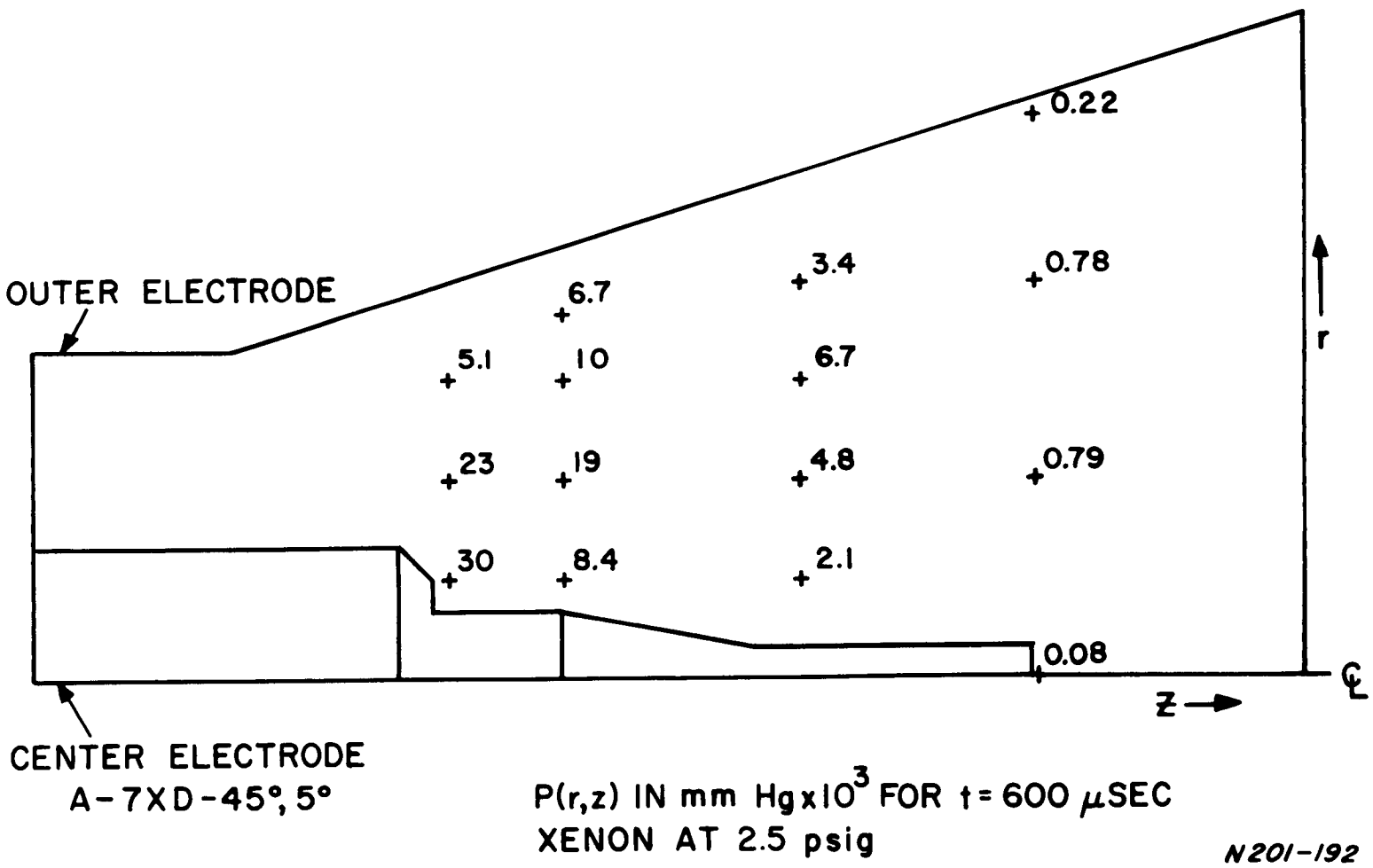

Figure 15. Propellant Distribution in Accelerator -600 μ sec after Valve Actuation

This nozzle allowed higher gas density at the outer electrode at the time of triggering and considerably less azimuthal inhomogeneity in the gas density distribution. The fraction of injected available propellant available at 650 μsec was 0.85. The efficiency, however, was 27.5% at 5000 sec. The performance curve (η_o vs I_{sp}) for the A-7XD, 45^o, 5^o accelerator is shown in Fig. 16.

A water cooled calorimeter[1] placed with its leading edge about 5 cm from the muzzle of the accelerator indicated that for the same conditions of operation the ratio of power in the exhaust stream to power input was 0.55. This compares with a previously measured value of over 0.70 for the A-7XD accelerator.

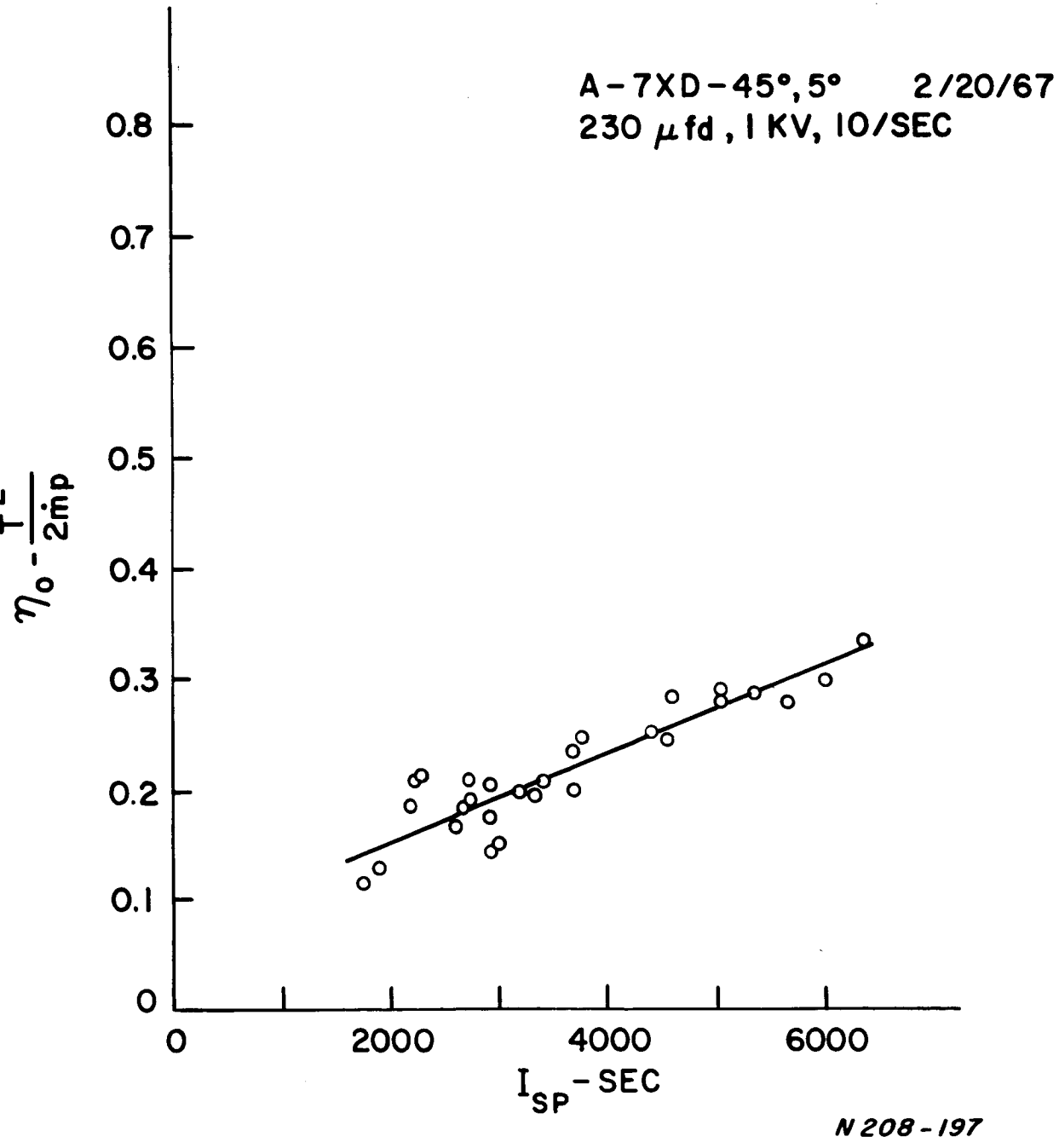

Figure 16. Efficiency vs I_{sp} for A-7XD-45°, 5° Accelerator

G. 2 Accelerator Geometry

In the light of the relative insensitivity of accelerator efficiency to propellant distribution, other factors previously found to influence performance were investigated. Changes in the accelerator electrode geometry were made for otherwise fixed conditions of operation. Outer electrodes of three different divergences, but with the same breech diameter of 12.5 cm and same 20 cm length, were substituted for the 27 cm muzzle diameter electrode which had been associated with highest engine efficiency. Of electrodes with 20 cm, 30 cm, and 12.5 cm maximum diameter, only the latter, a straight cylindrical electrode, provided significantly different performance. With it, the efficiency of the engine was reduced to 20% at 5000 sec I_{sp}.

Since the center electrode geometry was to a large extent fixed by the nozzle design, the only parameter investigated was the length of the 1.27 cm diameter section. In this case too, the electrode length shown in Fig. 1 resulted in a level of performance not significantly different from lengths 5 cm longer or 5 cm shorter.

G. 3 Voltage and Capacitance

The energy input into a fixed accelerator configuration was varied either by changing the capacitance or by changing the voltage. When capacitances of 218 μfd, 141 μfd and 337 μfd were used in the flexible array described previously, the efficiency of the A-7XD engine was peaked at 218 μfd, with $\eta_o \sim 27\%$ at 5000 sec I_{sp}. However, the efficiencies at the other capacitance values were only a few % lower. The efficiency-capacitance relationship followed approximately that established earlier, but at a level more than a factor of two lower than the original values.

Accelerator voltages as low as 700V and as high as 1100V were used with a fixed capacitance of 218 μfd. Once again, no profound changes in performance were evident.

G.4 Environmental Effects

Since a significant change in the performance of the accelerator was coincident with changes in the test facility rather than an obvious change in the geometry or operating inputs of the accelerator, further investigation of possible environmental effects was warranted. The effects of the presence of pumping system derived contaminants were referred to earlier. There is evidence that breakdown conditions for both the trigger and main discharge were influenced by such contaminants. In one test of the possible effects of hydrocarbon impurities, some acetone vapor was mixed with the xenon in the propellant reservoir. No effect either in ease of breakdown, or in accelerator performance was observed. Since neither the exact nature of the impurities or the mode of addition is known, a possible contribution in the form of environment influenced mass addition cannot be completely ruled out.

The effect of increased background pressure was observed at the time when the engine was operated with 286 μfd capacitance (see page II-7). Additional tests were run with the system background pressure increased to $> 5 \times 10^{-5}$ torr by valving off from the test chamber two of the three oil diffusion pumps. At 10 cps firing rate an increase in efficiency from 28% at 5000 sec to 32% at 5000 sec was observed. At a 5 cps firing rate, the efficiency was once more 28% at 5000 sec. Thus, there appeared to be some effect on performance due to background pressure, but such an effect was minor compared to the change in performance sought. In addition, tests at several repetition rates, down to 2 cps, in some cases, were standard procedures and had never shown disagreement, except in the case described above and on page II-7.

Alteration of the vacuum facility involved a structural modification which was investigated as a possible source for spurious influence on the thrust. A hole in the interchamber pumping plate through which the accelerator fired[1] was enlarged from 22" diameter to 35" diameter in order to improve access to the engine. The possibility of interactions between the accelerator

and this plate, resulting in spurious thrusts, was examined previously (see Ref. 1) and proved to be significant. Since any drop in performance might have been remotely associated with a change in the proximity of the accelerator to the plate, an aluminum ring of 22" diameter was affixed to the plate to simulate the previous conditions. No change in performance resulted from this modification, thereby ruling out the possibility of such an interaction.

H. Additional Measurements on the A-7XD-45°, 5° Accelerator

Since the A-7XD-45°, 5° accelerator produced as high a performance as could be achieved as a result of the numerous parametric changes which have been described, it was decided to investigate its characteristics in additional detail.

H. 1. Measurements of Magnetic Fields in the A-7XD-45°, 5° Accelerator

A small search coil having a rise time of 3×10^{-8} sec was wound on a 2 mm diameter form and placed in a quartz envelope for the purpose of mapping the B_θ component of the accelerator magnetic field. The voltage output from this coil, which is proportional to $\frac{dB_\theta}{dt}$, was integrated by a passive integrating circuit having an integration time constant of 6×10^{-5} sec., long compared with the accelerator discharge period of 10 microseconds. The probe and its integrating circuit had a calibrated response of 3 gauss per millivolt.

At a particular accelerator operating condition the probe was moved in both r and z. Reduction of the B_θ vs time oscillograms as shown in Fig. 17 allowed the spatial plotting of B_θ at a given time as shown in Fig. 18. For these plots the A-7XD-45°, 5° accelerator was running with xenon at 0.06 mg/shot, at 1 KV, and 1 shot per sec with a delay time of 450 microseconds.

It can be seen from Fig. 18 that B_θ has a large radial dependence for all time. This further corroborates previous assertions (see Ref. 1) that no simple thin radial current sheet exists during the acceleration process. Rather, the discharge current appears to follow constant gas density contours with large axial components at an intermediate radius between anode and cathode. The only discernable radial current sheet travels along the center electrode and finally evolves at 10 μ sec as a pinch off the tip of the center electrode. This correlates well with usual observation

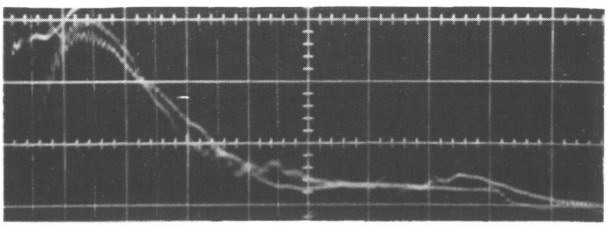

r = 3.2 cm, z = -17.8 cm
0.2 V/cm, 2 μsec/cm

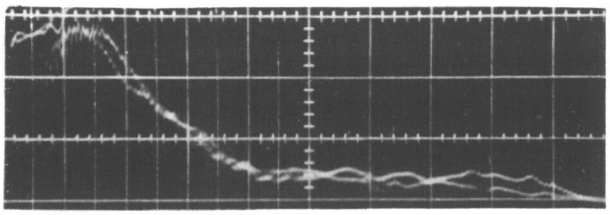

r = 3.2 cm, z = -13.3 cm
0.2 V/cm, 2 μsec/cm

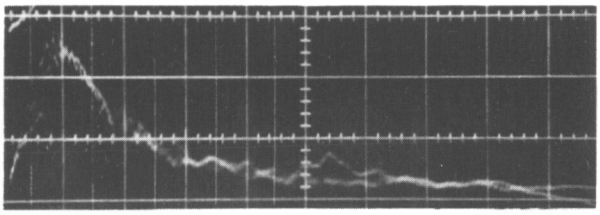

r = 3/2 cm, z = -8.9 cm
0.2 V/cm, 2 μsec/cm

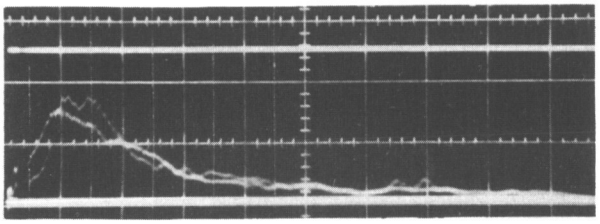

r = 3.2 cm, z = -4.4 cm
0.2 V/cm, 2 μsec/cm

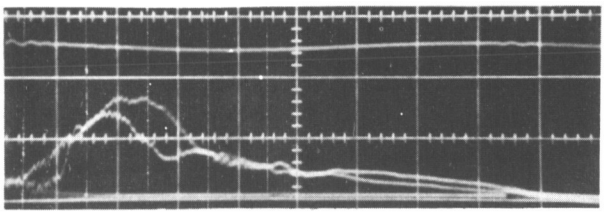

r = 3.2 cm, z = 0
0.1 V/cm, 2 μ sec/cm

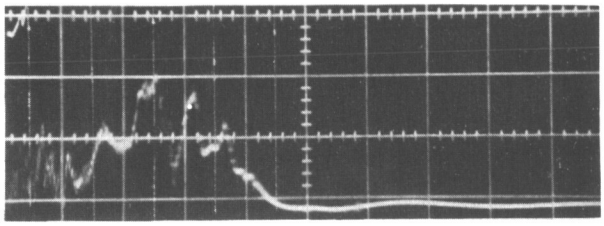

r = 3.2 cm, z = 8.9 cm
0.02 V/cm, 2 μ sec/cm

1 KV, 230 μfd, 0.6 mg/sec Xe.
r = 3.2 cm, z measured from tip of center electrode positive towards gun muzzle.

Figure 17. B_θ vs z for A-7XD, 45°, 5° Accelerator

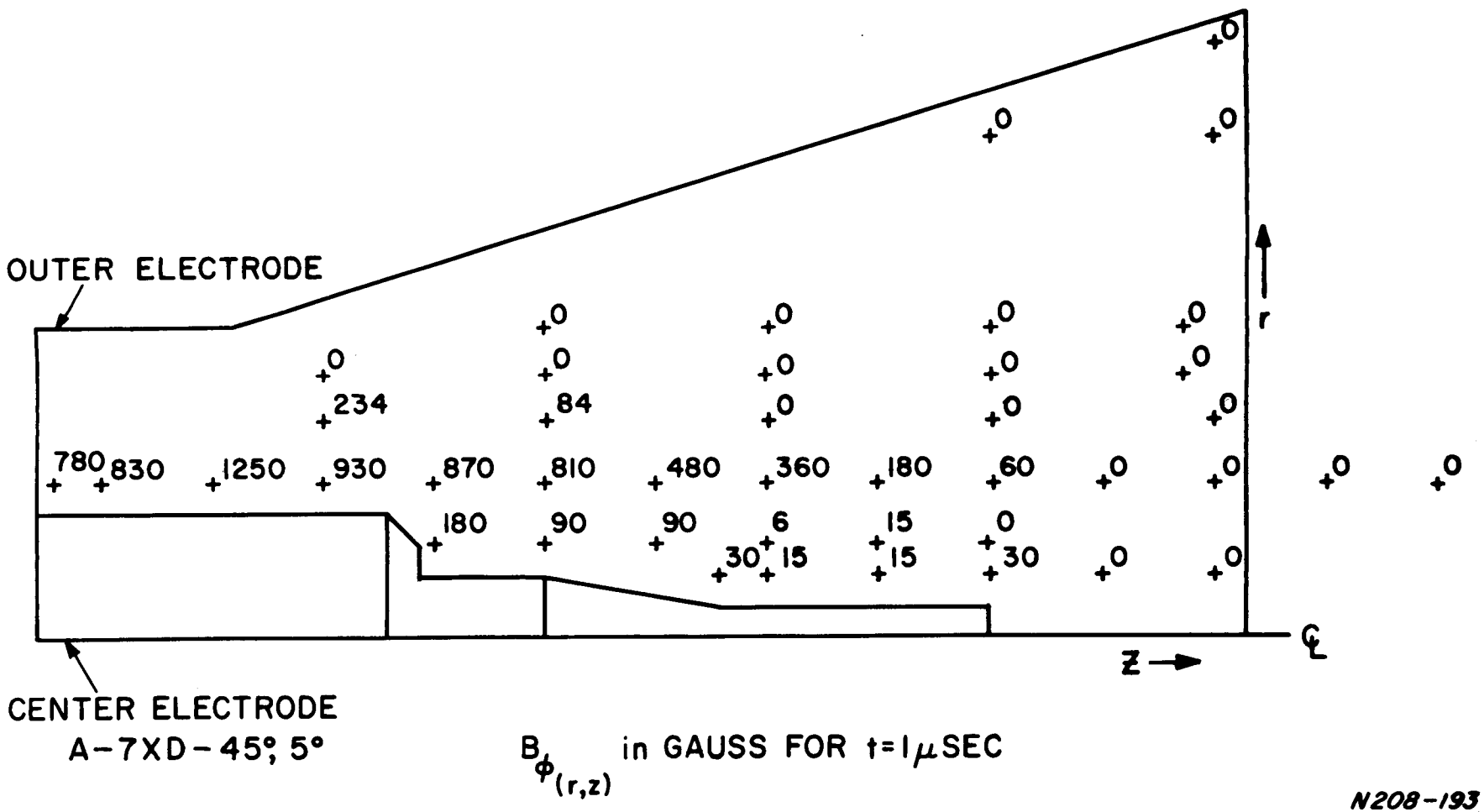

Figure 18. Distribution in A-7XD-45°, 5° Accelerator at different Times after Discharge Initiation

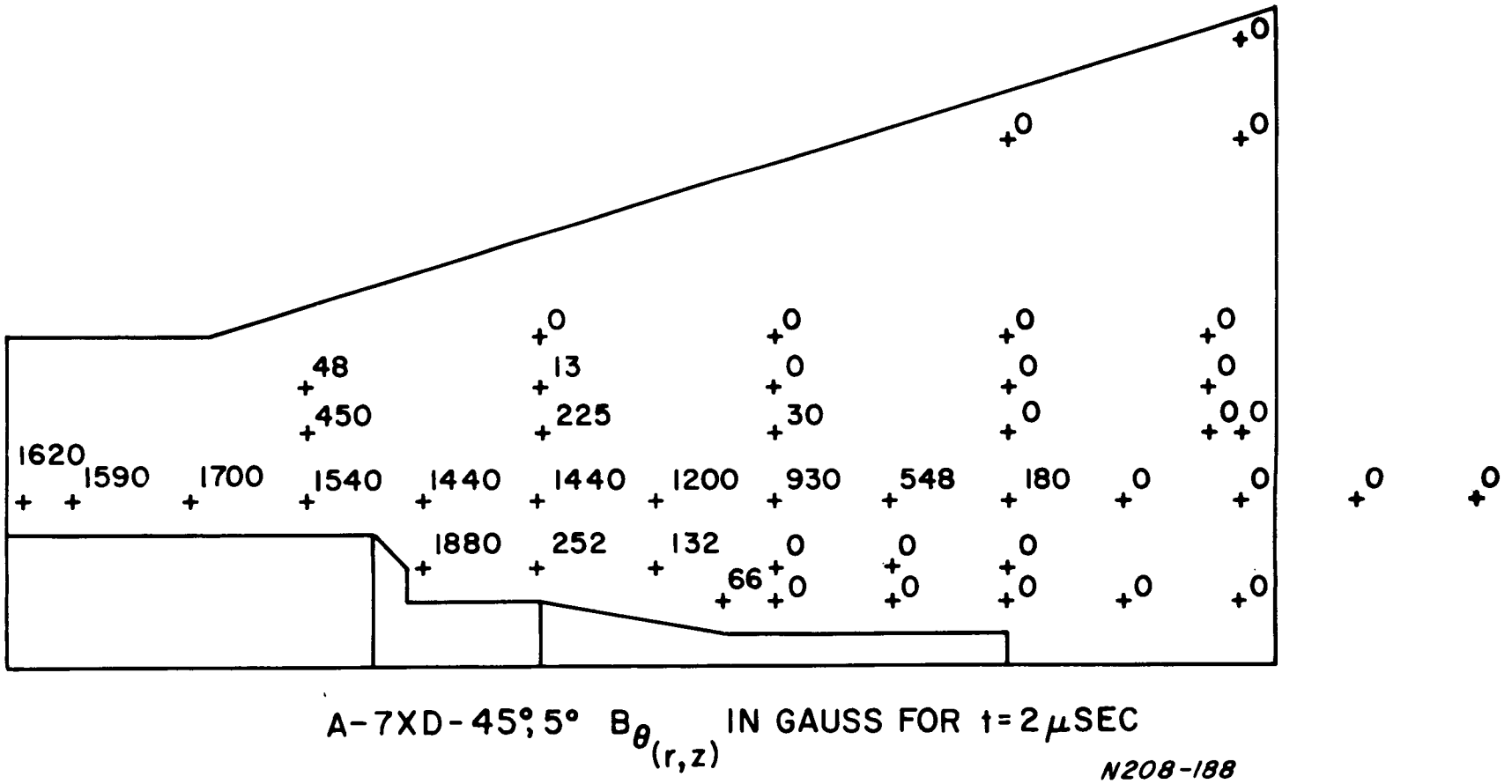

Figure 18(cont.). Distribution in A-7XD-45°, 5° Accelerator at different Times after Discharge Initiation

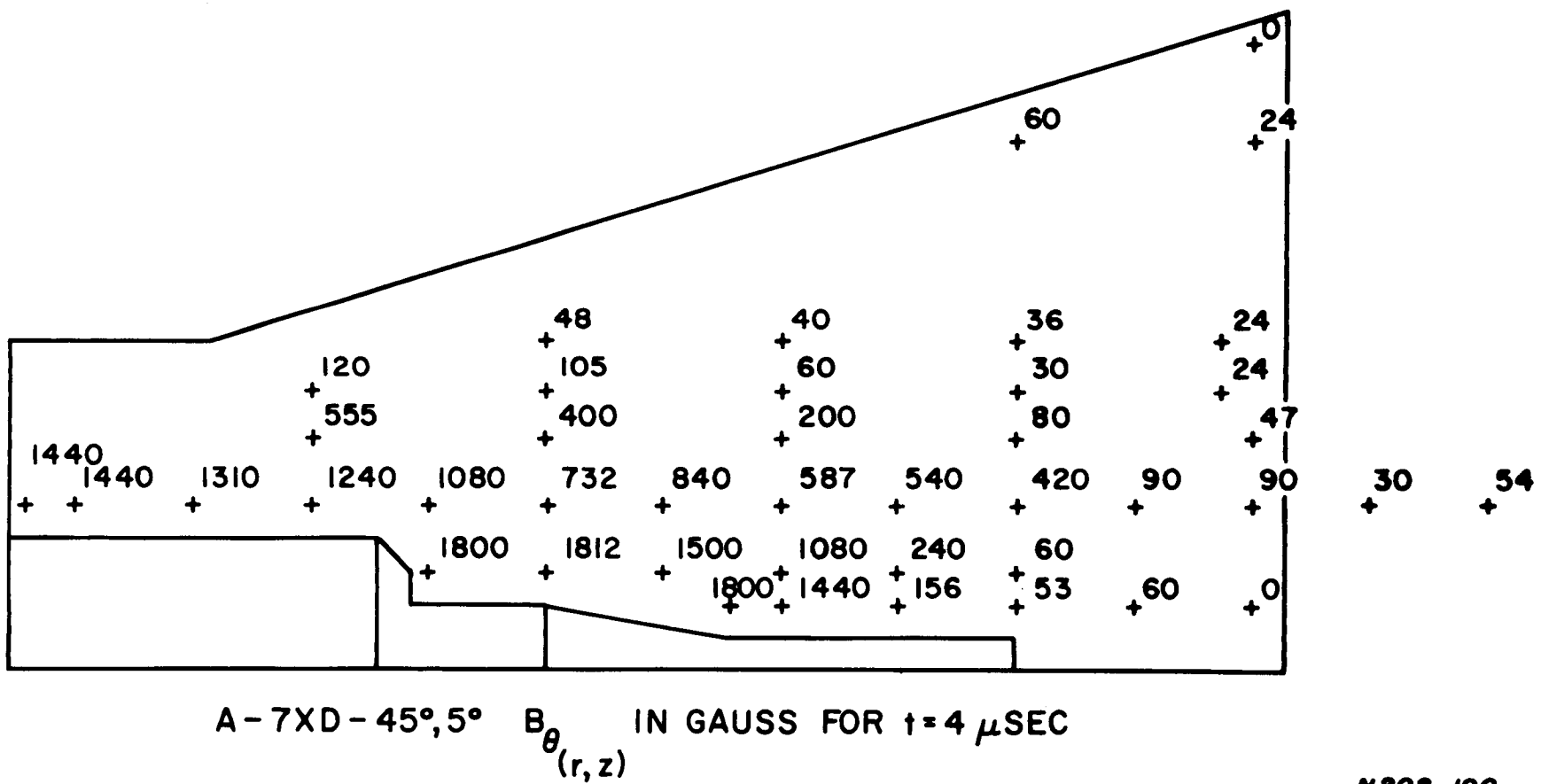

Figure 18 (cont.). Distribution in A-7XD-45°, 5° Accelerator at different Times after Discharge Initiation

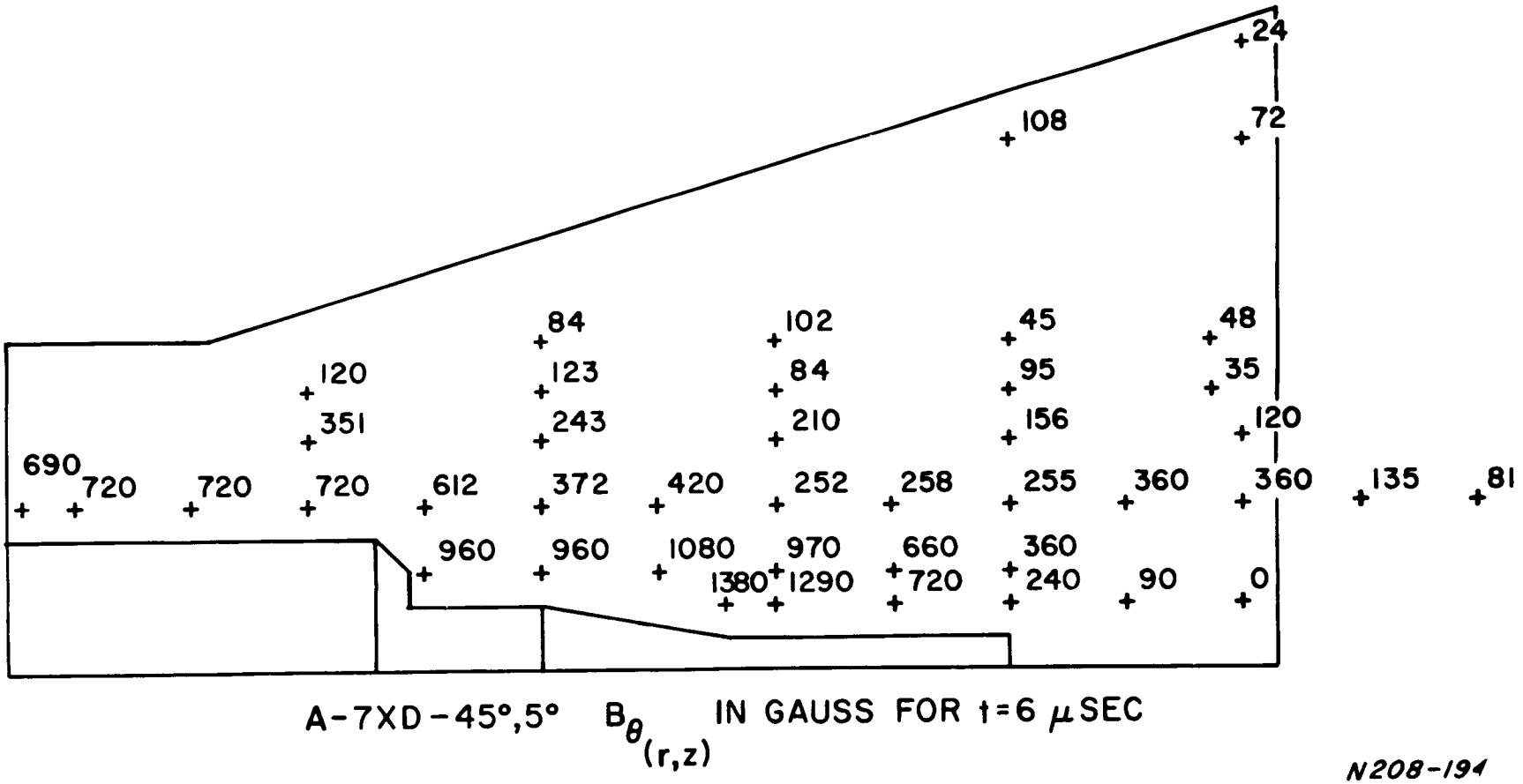

Figure 18 (cont.). Distribution in A-7XD-45°, 5° Accelerator at different Times after Discharge Initiation

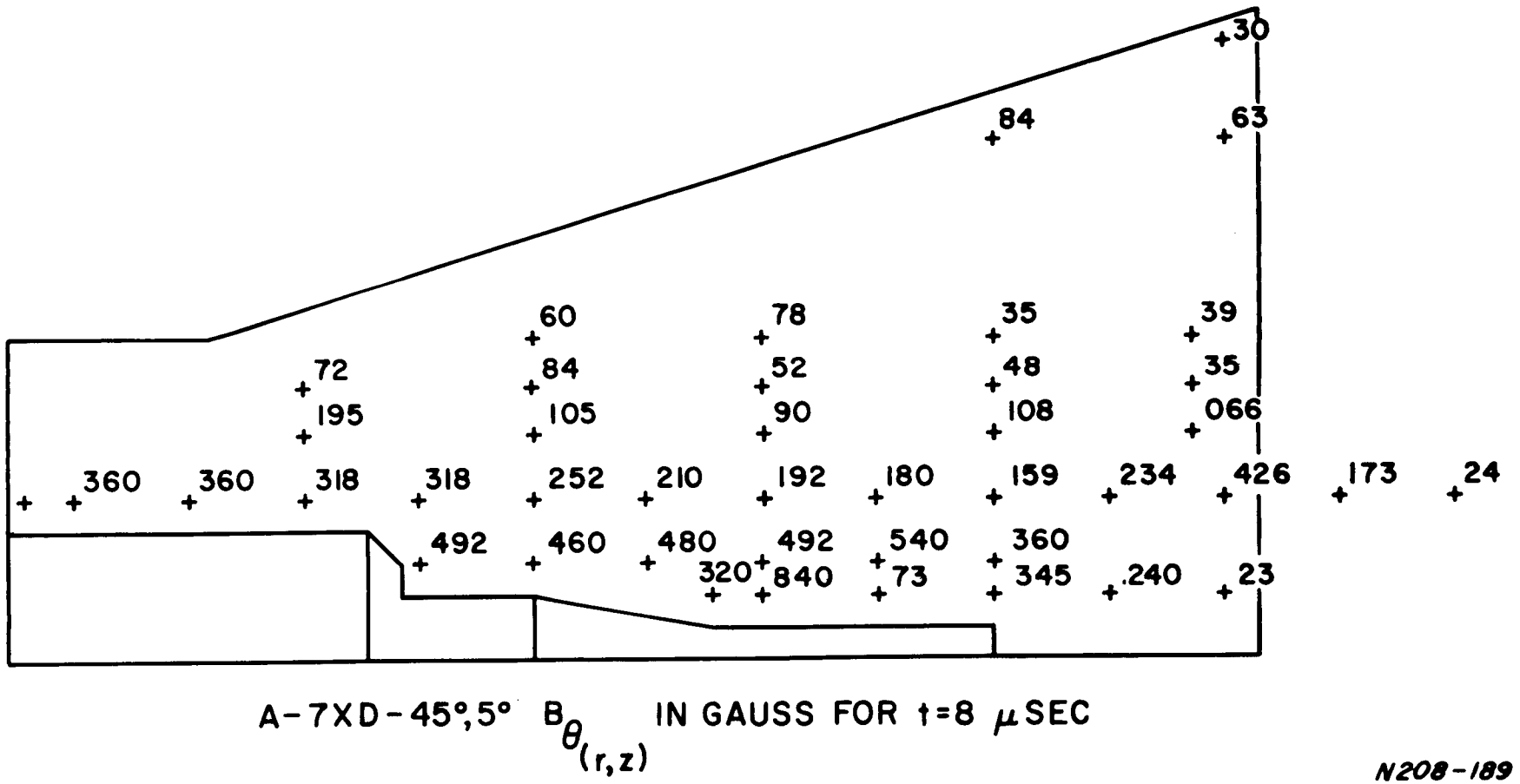

Figure 18 (cont.). Distribution in A-7XD-45°, 5° Accelerator at different Times after Discharge Initiation

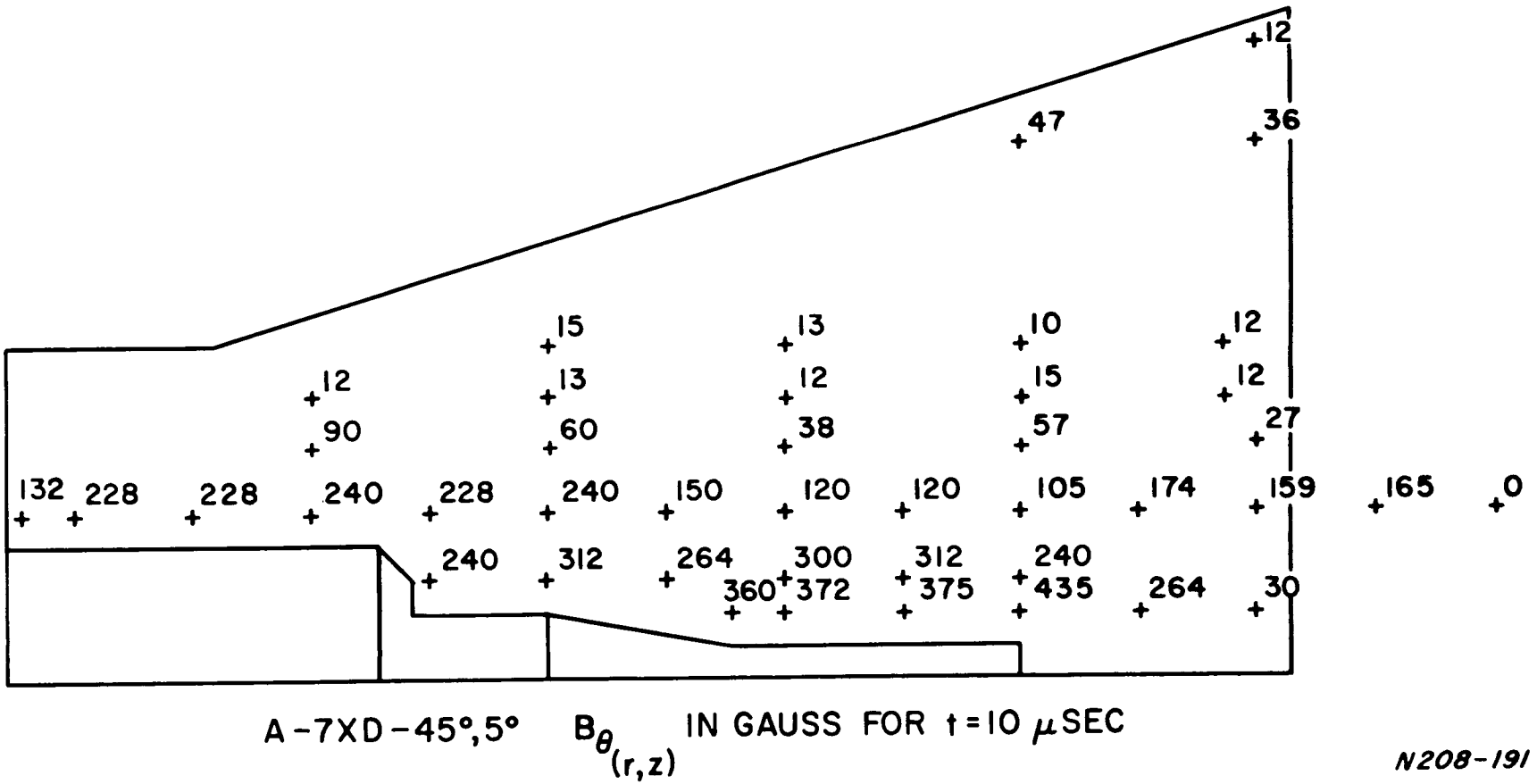

Figure 18 (cont.). Distribution in A-7XD-45°, 5° Accelerator at different Times after Discharge Initiation

of a sharp luminous plasma core at the tip of the center electrode during best accelerator operation.

The general quality and reproducibility of the magnetic field signals at a given point deteriorated with decreased mass flow. This is seen from the traces shown in Fig. 19. At any mass flow in the accelerator the reproducibility of the magnetic field signals decreased sharply for data taken beyond the tip of the center electrode. This non-reproducibility had not been observed for the A-7D accelerator operating with 144.5 μfd.[1]

H. 2 Gridded Probe Measurements in the Exhaust of the A-7XD-45°, 5° Accelerator

In order to determine the ion velocity distributions an electrostatic gridded probe used in previous[1] measurements in the exhaust of the A-7D accelerator was placed 2 meters downstream from the muzzle of this accelerator. The non-reproducibility of signal observed in B_θ probe measurements at the muzzle of the accelerator was even more pronounced at 2 meters downstream with the gridded probe signals. The erratic nature of the signal made it impossible to interpret the data. It should be noted that this was not the case with the A-7D accelerator, where reproducibility of signal was sufficiently good to obtain consistent quantitative results.[1]

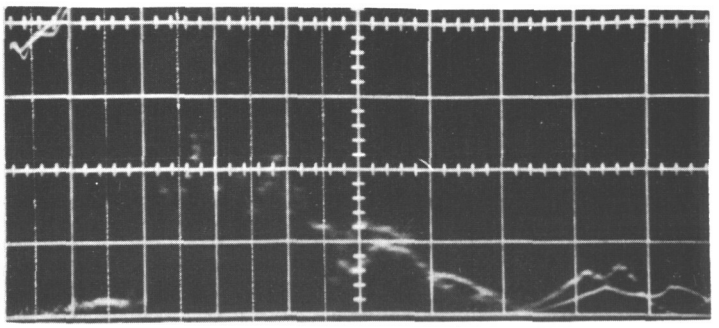

0.1 V/cm, 2 μ sec /cm

$\dot{m}$ = 0.2 mg/sec

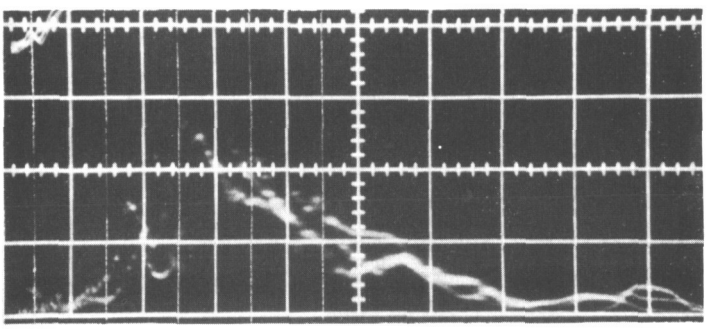

0.1 V/ cm, 2 μ sec/cm

$\dot{m}$ = 0.4 mg/sec

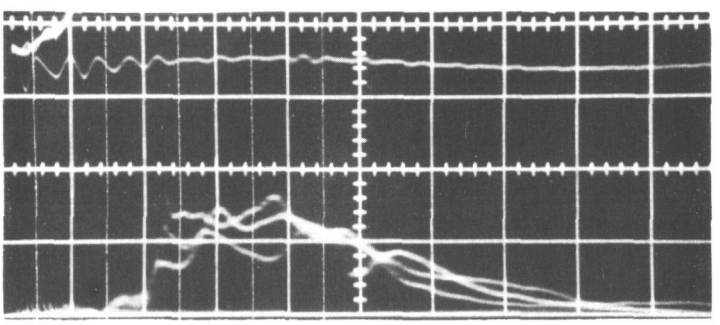

0.1 V/cm, 2 μ sec/cm

$\dot{m}$ = 0.6 mg/sec

Fig. 19. B_θ vs $\dot{m}$ for A-7XD-45°, 5° Accelerator
1 KV, 230 μfd
r = 1.9 cm z = 0

REFERENCES FOR SECTION II

1. B. Gorowitz, P. Gloersen, and T. Karras, "Study of Parametric Performance of a Two-Stage Repetitively Pulsed Plasma Engine (REPPAC) Summary Report, NASA CR 54846, Contract No. NASw-1044, 1966.

2. H. C. Miller, 'The Influence of Electrode Curvature Upon Electrical Breakdown in Vacuum. GE Report No. 65-RL-3929G, April 1965.

III. DEVELOPMENT OF THE ELM LIQUID METAL INJECTOR

A. Introduction

A means of reliable pulsed injection of small quantities of metal vapor has been studied with the aim of incorporating it into the repetitively pulsed plasma engine.

The demands on such an injector are severe. It must place the propellant so that a large fraction of it is optimally located for acceleration at the time the discharge is initiated. This operation must be performed anywhere from one to several hundred times per second, depending upon the engine's power level, with only a small energy consumption and negligible wear or deterioration in operation over many millions or even billions of injections. In addition the operation must be more rapid than the neutral atom transit time through the engine.[2]

The device that has been used to inject gases (xenon, nitrogen, etc.), an electromagnetically driven valve,[3] has been capable of satisfying only a few of these requirements. Its weaknesses lie in the high energy required for injection of an adequate supply of propellant and its questionable lifetime due to heavy bearing on the O-ring seat. Recent modifications have brought the energy requirement down to below a joule per shot, but the latter drawback still remains. For operation of a mechanical valve with liquid metals a boiler system would also be required, with all the high temperature problems and instabilities inherent in it.

The advantages of liquid metal propellants (storability, low ionization potential, high atomic mass) have been so compelling that they have been used in other electric propulsion devices.[4] It was thus felt that pulsed plasma engines must also use these propellants if they are to be considered for practical application.

A two prong study was begun on the device to be described in the following sections. One, under Air Force sponsorship, was intended to

investigate its general characteristics and theory of operation. As part of the program reviewed here work was begun to develop a reliable long life propellant injector capable of high repetition rate operation. The areas of emphasis involved long term testing of various materials, development of manufacturing techniques, and determination of optimum aperture size. The major goal of this phase of the program was the operation of a full size, pulsed plasma engine with a liquid metal propellant.

B. The Basic Concept - Exploded Liquid Metal Injector (ELM)

An injector system has been devised[5] that has many of the aforementioned advantages. The technique involves the pulsing of an electric current through a small body of liquid metal, contained by surface tension forces, in order to induce repetitive vaporization. Except for the propellant itself, no moving parts are used.

The most practical configuration uses a small cylindrical capillary with a small hole at its end. The capillary is drilled in an electrical insulator while the end wall containing the small hole is an electrical conductor. Figure III-1 schematically shows the geometry with a capacitor and switch in series with the capillary and metal wall.

Pressure behind the liquid metal filled reservoir forces liquid into the capillary completing the electrical circuit. Surface tension forces prevent any flow through the small hole in the metal wall. When the capillary is properly dimensioned the resistance of the filament will be greater than any other element in the circuit and so any energy stored on the capacitor will be dissipated within the filament when the switch is closed. If enough energy is deposited the liquid metal filament will vaporize and exit from the small hole through which surface tension had previously prevented the metal from passing.

The microscopic process of vapor generation involves complications that are not readily apparent: Initial heating causes expansion of the liquid metal and a consequent pressure build up within the capillary. The elevated pressure inhibits vaporization and so the filament remains in liquid phase

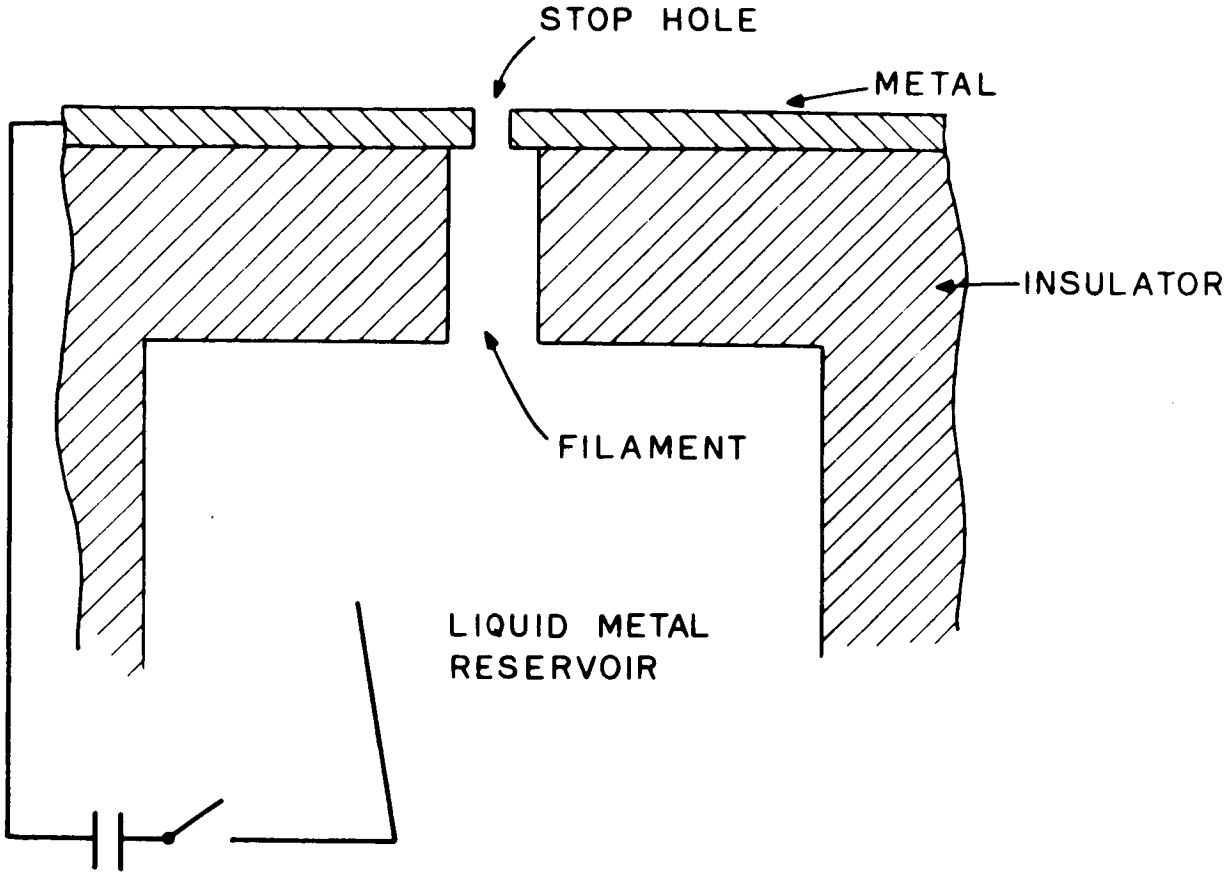

Figure III-1. Schematic of Filament ELM Feed

at an increasing temperature and pressure during a large part of the heating pulse. Conversion to vapor occurs only when the critical temperature of the liquid is reached or when the liquid vapor boundary on a PT diagram is crossed.

After the heating pulse is over, the pressure within the capillary will be maintained by the vapor pressure of the hot mercury. Thus vapor injection will continue until the filament has cooled. Only when the filament pressure and temperature are near the ambient conditions can the back pressure in the reservoir refill the capillary for the next shot.

The details of this process are discussed elsewhere.[6]

The liquid metal used in all tests up to this time has been mercury. Considerations of mass density and electrical conductivity make the fabrication of capillaries for other liquid metals very difficult. In addition, the low surface tension of these other liquid metals makes the stop hole that must be used very small. Appendix A analyzes in greater detail the relative suitabilities of potential propellants.

C. Specific Design

The most critical element in the design of the ELM injector is the dimensioning of the capillary and its stop hole. Appendix A gives the rationale for using capillaries between .0025" and .003" diameter and .016" to .021" long. The requirements of 15 micrograms of material and .075 Ω filament resistance (in each of 6 ELM units which would be fired in a single accelerator) were the primary criteria used.

The stop hole dimensions of .0008" diameter and .003" length are derived in Section G, and were based on the surface tension of mercury as well as considerations of gaseous conductance and liquid injection.

The capillary and stop hole apertures were placed in the center ($\pm$ .0002") of wafers .250" $\pm^{.0000}_{.0002}$" in diameter. The wafers could then be placed into a holder with an interior dimension of .250" $\pm^{.0002}_{.0000}$ insuring alignment of the stop hole and capillary. Since the surfaces of both

wafers were polished smooth no leakage of liquid through their interface was encountered. Care was also taken to insure a square smooth bottom on the holder and square burr free edges on the wafers. Only in this way could the desired alignment be achieved. Fig. III-2 shows a scale drawing of the region surrounding the capillary.

After insertion of the wafers into the holder a .250" O. D. O-ring was pushed in above them. This served to hold them in place and allowed a seal to be made between the glass tube forming the reservoir and the capillary wafer. Fig. III-3 shows a photograph of these pieces aligned as they would be before assembly.

The mechanical arrangement for testing was completed in the manner shown on Fig. III-4. The assembly was oriented so that injection occurred downward into a dry ice cooled cold trap ($< -50^{\circ}C$).

When the reservoir was filled, the contactor shown on Fig. III-4 was immersed. The firing circuit was then attached between the contactor and the flange containing the wafer holder. Fig. III-5 shows the circuit originally in use. Fig. III-6 shows the circuit adopted later to reduce extraneous losses. Appendix B discusses the reasons for this change and the basic characteristics of the circuits.

D. Wafer Materials and Aperture Fabrication

A wide variety of materials and fabrication techniques have been used on the ELM wafers and their apertures.

Early attempts were made with a plastic material (Kynar) and Lavite for the capillary wafer and stainless steel for the stop hole wafer. However, these were soon abandoned. The plastic had too low a softening point and stainless steel suffered mass transfer at the stop hole due to its contact with the hot mercury.[7] The Lavite was satisfactory for a time but its grains tended to come loose over extended runs.

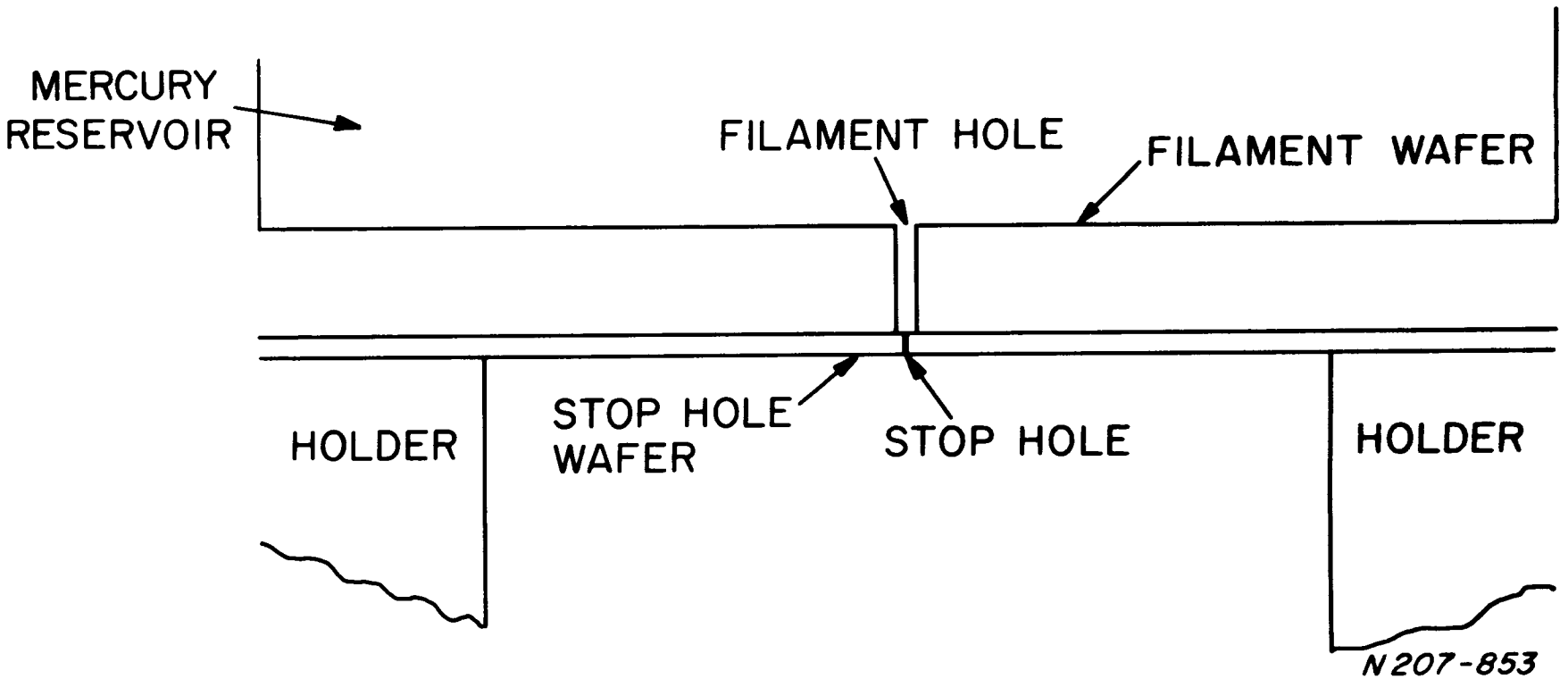

Figure III-2. Region Surrounding Aperture Assembly

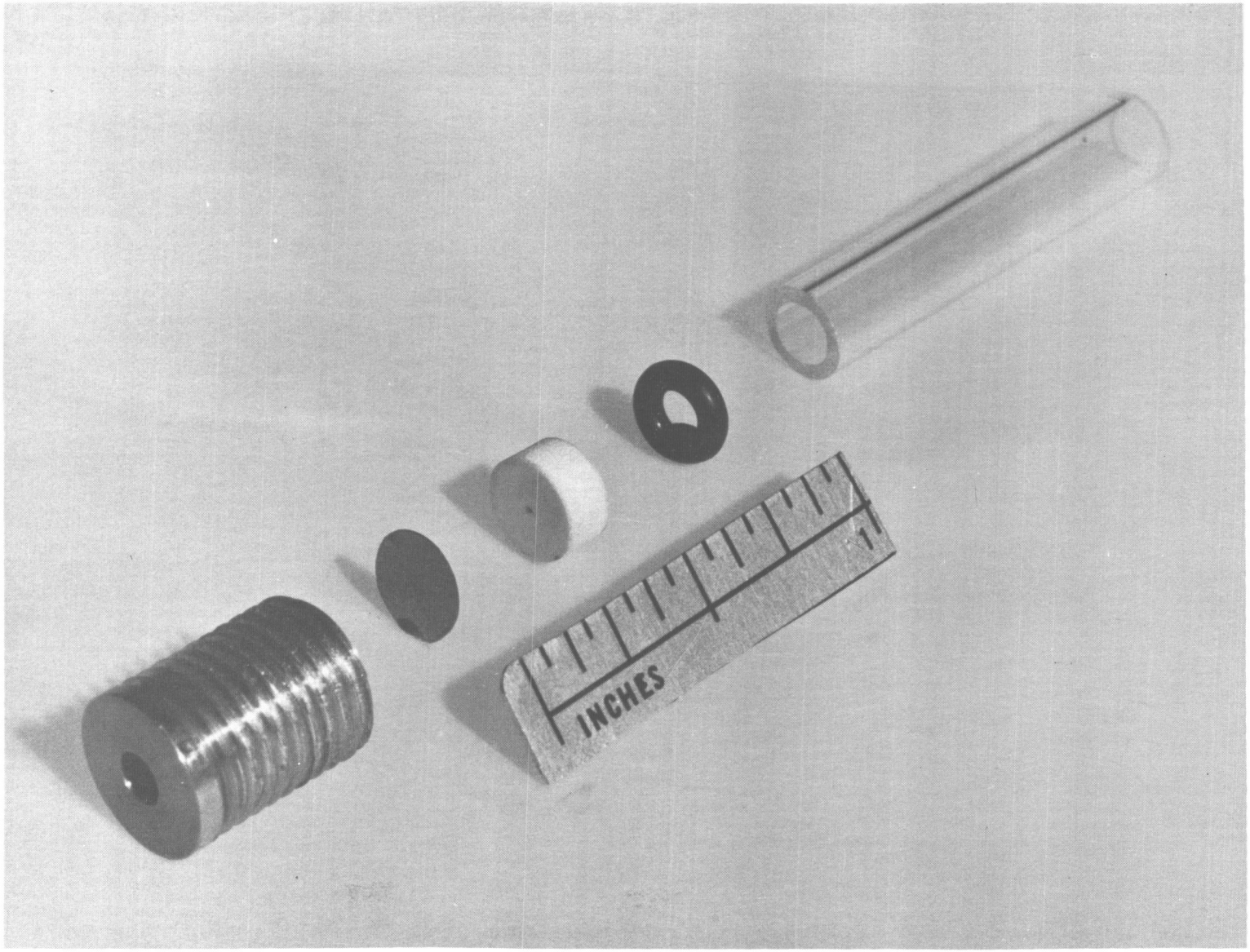

Figure III-3. Photograph of ELM Assembly

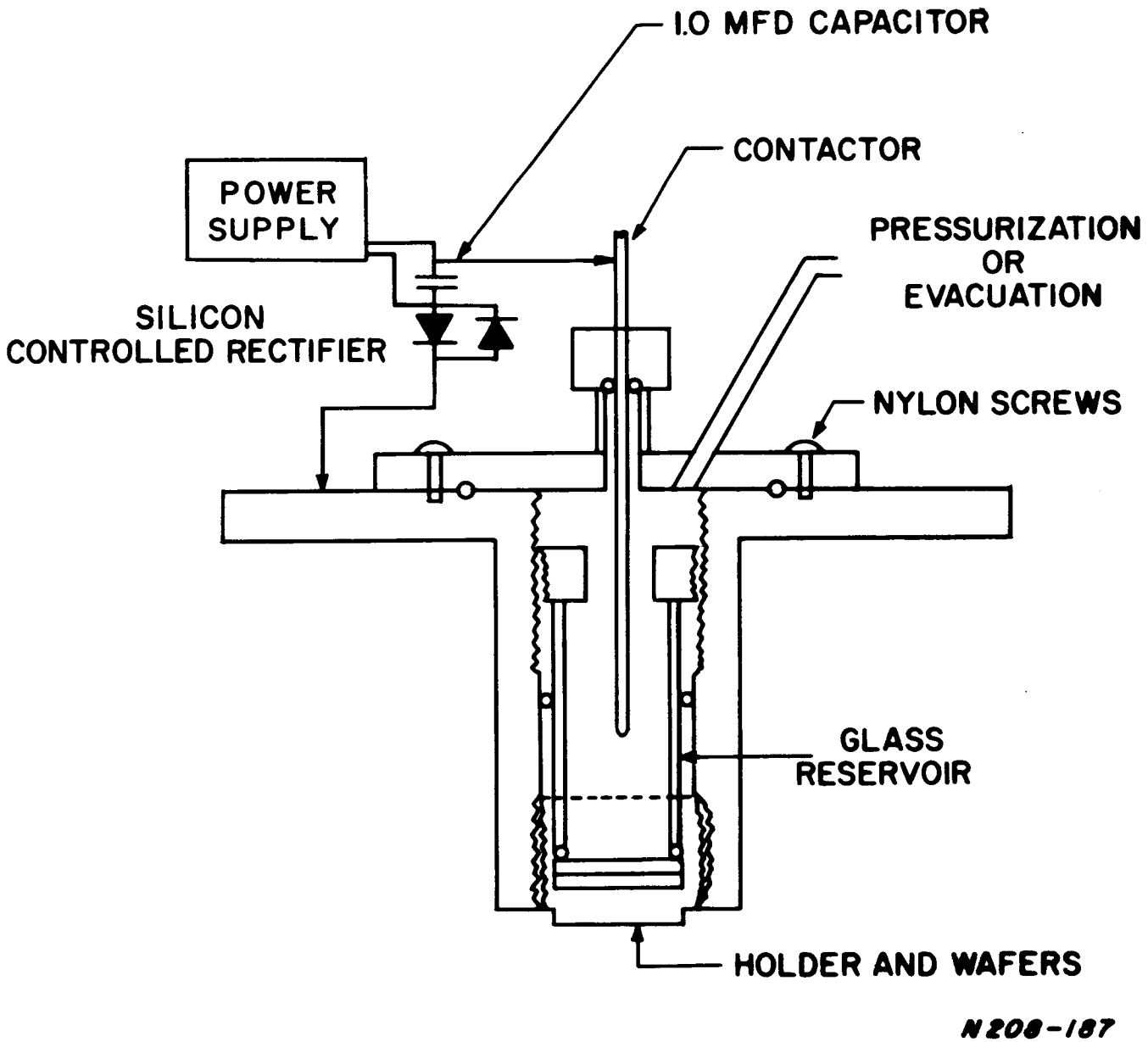

Figure III-4. ELM Experimental Assembly

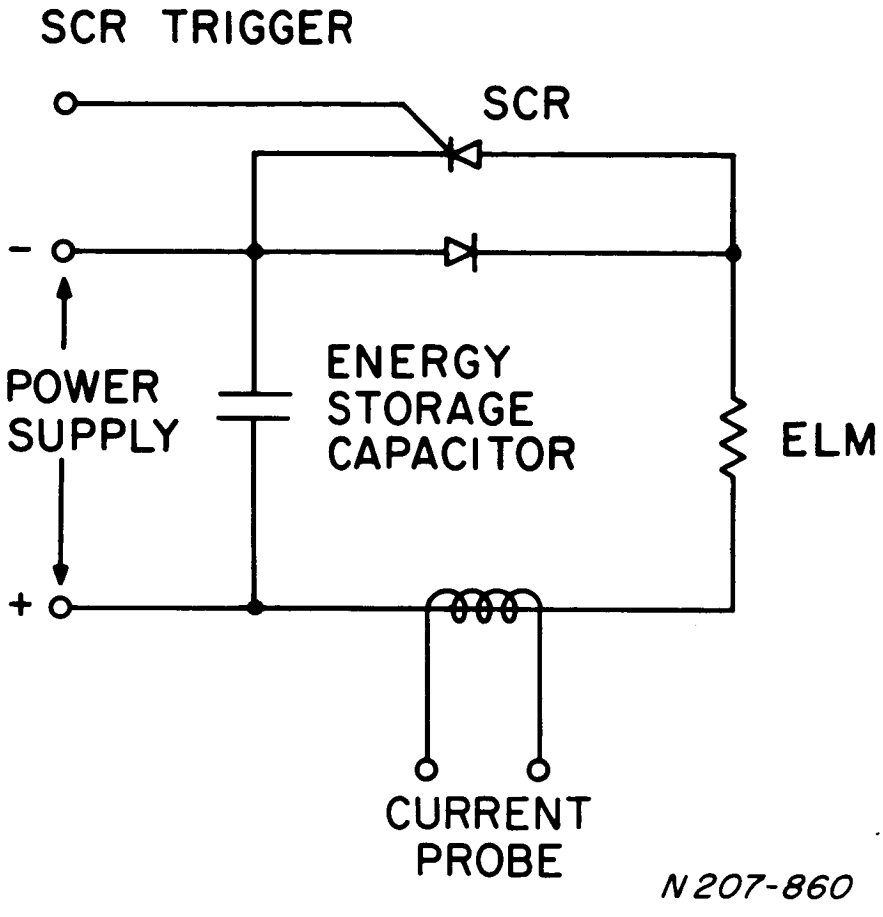

Figure III-5. Original ELM Firing Circuit

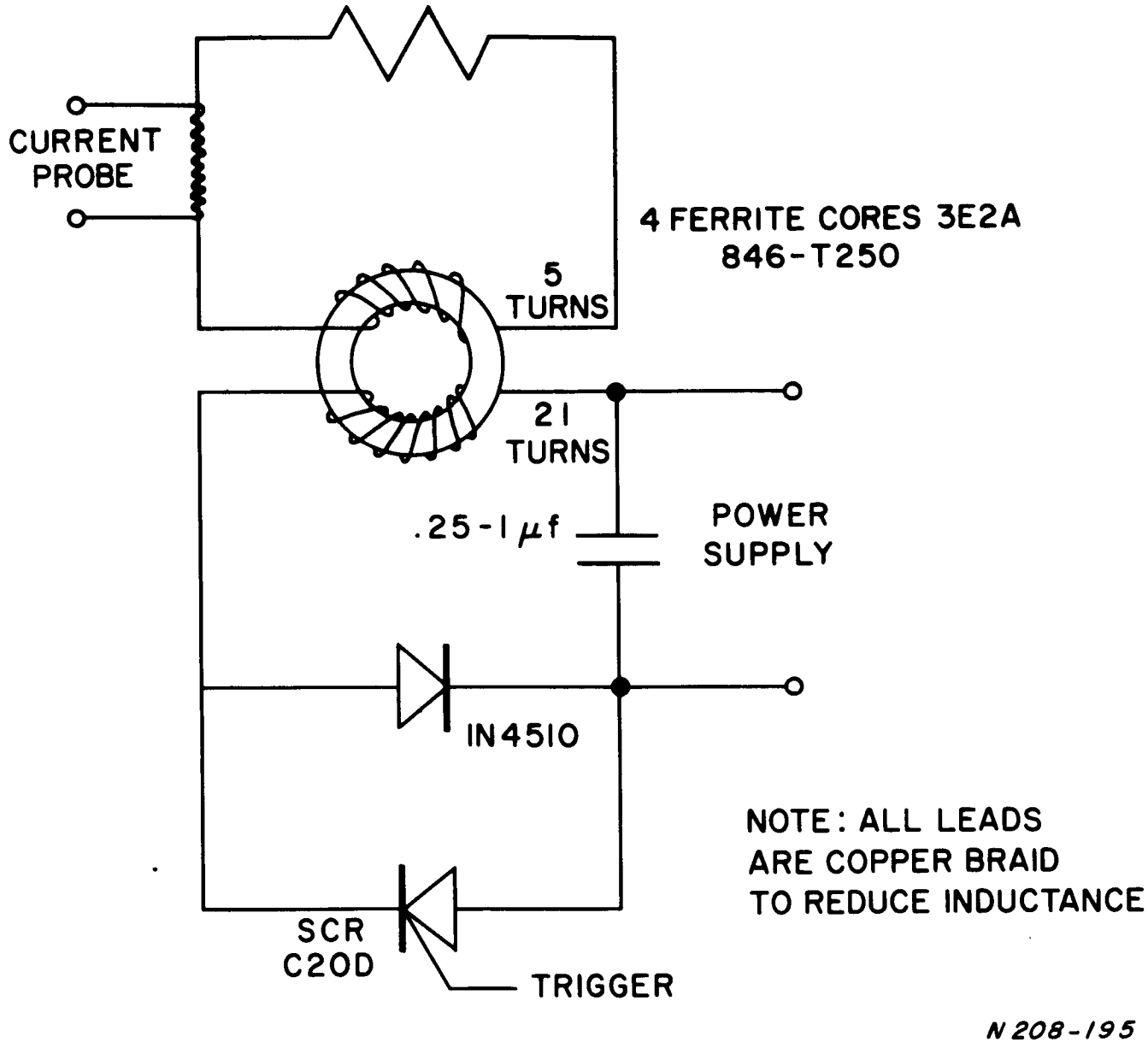

Figure III-6. Inductively Coupled ELM Firing Circuit

The materials chosen for succeeding tests were carefully selected to withstand the failures observed in the early materials. Thus refractory metals (i.e., molybdenum and tantalum) were chosen for the stop hole wafer because of their high temperature capability, thermal conductivity and lack of reaction with hot mercury.[7]

The required characteristics for the insulating material could not be so precisely specified. High strength to withstand the pressures generated, high temperature capability, and a lack of reactivity with mercury were obviously important. However, a resistance to thermal shock, a homogeneous structure (i.e., no grains to break loose or crystal axis to break along) and machineability were considerations that had to be included. The most promising materials appeared to be boron nitride, pyrolytic boron nitride, a specially deposited pyrolytic graphite, sapphire, Lucalox, and quartz.

Boron nitride had the advantage of being easily machineable, impervious to mercury, and of high temperature capability. Unfortunately its grain structure and lack of strength detracted from its usefulness. Pyrolytic boron nitride solved the grain problem since it is deposited in close fitting layers that are far more difficult to separate than grains. The lack of strength and hardness were present here also, however. Sapphire, Lucalox, and quartz in principle avoided these difficulties, and they were far superior for the thermal shock; but their machineability was a problem.

A major factor in the use of each of these materials was its compatibility with one of the various methods used for making the apertures. No great difficulty was encountered in making the exterior wafer dimensions. However, locating and making the holes was another matter.

The most straightforward technique, and in many ways the most successful, involved drilling of the holes by an outside vendor. Straight, circular, well located holes always resulted . Unfortunately the cost and

lead time required made alternatives attractive.

The obvious alternative of drilling holes in-house was also attempted. The special techniques and machinery required for the task were not available though, and only marginal success was achieved. Consequently this technique was abandoned.

The availability of a commercial laser device and its ability to penetrate even the most difficult material (e. g. diamond) prompted its use for drilling holes in both wafers.

Since the laser melts and vaporizes material in order to produce a hole, a steep taper results. The entrance of the laser beam produces a crater that narrows as it approaches the opposite surface. Fig. III-7 shows a stop hole from both sides as laser drilled in a molybdenum wafer. A similar appearance can be seen in pictures of laser drilled capillary holes. Because of the lower thermal conductivity the craters are not as extreme. This can be seen in Fig. III-8.

The stop holes produced by laser drilling molybdenum were acceptable. The only size requirement was that the narrowest section of the hole contain the propellant and any taper only served to increase the gaseous conductance. The short lead time and low cost of stop holes produced in this way were thus so attractive that standard drilling was no longer used.

The requirements on the capillary holes were considerably more severe. Even a moderate taper was found to lead to destruction of the capillary. This resulted from the fact that the narrow sections of the filament had a higher resistance per unit length and so absorbed a higher fraction of the energy deposited in the filament. Since these narrow sections also contained less material per unit length they were less capable of absorbing the added energy and damage to the adjacent capillary walls could result. In addition, since computation of the volume of a cratered capillary was difficult, the energy calculated for vaporization was often in error, leading to further damage of the capillary walls (see Section E).

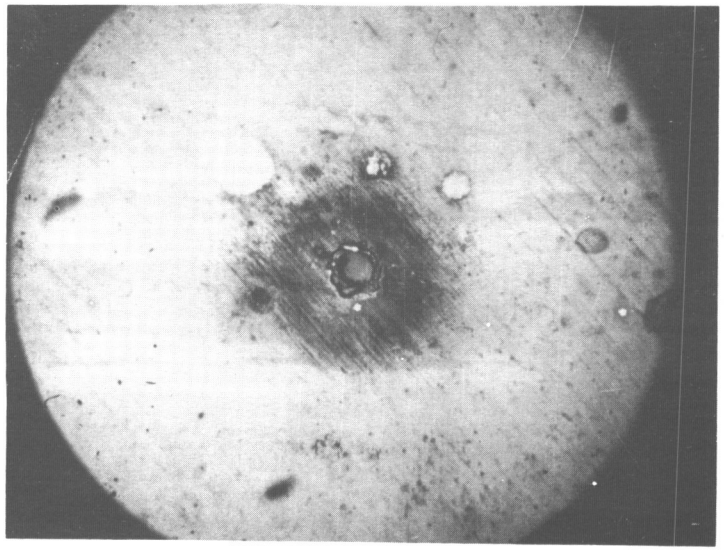

Mating Surface with
Capillary Wafer

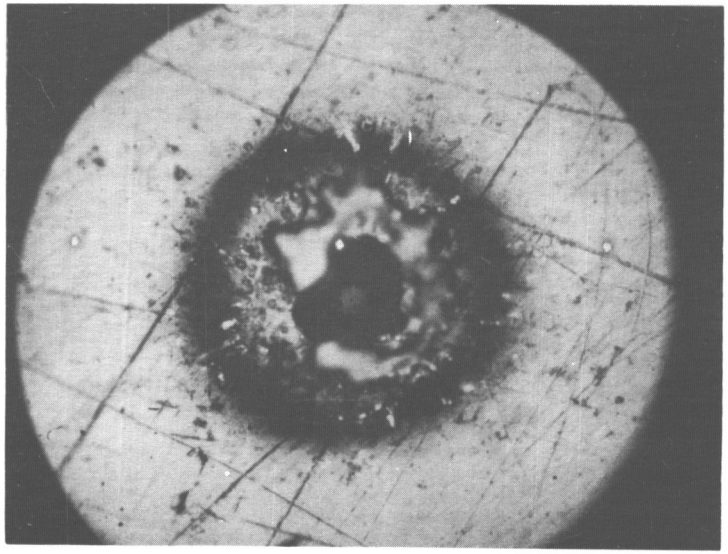

Surface toward Vacuum
(Entrance side for laser beam
during drilling)

Material: Molybdenum
Size: .003" thick
.0006" Min. Diam. of Hole

Figure III-7. A Laser Drilled Stop Hole from Both Sides

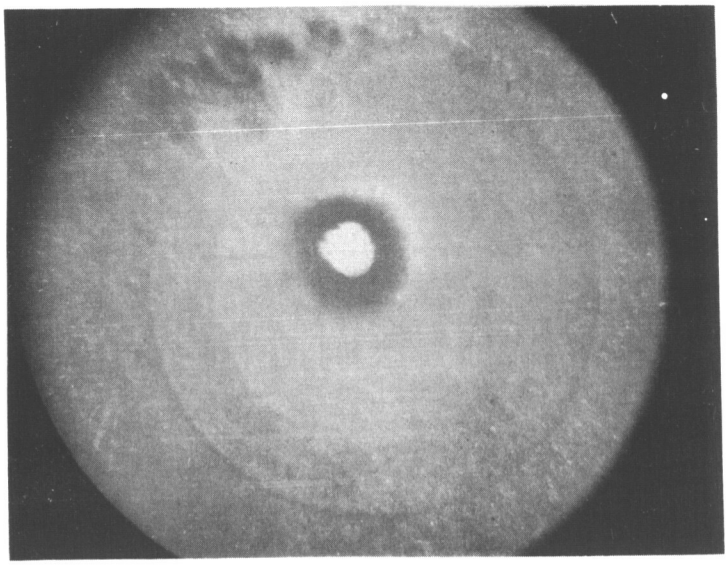

Exit Side for Laser Beam During Drilling

Size: .0026" Diam. at Narrowest Point
.017" Thick

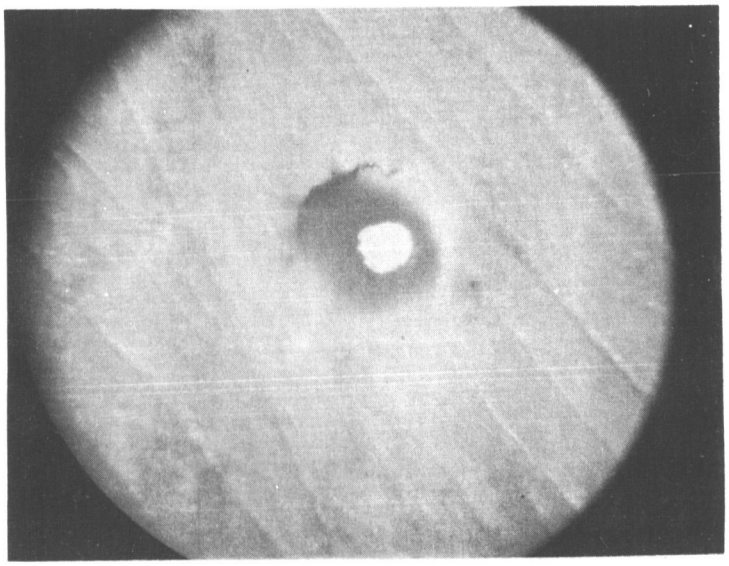

Entrance for Laser Beam During Drilling

Fig. III-8. Photographs of Laser Drilled Filament Holes in Hot Pressed Boron Nitride from Both Ends of Filament. 100x Magnification

The laser drilling process was the easiest way of producing capillary holes in many of the hard glassy materials (i.e., sapphire, Lucalox, quartz). For this reason considerable effort was expended in trying to obtain cylindrical laser drilled holes with these materials.

The smallest taper that was obtained was in capillaries 20% larger at their wide points than at their narrow points. However, this meant an almost 50% resistance change and usually led to destruction of the wafer (See Section E). Sapphire was much more likely to fail (fracture) in this way than a homogeneous material such as Lucalox because of weakness along certain crystal axes, but no material drilled with the laser gave anything but erratic performance. Table 1 gives the result of the two drilling processes with various materials.

Mechanical drilling was once again used as the means of producing the capillary holes, while laser drilling was used for the stop holes.

Several hard glassy materials investigated during the above period were believed to be very promising. Lucalox had shown an extraordinary resistance to destruction during actual tests as well as rating well on most of the characteristics discussed earlier. Quartz, though untested, rated even better. (Sapphire had already been rejected because of its tendency to fracture). For these reasons some way of making the capillary holes in these materials continued to be sought. Lucalox was found to be machineable in an unfired or partly fired state. Thus the holes could be drilled and the wafer fired afterward. The procedure is not consistent in the quality of pieces produced but a sufficient number has been obtained for test.

Another technique, untried at this time, would use casting and forming about a wire. Lucalox could be fabricated in our facility in this manner and an outside vendor has stated that the same process can be applied with quartz.

As a result of the manufacturing difficulties just cited, all tests were performed with boron nitride, pyrolytic boron nitride, and Lucalox capillary wafers. All three had holes produced by standard drilling techniques but the

TABLE 1

Results of Drilling Various Materials

	Mechanical Drilling	Laser Drilling	Alternatives (Not yet attempted)
Boron Nitride	Cylindrical hole	Tapered hole	------
Pyrolytic Boron Nitride	Cylindrical hole	Tapered hole	------
Sapphire	Very difficult	Tapered hole	------
Lucalox	Cylindrical hole if drilled in un-fired state	Tapered hole	Slip cast about wire (in-house)
Quartz	Very difficult	Not successful	Form about wire (outside vendor)
Molybdenum	Cylindrical hole	Strongly tapered hole	------

last had to be drilled in the unfired state. Laser drilled molybdenum wafers were always used for the stop hole.

The durability of each of these materials will be discussed in the following sections but Table II summarizes their characteristics.

E. Over Voltage and Under Voltage

Operation of the injector at voltages significantly above or below those required to vaporize the liquid within the capillary invariably leads to stress upon the walls.

Excess energy above that needed to vaporize the entire filament leaves voltage on the capacitor after vaporization has taken place. A microdischarge then occurs between the end of the unvaporized liquid through the vapor and to the conducting stop hole wafer. Fig. III-9 shows the current waveform being distorted on its trailing edge as the applied voltage is increased. It appears that the waveform is truncated at the time of vaporization and the excess voltage dissipates itself as the low level fluctuations visible thereafter. Spark pits can be seen surrounding the stop hole after such operation (see Fig. III-10).

Stop hole wafer spark pitting can be seen when only five or ten excess volts have been applied. However, much larger excess voltages are necessary to damage the capillary walls. Only when hot pressed boron nitride was used were capillary walls at all affected at even moderate overvoltages. (see Table II). Figure III-11 shows the ends of a pyrolytic boron nitride capillary subjected to overvoltage.

The criteria for overvoltage are not simply that the energy supplied is more than enough to vaporize all the liquid in the capillary. It occurs at some lower energy than that.[6] Table III gives data that indicate at what voltage current waveform distortion begins for several different capillaries. It is obvious that a large capillary can absorb more energy without being overvolted than one which is smaller.

127 volts applied

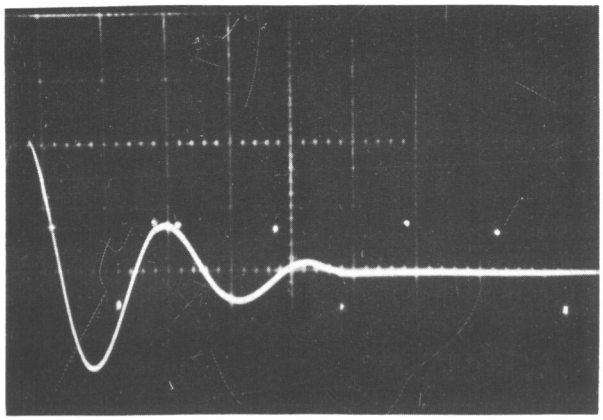

129 volts

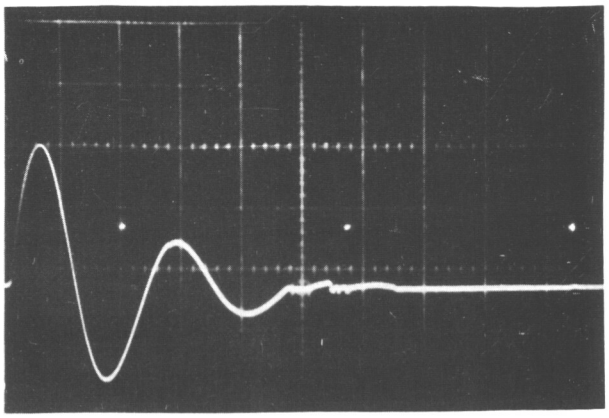

141 volts

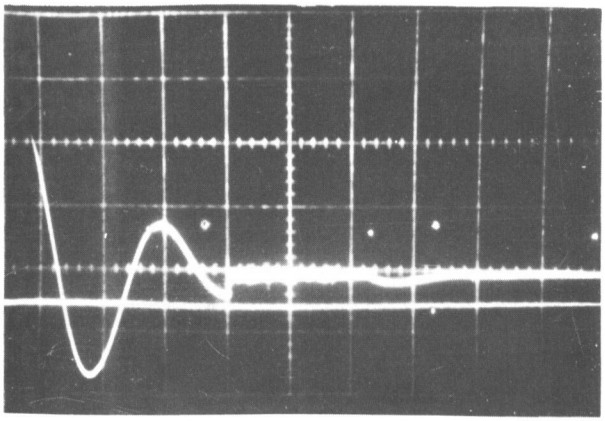

145 volts

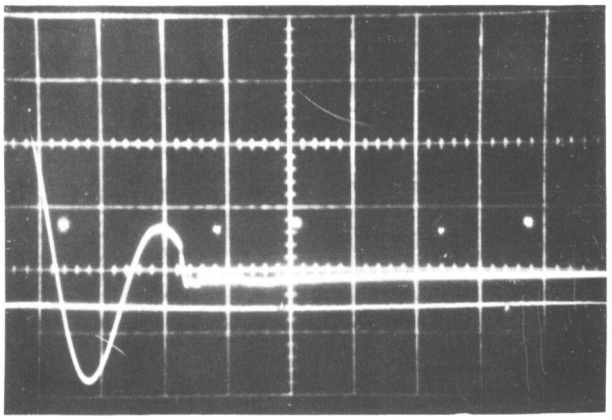

154 volts

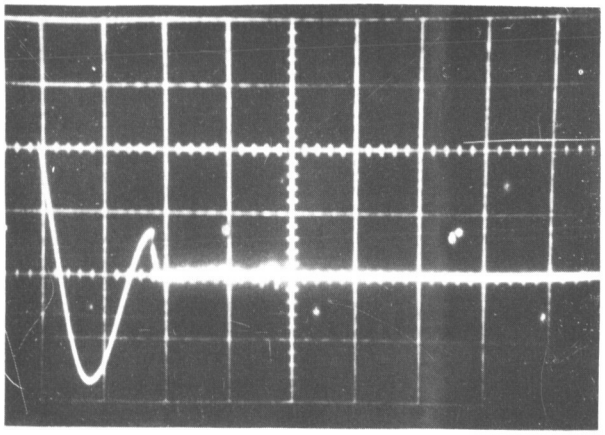

5 μsec/cm 25 amp/cm

Figure III-9. Gradual Distortion of Current Waveform by Overvoltage

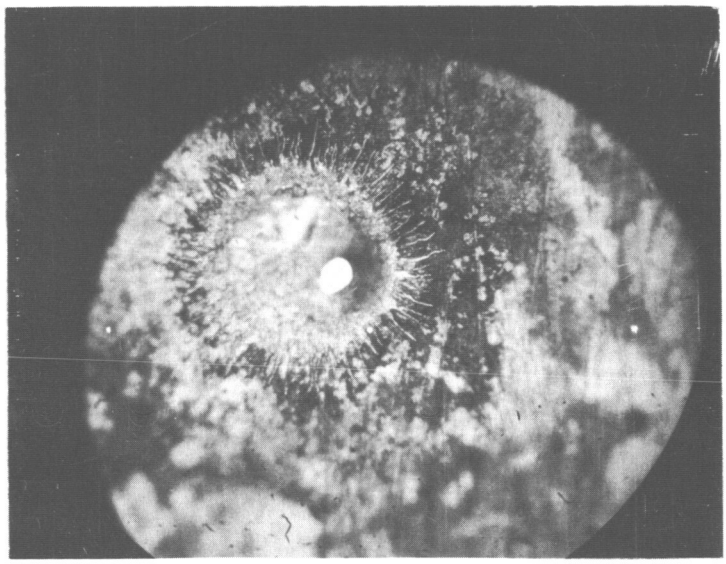

Size Disc: .0009" Diam
.003" Thick

Fig. III-10. Spark pitting of stop hole in molybdenum disc.
200x Magnification

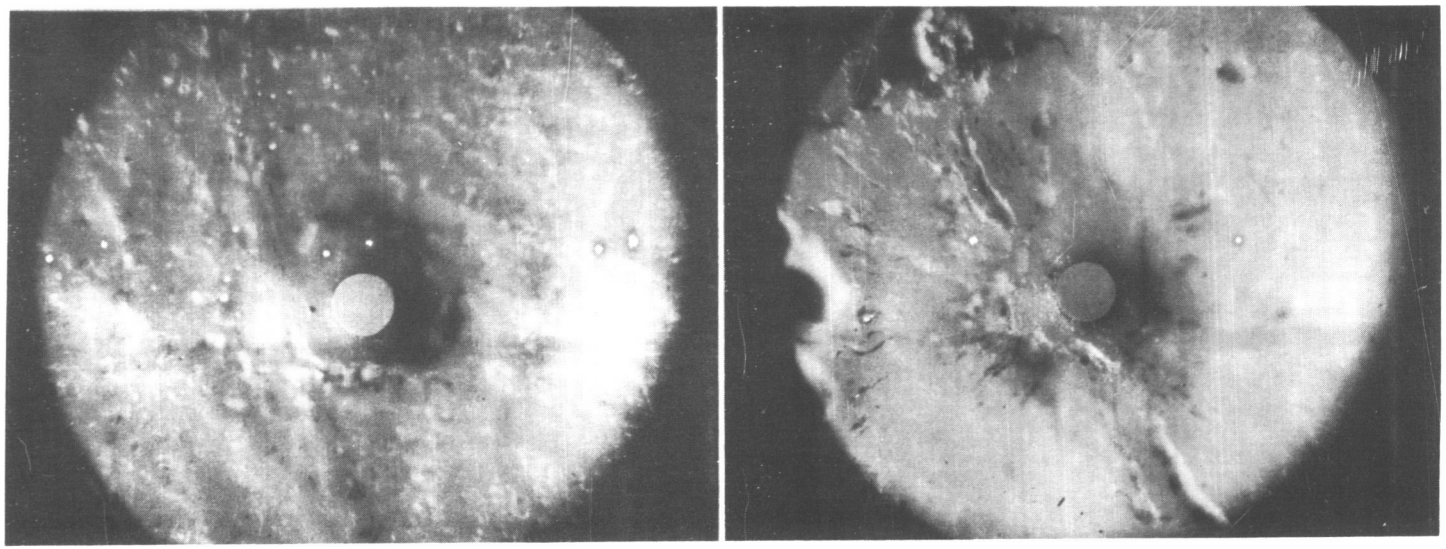

Side Facing Stop Hole

Side Facing Mercury Reservoir

Pyrolytic Boron Nitride - .0031" Diam
.017" Thick

Figure III-11. Capillary Damaged by Overvoltage

It is interesting to observe that if the overvoltage is moderate and damage to the capillary walls gradual the only effect may be a slow thickening of the filament. In this way an oval capillary can be made round or one of circular cross-section made larger. Experiments indicate that the process is self limiting in that the capillary grows until it contains so much liquid that it is no longer being overvolted.

Undervoltage, the condition when too little energy is supplied to vaporize a significant fraction of the filament, is usually more damaging than overvoltage. The danger is not with extremely low voltage. In that case the filament is just heated slightly and no significant expansion takes place.

However, if only a little less energy than is required for some vaporization is used, the filament heats and expands 5% - 6% or more. (See section B and reference 6). The high pressures are unrelieved by vaporization and since the liquid cannot leave as fast as the vapor could, the high pressures remain for a much longer period. After a few such vaporizations the walls are likely to be effected. The specific failure mode of course depends upon the material. Table II shows what happened with each material.

Figure III-12 shows moderate damage created by undervoltage on a pyrolytic boron nitride wafer. Only the ends have failed and so the capillary can be reused by polishing off the damaged sections. Only in cases of extreme damage (Fig. III-13) as would occur from many undervolted shots will a capillary become useless.

An empirical determination of the energy necessary for vaporization can be made from data similar to that shown on Table III. The threshold energy for vapor injection can thus be seen to be $\sim 3 \times 10^{-3}$ joules per shot. Anything below this can be labeled undervoltage and may produce capillary damage.

TABLE II

Failure Modes for ELM Components

Wafer	Effects of Under Voltage	Effects of Over Voltage	Effects of Long Term
Molybdenum Laser drilled stop hole	Possible slight deformation due to excess pressure	Spark erosion surface mating capillary, even at small over-voltage	None Observable
Hot Pressed Boron Nitride Mechanically drilled capillary	Walls easily destroyed through loosening of grains	Grain loosening at moderate over-voltage	Gradual grain loosening ~ 500, 000 shots
Pyrolytic Boron Nitride Mechanically drilled capillary	Walls damaged at ends of capillary through layer separation	Layer separation at large over-voltage	Gradual layer separation ~ 5, 000, 000 shots
Lucalox Mechanically drilled capillary (unfired)	Cracking when under extreme stress	Occasional cracking at extreme over-voltage	None Observable

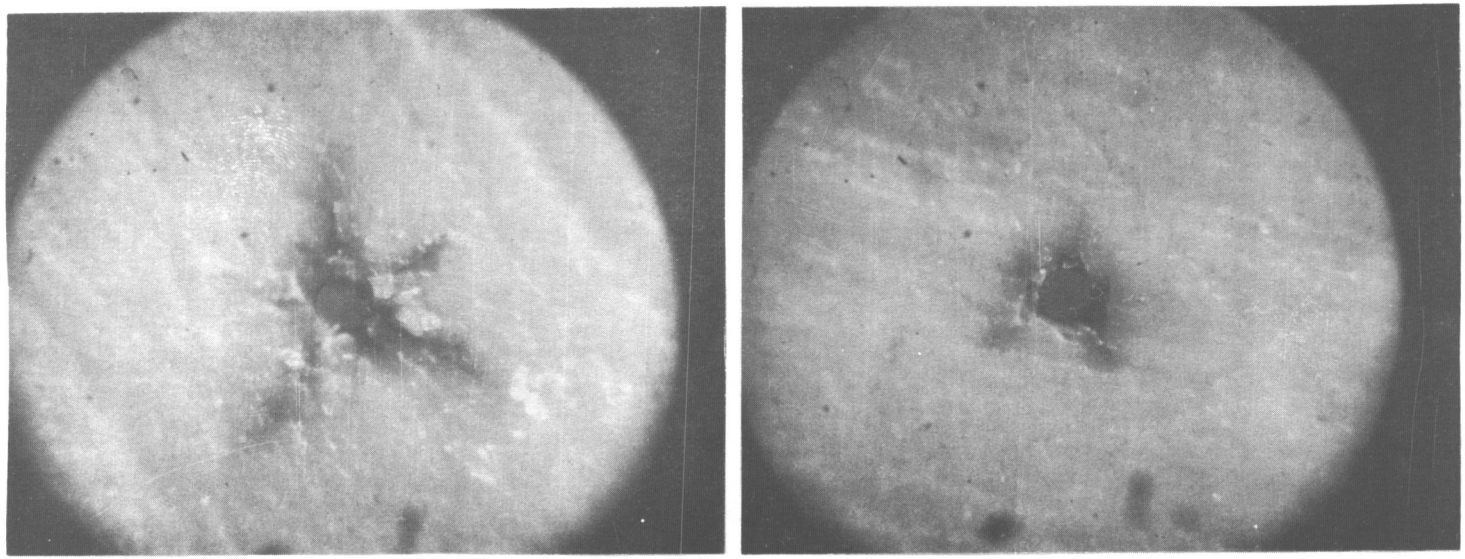

Side Facing Stop Hole

Side Facing Mercury Reservoir

Pyrolytic Boron Nitride - .0025" Diam.
.017" Thick

Figure III-12. Capillary Damage Caused by Short Term Undervoltage

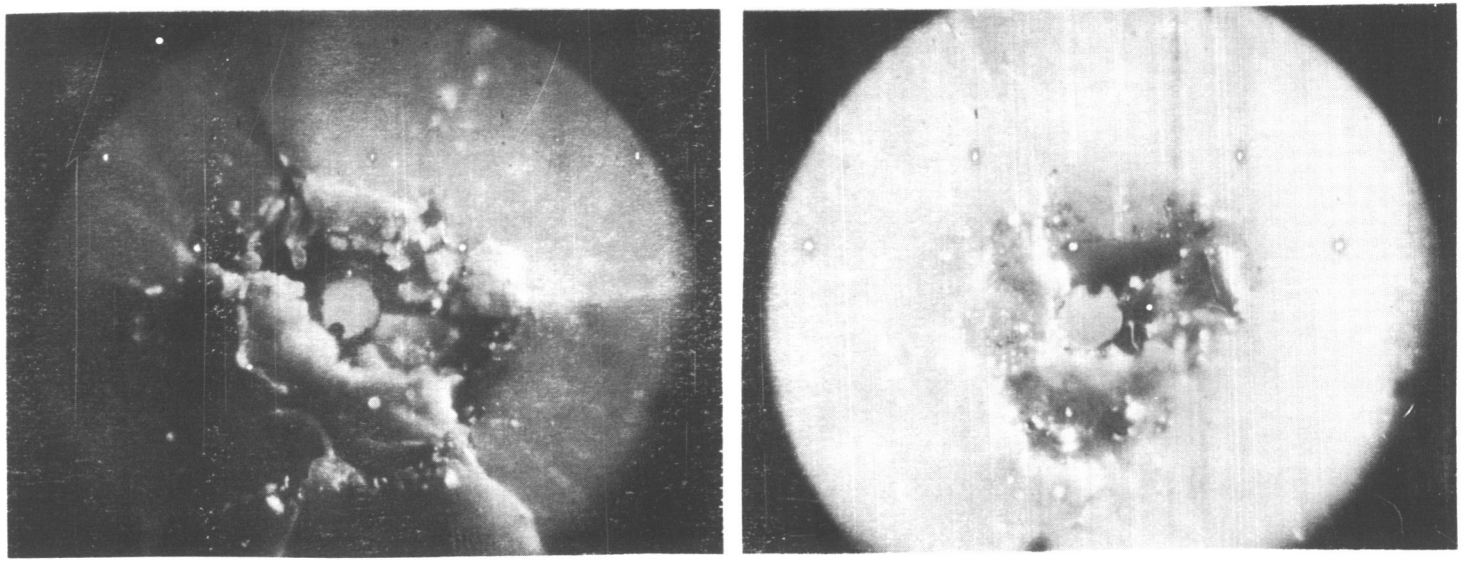

Side Facing Stop Hole

Side Facing Mercury Reservoir

Pyrolytic Boron Nitride - .003" Diam.
.017" Thick

Figure III-13. Capillary Damage Due to Long Term Undervoltage

TABLE III

Energy Inputs for Various Filament Dimensions

Filament Wafer Material	Filament Dia.	Filament Length	Voltage of Onset of Current Waveform Distortion	Minimum voltage without damage	Capacitance
Pyrolytic Boron Nitride	.0025"	.016	100 V	85	1 μf
*Boron Nitride	.0042	.016	159	145	1 μf
Boron Nitride	.003	.019	189	150	1/4 μf
Lucalox	.003	.016	125	107	1/2 μf

*-Low resistance filament using high loss switching circuit.

F. Diagnostic Tools

A wide variety of diagnostic methods have been used to obtain information regarding ELM operation. Table IV lists the most important techniques and their purpose.

The first six were simple techniques and consequently were used as a matter of course during some stage of every run. Knowledge of the capillary's condition before and during every run (4 and 5) was a primary consideration of many of the tests described in this report, as were measurements of the energy input and mass output (1, 2, and 3).

Techniques 6 and 7 were special test devices designed to verify special characteristics of the injection process. The make and break detector (6) allowed verification of when vaporization was actually taking place by a meansurement within the capillary itself. It also allowed a quantitative determination of the time required for capillary refilling. The vapor detector (7) gave a direct indication of the fact that vapor injection had occurred. It was capable of responding to high repetition rates (greater than 200 pulses per second) as well as surviving an indefinite number of shots. Both techniques are discussed in greater detail in reference 6.

The gas density probe is a familiar device[2] used for quantitative determination of gas density distributions. Its use was limited in this study to verifying the velocity of the vapor front under a variety of conditions.

G. Control of Mass Injection

It has been found that the quantity and phase of the injected mercury can be controlled by variation of the applied energy and the pressure backing the reservoir. When the back pressure is raised above a certain critical value some liquid escapes with the vapor. When the reservoir pressure is maintained below this value, variation of the input energy over a certain range can control the amount of vapor that is injected. The injection of only liquid in an amount independent of the firing rate is from hereon called leakage. The injection of a fixed amount of liquid per shot

TABLE IV

DIAGNOSTIC TOOLS

	Device or Technique	Quantity Measured
1.	Voltage probe on ELM Capacitor Reading on oscilloscope	Input Energy
2.	Current probe in series with ELM	Heating of ELM Load resistance
3.	Reservoir level measurement	Quantity of liquid expelled
4.	Bridge measurement of d. c. resistance of filament	Indirect measure of size and condition of capillary
5.	Microscope	Measure aperture dimensions and observe condition
6.	Make and break detector	Time at which capillary ceases and begins to conduct current (vaporization and refilling time interval)
7.	Vapor detector	Detects vapor leaving ELM for long periods at high repetition rate
8.	Gas density probe	Vapor distribution as a function of time.

shall be referred to as liquid injection. Either is clearly undesirable for firing of a plasma thruster since liquid is being injected rather than vapor.

The size of the stop hole and the applied reservoir pressure were originally thought to be unimportant as long as mercury was kept from leaking out when no firing was taking place. Succeeding tests showed that the gaseous conductance of the tube formed by the walls of the stop hole could limit the vapor flow.

Using equations for viscous flow, the product D^4/ℓ (where D is the hole diameter and ℓ its length) was evaluated for various stop holes and then compared to the injected mass from each of them. While the effect of other parameters (the applied voltage, the back pressure, the filament size) blurred quantitative results, it was clear that a stop hole at least as conductive as one .0011" in diameter and .003" long was required for the injection of more than 12 micrograms/shot.

However, in going to these large stop holes (i.e., larger than .00075) another problem was encountered. The pressure backing the reservoir had shown little effect with stop holes having a diameter of less than .00075", but with larger stop holes a marked increase in mass injected per shot was observed beyond some critical pressure. Fig. III-14 shows this dependence for a .00107" and a .00082" diameter stop hole. As the stop hole size was increased, the value of this critical pressure was reduced until, for stop holes .0015" in diameter only a small flat range (50 mm hg wide) of injected mass vs back pressure could be located. For stop holes smaller than .0008" diameter the critical pressure rose beyond the range of the commonly used back pressures and the anamolous increase in injected mass per shot (presumably liquid injection) was not observed.

The desired mode of operation can thus be expected with a laser drilled stop hole having a maximum diameter of about .0008" and backed by a pressure of 8" to 10" of mercury.

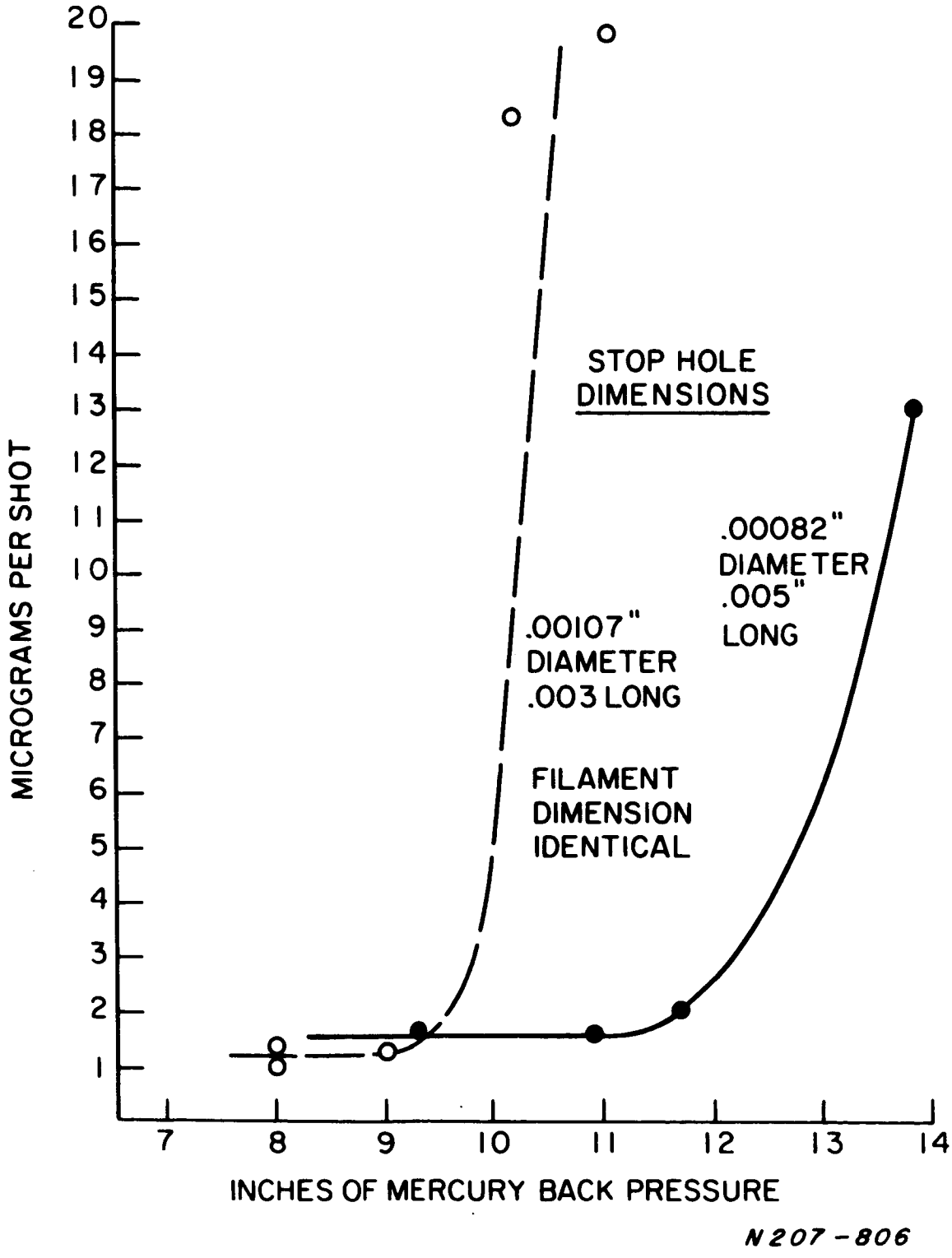

Figure III-14. Injected Mass Dependence Upon Back Pressure

Once these parameters have been fixed the amount of injected vapor can be controlled through variation in the applied voltage (i.e., deposited energy).

The ELM model, as originally conceived, predicted that the liquid metal filament would be heated uniformly and that no vapor would emerge until all of the filament had been vaporized. Subsequent tests with the vapor detector have indicated vapor flow at voltages considerably below that required to vaporize all the mercury within the filament.[6]

Direct measurement of reservoir level (measurements of the mass caught in a dry-ice cooled catcher have been found to be within a few percent (3%) of that lost from the reservoir) has established this phenomenon on a quantitative basis. For a small range of voltages short of that required to vaporize the entire filament the injected mass can be varied from less than one microgram per shot up to some large fraction of that contained within the filament. Fig. III-15 shows the variation in injected mass per shot as a function of applied voltage using a capillary designed for insertion into a large plasma gun. Similar behavior was observed in tests of capillaries of different sizes reported elsewhere.[6]

The procedure preliminary to operation at a specific vapor injection rate thus always involved determination and setting of the back up pressure suitable for the stop hole in use and the appropriate voltage for the amount of vapor desired. Operation with a higher pressure could cause liquid injection or leakage and too low a pressure might not provide adequate contact between the mercury filament and the conducting stop hole wafer (sparking could then result in pitting of the stop hole wafer and alteration of the place in which the energy is being deposited). Operation with too much or too little energy could also lead to damage and so this value had to be preset also.

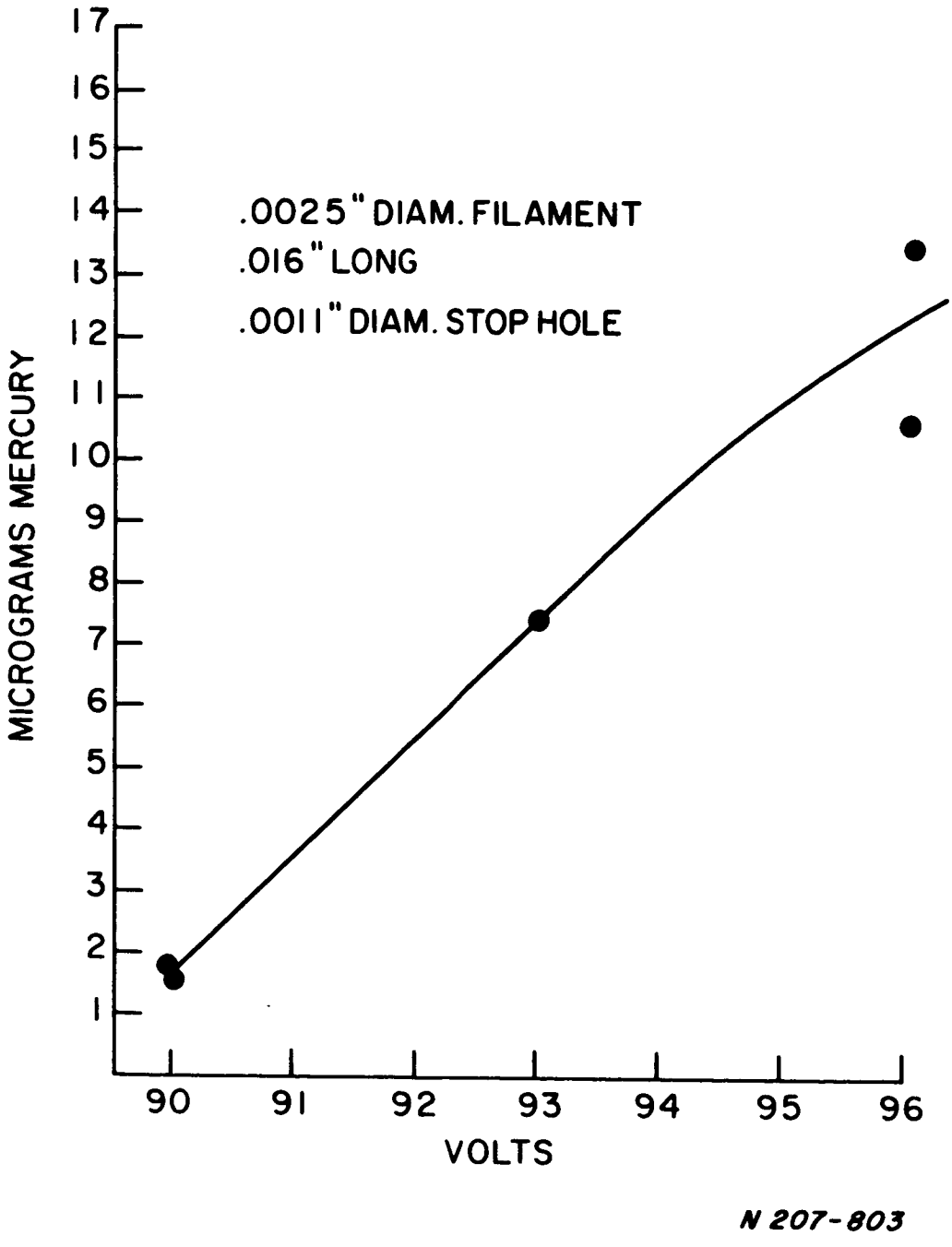

Figure III-15. Injected Mass Dependence vs Applied Voltage

H. Elm Testing

The testing procedure was ordinarily conducted in the following manner.

1. The ELM test assembly was bolted into place and the region behind the reservoir was evacuated along with the vacuum chamber.
2. After the background pressure within the vacuum system dropped to the range of 10^{-6} torr the reservoir was closed off and pressurized up to 8" - 10" of mercury with argon.
3. The resistance of the mercury filament and the mercury level within the reservoir were measured.
4. Since the indicated resistance was always higher than the dimensions of the filament would justify, a resistive layer between the mercury and the stop hole wafer was postulated. Operation at very low voltages tended to destroy a large part of this extraneous resistance. Re-exposure to the atmosphere or long term exposure to the vacuum without the mercury in contact tended to recreate it.
5. A series of conditioning runs were then made at low voltages. If these runs were not sufficiently long or if the assembly had not been adequately outgassed first, liquid injection occurred.
6. Once the resistance of the filament was brought close to the expected level by the above technique the desired voltage for the test was computed. In general this voltage was a little less than was required for vaporization of the entire filament. Compensation was made for losses due to extraneous resistances in the discharge circuit (see Appendix B).
7. A run was then completed by firing the discharge circuit through the ELM filament at the rated voltage for the desired number of shots. Measurement of the reservoir level gave the amount of mass that was injected. The mass per shot could then be easily computed.

The goal of these tests was to establish how much vapor could be injected and for how long at various repetition rates without damaging the wafers.

The basic design of the thruster (see section J) called for the use of six ELM assemblies, each injector to have the capability of operating at 140 pps while injecting anywhere from 2 to 18 x 10^{-6} grams per shot. If all the mass within a filament was to be injected, a capillary .0025" in diameter and .018" long could do this while varying the voltage on a 1 μf capacitor from 90 volts to approximately 105 volts. Table V shows the mass injected and the corresponding voltage for capillaries .0025" in diameter.

The maximum injected mass is considerably below the theoretical maximum because voltages above 100 volts tended to produce characteristics symtomatic of overvoltage. Consequently only operation at lower mass flow was investigated in detail with capillaries of this size.

A variety of filaments of other sizes have been investigated. The results of these tests have been reported elsewhere.[6] The results of tests with a .003" diameter capillary will be reported here since that size could be used to inject the quantities of mercury necessary for low I_{sp} operation of the plasma gun. Table VI shows the injected mass from two filaments with this diameter. From the data shown in Tables V and VI, it is clear that the mass per shot required for engine operation from 3000 to 10,000 seconds can be achieved. Another portion of the ELM test program involved the determination of the range of repetition rates and life times which could be obtained with a single injector unit. Repetition rates of from 10 to 50 pps were initially used during tests. However, repetition rates as high as 200 pps were later used for short times and repetition rates of 167 pps became standard.

While the 10 pps repetition rate was in use a long run of 152 hours (5.5 x 10^{6} shots) was completed using a pyrolytic boron nitride capillary and injecting 0.75 μgm of mercury per shot. No degradation of operation was observed during this run but examination of the capillary disclosed that slight erosion had

TABLE V

Mass Injected by Filaments .0025" in Diameter

Filament Length	Mass/Shot	Voltage
.015"	.75 μ grams	80 volts
.015	2.4	93
.015	7.4	95
.015	12.4	97
.016	1.6	90
.016	7.5	93
.016	11.	96
.016	13.5	96

TABLE VI

Mass Injected by Filaments .003" in Diameter

Filament Length	Mass/Shot	Voltage	Capacitance
.016	1 μ gram	117	1/2 μf
.019	1.3	176	1/4

---

occurred. At the standard repetition rates a run of 2.7×10^7 shots was completed using a lucalox capillary and injecting 1.0 μ gm of mercury per shot. This latter run was of a shorter duration (24 hours) but the greater number of shots and the perfect condition of the wafers at its termination show that it is of much greater significance. Table VII lists the characteristics of these two runs along with several others of similar duration.

It is important to note that the limiting factor in all successful runs (except the last, noted above, in which time was the limiting factor) was the capillary walls containing the mercury filament. The stop hole wafers lasted indefinitely if not subjected to extensive overvoltage runs and were several times used for more than 2×10^7 shots.

The two materials found to be most satisfactory for the capillary wafers were by no means so invulnerable. Hot pressed boron nitride invariably failed at less than a million shots while the pyrolytic form of this material failed in about 10^7 shots. The detailed mode of this failure is reported elsewhere.[6] Lucalox, which when produced properly and operated under the specified conditions seemed to last indefinitely, could crack under the stress of only a few shots if the injected energy for a given capillary size was wrong.

Since operation with carefully controlled energy injection has shown very long lifetime to be possible, Lucalox is recommended for future application. When used with a molybdenum stop hole wafer, long life SCR's and diodes and a voltage overrated capacitor[8] useful lifetimes of at least tens of millions of shots, and possibly orders of magnitude more, can be obtained.

The major difficulty encountered during long term tests has been the inability to raise the injected mass much above one microgram per shot. When the energy required for more mass was supplied, distortion of the current waveform took place indicating sparking at the stop hole. The character of the distortion was essentially that of overvoltage. However, previous short term tests showed no such limitation. Reference 6 gives the reasons for this.

Several of these long term high mass injection runs performed early in the program are summarized in Table VII. Since the capillary material was pyrolytic boron nitride rather than Lucalox the lifetimes were of course limited to several million shots. As much as 18 micrograms per shot has been reported over a similar lifetime with a .0042" diameter capillary.[6]

Thus, while the actual combination of high mass flow (i.e. > 5 micrograms/shot) and long lifetime (> 10^7 shots) has not been run such performance should be possible when Lucalox capillaries are used with an appropriate firing circuit.[6] This is supported by the similarity of lifetime already obtained between high and low mass flow runs using pyrolytic boron nitride capillaries. Table VII lists the best lifetimes achieved at this time at the various mass flows.

TABLE VII

Characteristics of Several ELM Runs

Capillary Material	Filament Diameter	Filament Length	Stop Hole Dia.	Backup Pressure	Capacitance	Voltage	Rep Rate	Mass/ Shot	No. of Shots
Lucalox	.003"	.016"	.007"	6" - 8" hg	1/2μf	117V	167 pps	1.0 μ grams	27.2×10^6
	Assembly perfect at end of run. After a total of 3.89×10^6 shots very slight wear was observed.								
Pyrolytic Boron Nitride	.003"	.0189	.00075"	6" - 9"	1/4 μf	169V	167	1.3 to 3.6*	13×10^6
	Capillary destruction terminated run								
Pyrolytic Boron Nitride	.0025"	.015"	.00067"	10"	1 μf	80V	10 pps	.75	5.5×10^6
Pyrolytic Boron Nitride	.0025"	.015"	.00109"	10"	1 μf	95V	50 pps	7.4	2.6×10^6
Pyrolytic Boron Nitride	.0025"	.015"	.0015"	10"	1 μf	97V	50 pps	12.4	1.1×10^6
	Assembly ran at 2.4 to 12.4 micrograms per shot for a total of 5.5×10^6 shots before significant erosion was observed.								

*-Gradual shortening of capillary through erosion led to more efficient use of energy[6].

I. Characteristics of the ELM Exhaust

The most important characteristics of the injected mercury flow are composition (i. e., vapor and liquid if any), spatial distribution, time dependence, and repeatibility.

The composition of the exhaust was studied in several ways. The gas density probe and the vapor detector were placed in the exhaust stream and always detected quantities of vapor when vapor was believed to be injected. Liquid droplets would not register on these devices. In addition, visual observation was capable of detecting one tenth of a microgram per shot if it was being expelled in the form of spherical droplets, and none was ever seen when vapor injection was supposed to be taking place. However, when leakage was suspected and actual measurement showed several micrograms of mass injection per shot, the droplets could be seen by the unaided eye. Finally, the pattern of deposition on the cold catcher was also most easily explicable as vapor deposition.

While none of the above observations is a direct measure of the fraction of liquid droplets present they are strong indications that the vapor fraction is very high.

The vapor detector and the gas density probe also yield information regarding the time dependence and repeatibility of the vapor injection. Indications of a vapor pulse a few tenths of a millisecond wide were obtained several cm downstream. Similarly, the time for the vapor pulse to arrive at this position was also a few tenths of a millisecond. One would expect the spread in temporal pulse width to be comparable to the propagation time in a thermally accelerated vapor jet.

At the same position downstream the vapor detector produced a uniform response to pulses produced over a run of several hours.

Within the capillary itself the make and break detector indicated an absolute maximum pulse width of 50 microseconds, with a likely width for the bulk of the injection being considerably smaller. Once more, this

corresponds to expectations of the model.[6]

The spatial distribution of the exhaust has been qualitatively analyzed on the basis of the deposited pattern on a cold catcher. The indications obtained in this way were of a high density core with a half angle of less than 10^{o} surrounded by a decreasing density plume out to angles of 30^{o} and beyond. Very little material was present at these extreme angles but long runs did yield a visible deposit.

Some ability to vary the deposited pattern was found through variation of the stop hole shape and position. No systematic study of this was made however, and symmetrical exhaust plumes were generally encountered.

Overall, the picture of a sharp narrow pulse in space and time surrounded by a more diffuse cloud emerges. Combined with the results of using a single injector for gun firing, to be discussed later, the expectation of a satisfactory propellant distribution in a full scale gun seems to be borne out.

J. Engine Design

A large full scale version of the A-7D xenon propellant[1] accelerator was constructed for use with the ELM feed. Molybdenum was chosen as the electrode material because of its high electrical conductivity, low susceptibility to sputtering and high temperature capability. The center electrode was machined from solid material (see Fig. III-16 for a photograph with an ELM assembly partially screwed into place) while the outer electrode was machined from copper and plasma sprayed with molybdenum.

The ELM assemblies were inserted into the inner electrode wall as shown in the exploded view of Fig. III-17. Six separate assemblies injecting up to eighteen micrograms each were to be used. There was some question whether this is a sufficient number of units to maintain a uniform vapor distribution, but since six nozzle holes were able to produce an adequate uniformity with early models of the gas fed accelerator the likelihood of success here was believed to be high.

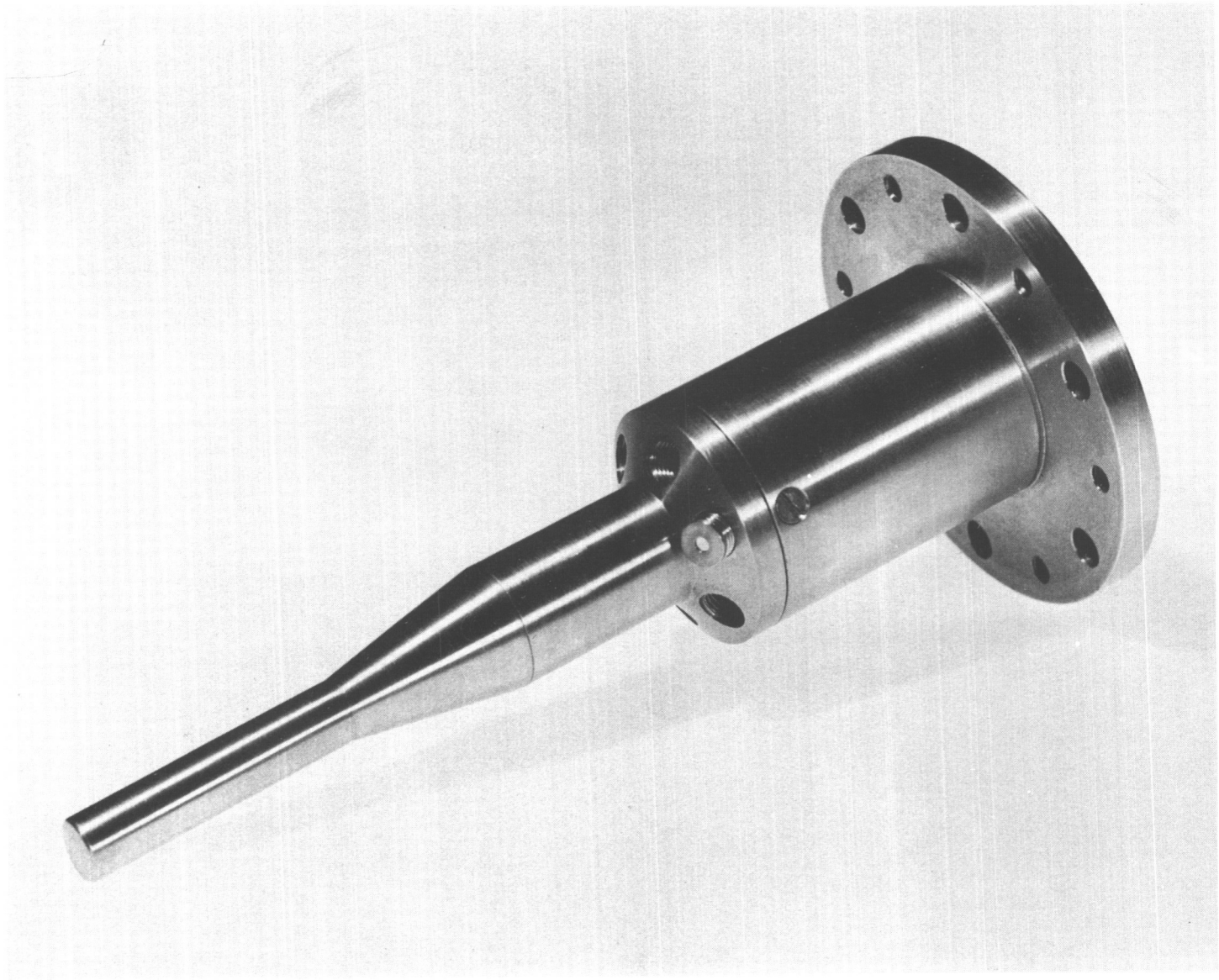

Figure III-16. Center Electrode of Liquid Metal Plasma Accelerator

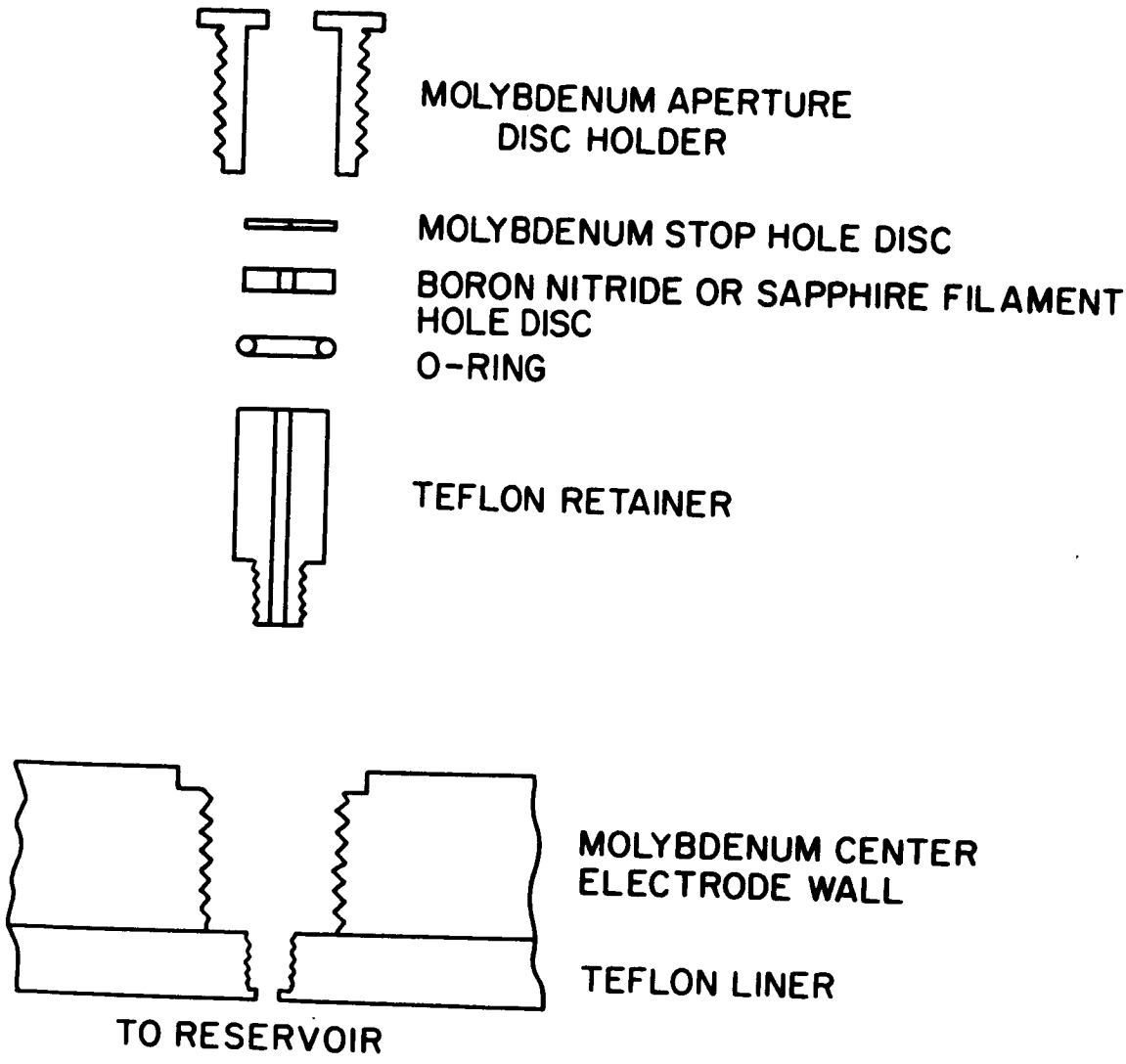

Figure III-17. Exploded View of Elm Aperture Assembly as Inserted into Accelerator Wall

Parallel with this effort, preliminary experiments at firing a smaller thruster with a single ELM injector were begun.[6] The general design of the single ELM assembly used in that experiment was identical to that shown here.

These early attempts at firing uncovered the fact that the ELM firing circuit has to be electrically isolated from the high voltage gun circuit. Otherwise filament resistance can flow through the filament and possibly destroy it. This happened during several different attempts to fire the small thruster.[6]

In order to isolate the ELM feed circuit, it was separated from the negative electrode by an insulator. Thus the current forced through the filament by the main discharge could be completely ignored.

Tests with this arrangement were satisfactory[6] and so design modifications were made on the large accelerator.

A drawing of the center electrode design is shown in Fig. III-18. The modified wafer assembly and holder is shown in Fig. III-19. A gravity feed system to the reservoir was included with an inductive transducer to measure the liquid level. A bladder system, such as is used in certain ion engine feeds, would be superior to the gravity feed, particularly since it could be used under zero g conditions, but its added complexity was avoided at this time.

Figs. III-20, 21, and 22, show the engine after it had been modified.

Table VIII lists the number of micrograms of propellant required per shot for a fixed efficiency and specific impulse with various amounts of energy initially stored on the capacitor. The repetition rate for an accelerator operating level of 10 KW is also listed.

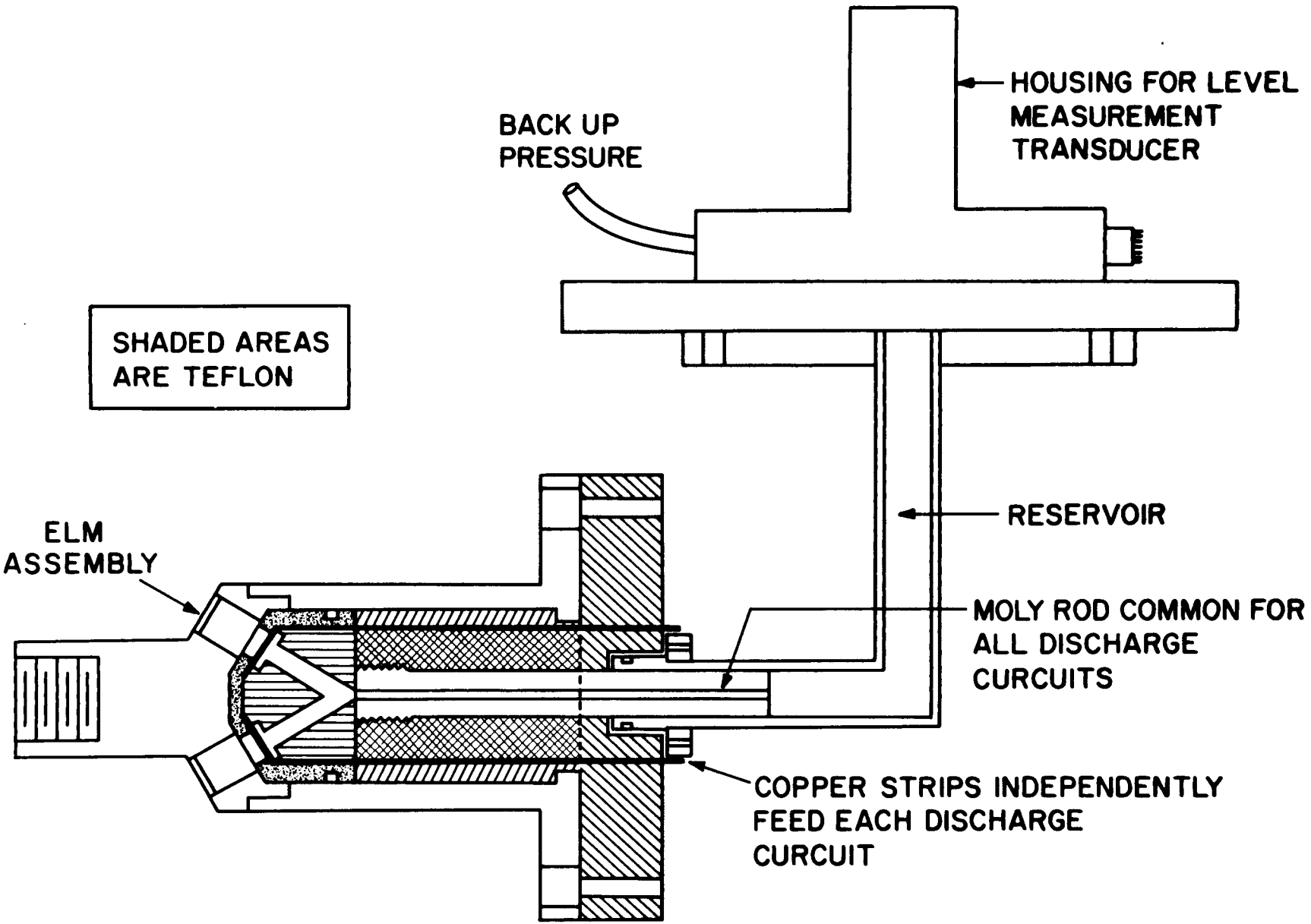

Figure III-18. Cross-Section of ELM Feed into Center Electrode

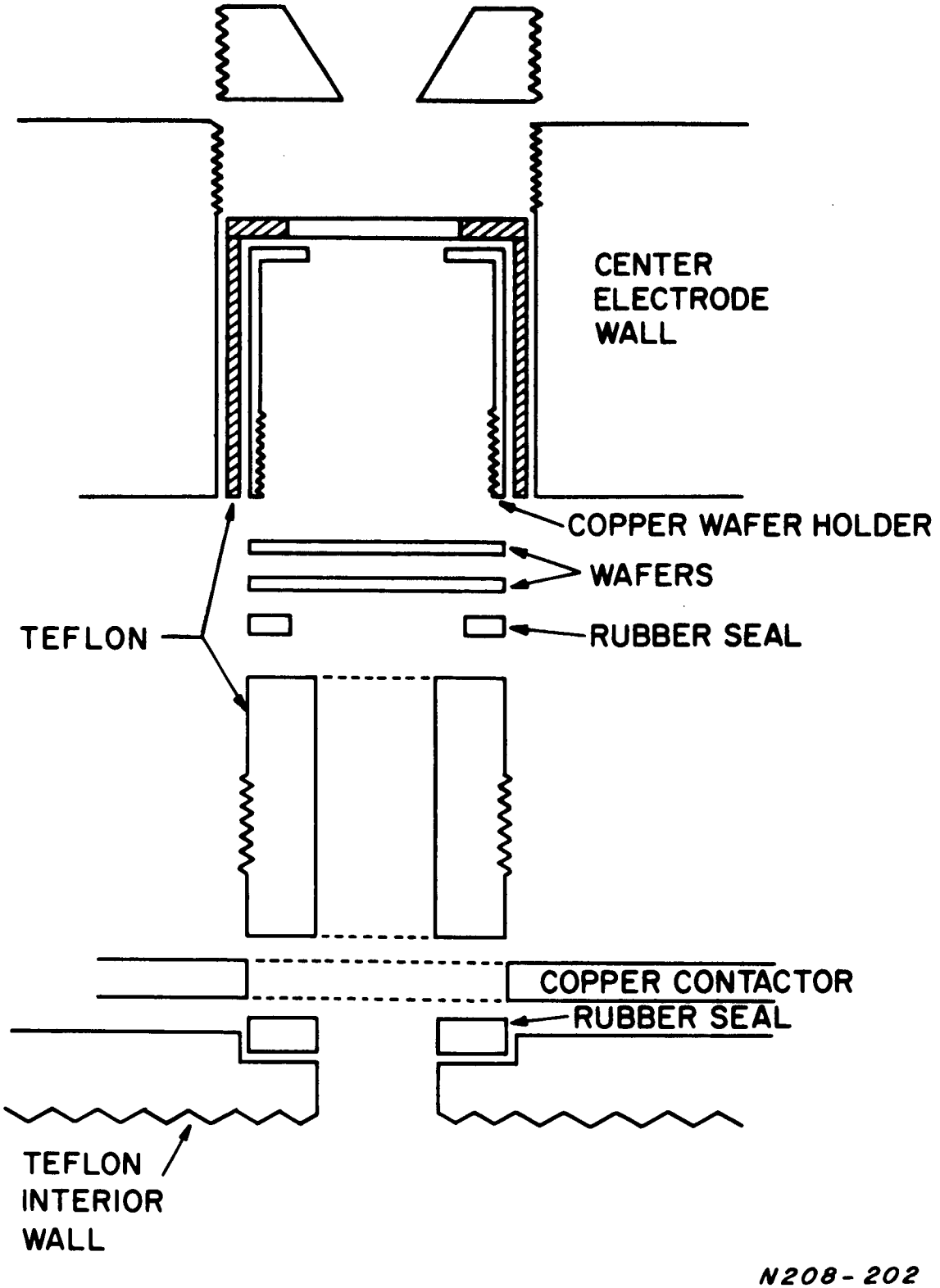

Figure III-19. Blow-up of Wafer Assembly in Center Electrode Wall

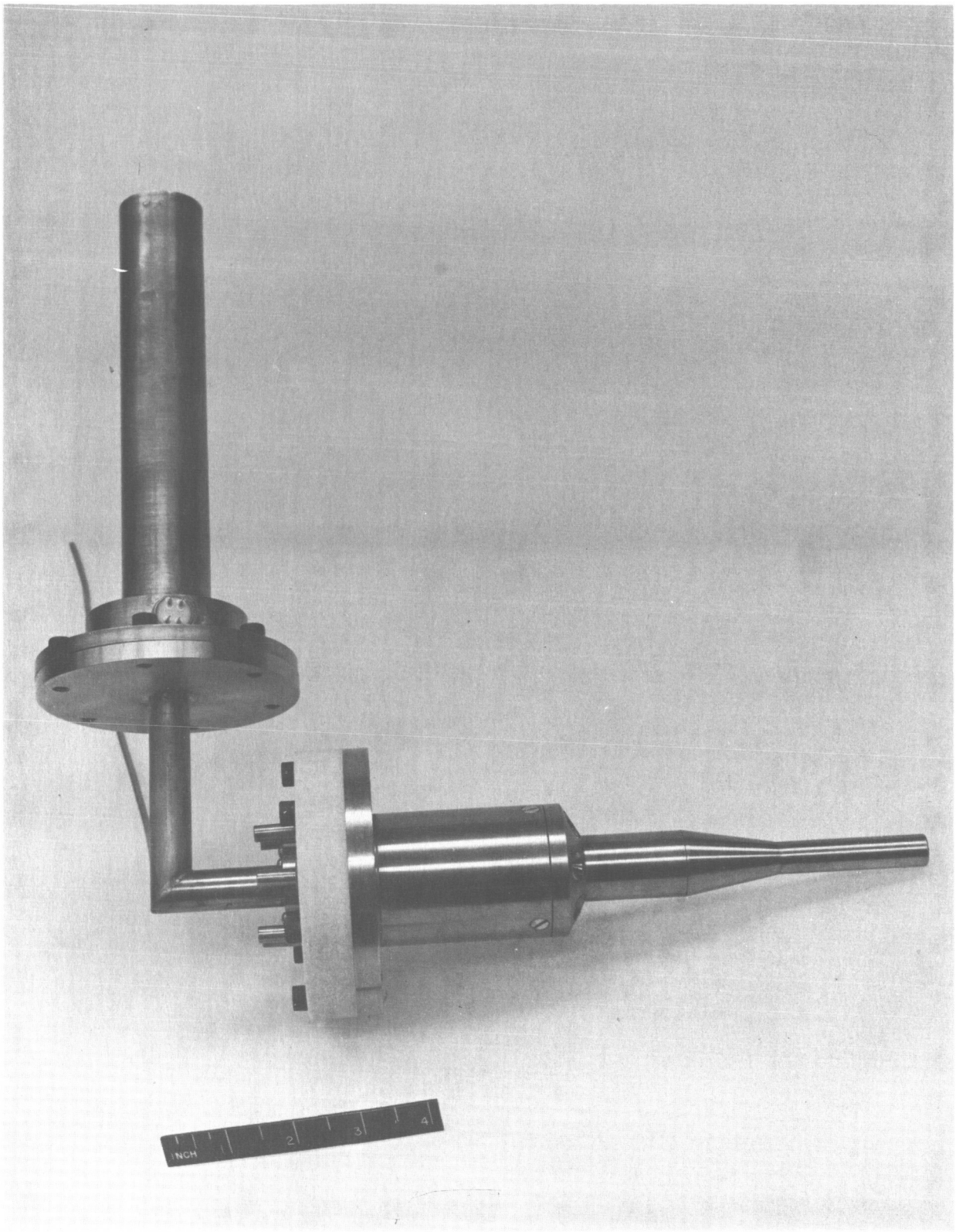

Figure III-20. ELM Fed Thruster with Outer Electrode Removed

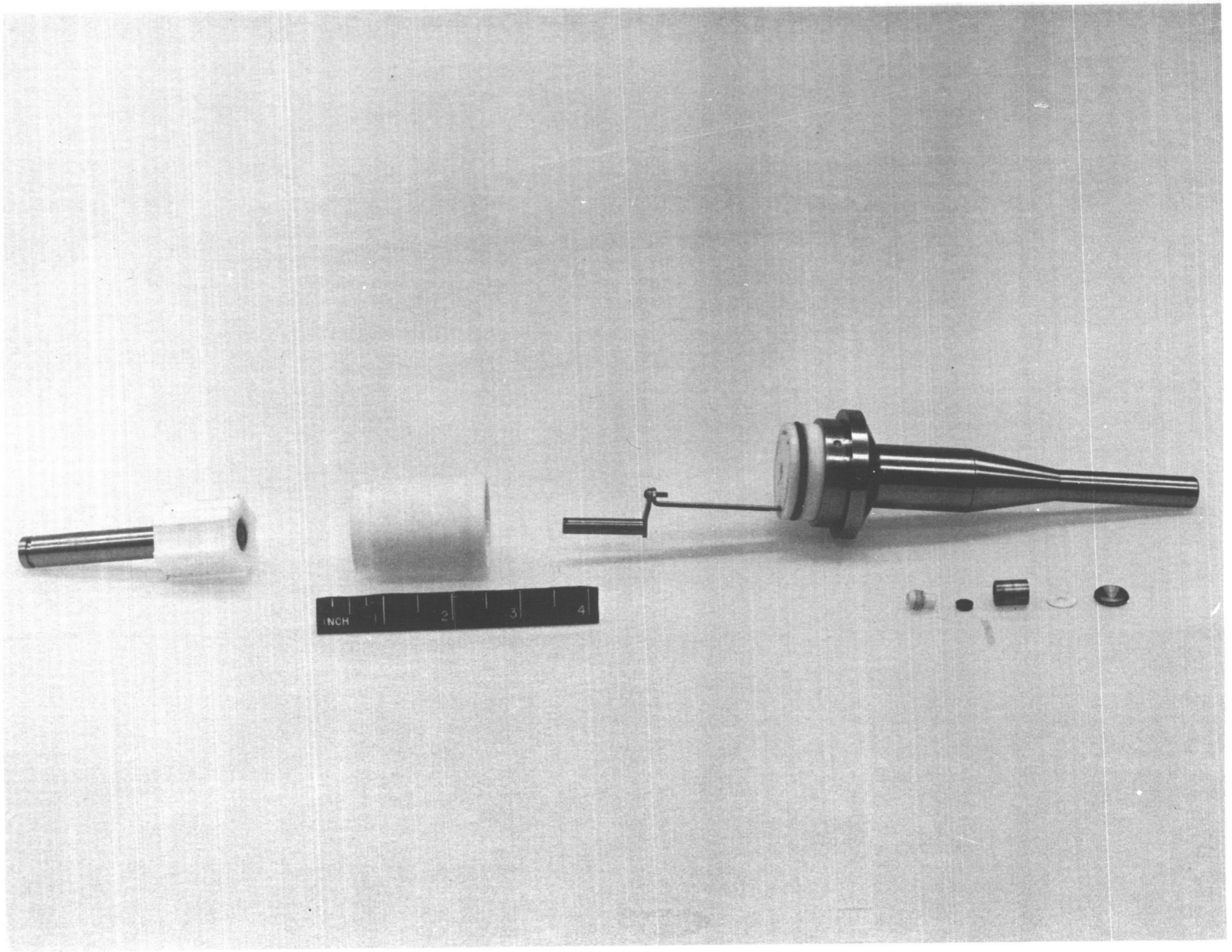

Figure III-21. Exploded View of Central Electrode Assembly, Tip and Interior

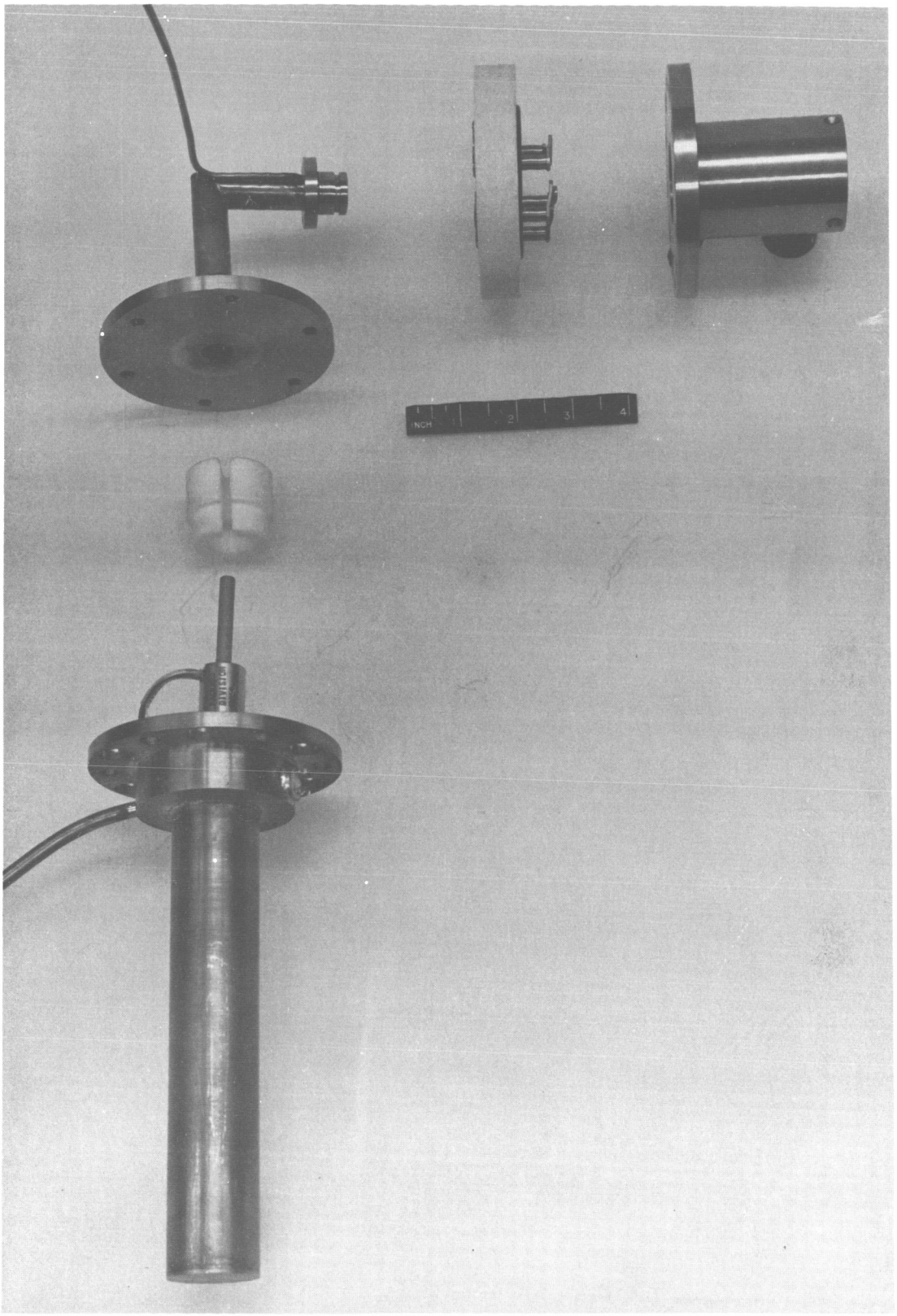

Figure III-22. Exploded View Central Electrode End Housing and Reservoir

TABLE VIII

ELM Requirements Assuming η_o = 70%, I_{sp} = 5000 sec.

Joules / Shot	Total Micrograms / Shot	Micrograms /Shot Unit	Shots/Sec. at 10 KW
50	28	4.67	200
100	56	9.34	100
150	84	14.01	66.7

K. Summary of ELM Program

ELM injectors have been operated at repetition rates up to 200 pps and survived without degeneration for almost 40 million shots at mass flows of 1.8 μgrms/shot. The key to this success was the use of Lucalox capillary wafers and molybdenum stop hole wafers.

During short term runs ($\sim$1 million shots) propellant masses of as much as 18 micrograms per shot have been injected using a pyrolytic boron nitride capillary. Indications that pyrolytic boron nitride capillaries would be limited in lifetime due to eventual erosion led to the use of Lucalox capillaries and the exhibited long term operation mentioned above. However, time limitations have prevented extended operation at mass inputs.

A large molybdenum gun has been designed and constructed based upon tests with a smaller thruster. Actual firing has not taken place because six matched injectors are not yet available.

REFERENCES FOR SECTION III

1. B. Gorowitz, P. Gloersen, T. Karras, "Steady State Operation of a Two Stage Pulsed Coaxial Engine". AIAA Paper 66-240.

2. T. Karras, B. Gorowitz, P. Gloersen, "Neutral Mass Density Measurements in a Repetitively Pulsed Coaxial Plasma Accelerator". AIAA Journal 4, 1366-1370 (1966).

3. B. Gorowitz, P. Gloersen, K. Moses, Rev. Sci. Inst. 31, 146, 1960.

4. R. C. Speiser, et al, "Cesium Electron Bombardment Ion Engine", AIAA Paper 65-373. G. L. Cann, et al, "Lithium Plasma Thruster Performance," AIAA Paper 65-295.

5. T. Karras, B. Gorowitz and P. Gloersen, "Propellant Injection into a Coaxial Plasma Accelerator". AIAA Paper No. 66-241, (March 1966).

6. T. W. Karras, et al, "ELM: Valveless Propellant Injection" Final Report, Contract AF33(615)-5016.

7. C. M. Scheuermann, et al, Astronautics and Aerospace Engineering, December 1963.

8. B. Gorowitz, and T. W. Karras, "Life Tests on Capacitors for Pulsed Plasma Engine Application", G. E. TIS R65SD26.

IV. CONCLUSIONS

The fact that it has not been possible to reproduce the high levels of performance observed early in the program might be attributable to any or all of the following possibilities.

1. The performance measurement techniques used (i.e. propellant input , power input, and thrust) during the periods of either high or low performance were not valid.
2. There was a subtle change from the original engine operating characteristics which has not yet been identified and eliminated.
3. There was a change in environmental conditions which removed unaccounted for inputs which had previously served to enhance engine performance.

Of these possibilities, it is our opinion that the first can be ruled out on the basis of the results of rigorous review of the techniques and independent measurements on the part of different experimenters. It is now believed that both of the latter possibilities applied during the course of the program. It should be remembered that the changes in overall efficiency and specific impulse described above were generally accompanied by changes in such factors as current and voltage waveform, magnetic field distributions and neutral and ionized species density distributions. In some cases which have been mentioned the non-reproducibility of signal was such as to clearly indicate the erratic behavior of the accelerator. It should also be remembered that the deterioration in observed performance took place in two stages. One of these changes in performance was associated with a change in valve operation and propellant distribution. The influence of propellant distribution, as determined by valve action, nozzle design and discharge triggering time has been considered in some detail in this and in earlier reports. It is apparent that the achievement of peak performance by the pulsed plasma engine can be closely associated with optimization of the propellant input, both from the viewpoint of providing maximum propellant availability on a given mass injection basis, and from the viewpoint

of establishing a propellant distribution which will be appropriately matched to the discharge and magnetic field distributions in the accelerator.

The other change in performance was associated with changing environmental conditions (i.e., establishment of a "clean" vacuum) and thus may be related to the third possibility mentioned. The quantitative contribution of a contaminant such as diffusion pump oil vapor or droplets has not been precisely determined, nor has been the exact mechanism of any possible contribution. Tests simulating the original conditions of contamination, even if these conditions were sufficiently well known, would involve considerable experimental difficulty, but they should be performed if the possible causes of lower efficiency are to be pursued further.

A more fundamental part of a program to improve the present relatively low level of pulsed plasma engine performance reported by these and other investigators is a greater knowledge of the details of discharge breakdown, ionization, and energy transfer phenomena. These fundamentals were to a great extent neglected while empirically determined parametric changes brought positive and promising increases in accelerator efficiency. It was believed that, within the limitations of time and funds, a more detailed program of investigation of accelerator characteristics should be performed on the most efficient accelerator available rather than on each accelerator which was studied. Since recent exhaustive parametric changes have exerted little influence on accelerator performance, it is recommended that more detailed accelerator diagnostics be a prime requirement of any continuing programs devoted to the eventual development of a feasible pulsed plasma thruster.

The portion of the program which was devoted to the development of a metal propellant feed for the pulsed plasma accelerator has progressed to the point where a prototype of six similar units which would constitute such a feed has been successfully tested. The materials and fabrication problems associated with a single injector have largely been solved. Some of the potential interface problems associated with the operation of the ELM in a plasma

accelerator have been identified and circumvented. Other requirements pertinent to this application include the following: establishment of an appropriate propellant distribution in the accelerator either by changes in the propellant pulse shape or adjustment of the number and or placement of injector units, the injection of an appropriate quantity of propellant for the thrust and specific impulse range anticipated, the determination of the need for auxiliary triggering for maximum propellant utilization, and the determination of the limits of injector reliability and life in the operating environment of a plasma accelerator. For this reason, the problems which may be faced in its operation in an accelerator should be uncovered at the earliest possible time by actual operation of ELM systems in a full scale plasma accelerator. In addition, the fundamental characteristics of the energy transfer, heating, vaporization and injection process should be studied in considerably greater detail than has been described above.

APPENDIX A.

Aperture Design and Propellant Evaluation

In order to evaluate a specific design for the ELM filament, a computation was made of the filament size that would be necessary. This involved a simultaneous solution of the two equations

$$R = \rho_r \frac{\ell}{A}$$

and $$M = \rho \ell A$$

where

ρ_r is the liquid metal resistivity

ρ is the liquid metal density

ℓ is the filament length

A is the filament area (πr^2)

R is the filament resistance

and M is the mass of liquid metal within the filament

The first computation was performed for the metals cesium and mercury under the constraints found to be useful for coaxial gun firing ($R \gtrsim 0.1$ ohms and $M \gtrsim 1.5 \times 10^{-5}$ grams. The resistance must be this high so that the filament absorbs most of the energy. The injected mass is dictated by the number of ELM assemblies that are convenient for the gun design. These constraints are discussed more fully in section III). The results of this computation are shown on Table A-I.

TABLE A-I

	Density g/cc	Resistivity micro ohm -cm	Filament Area cm^2	Filament diameter mills	Filament length mills	ℓ/d
Cesium	1.87	30.6	1.72	5.84	185	31.6
Mercury	13.6	95.8	3.25	2.52	13.5	5.35

Filament length and diameter for two liquid metals and $M = 1.5 \times 10^{-5}$ gms $R = .1$ Ω

Clearly, mercury is superior in the filament length to diameter ratio required. The capillary required for cesium is far too long for the drilling techniques currently available. Holes having an ℓ/d ratio of about 7 to 10 are the best that can be managed for holes as small as are needed here.

In order to push the design to the limits of fabrication the equations were solved again using $\ell/d = z$, ρ, ρ_r, and R as constants and M and d as the independent variables.

$$M = \frac{\rho z^4 \rho_r^3}{R^3 \pi^2}$$

$$d = \frac{2 z \rho_r}{R \pi}$$

The value of z used was 7, corresponding to commonly available manufacturing and R = .1 as indicated earlier. Table A-II shows the results.

Once more, only mercury shows itself to be adequate for operation with a plasma accelerator. For operation with a thruster using only fifteen micrograms of propellant per shot, 42 filaments containing cesium would be required. For a thruster needing more propellant per shot the situation would be even worse.

The only way out of this difficulty is to loosen the resistance requirement and thus sacrifice energy efficiency and complication in the electronics. Table A-II shows the results if the required resistance is reduced to 0.02 ohms. Only now does cesium begin to sound like a reasonable propellant for plasma thruster.

However, before operating in such a low resistance mode, where the resistance of the rest of the circuit is comparable to the filament resistance, further study will be necessary. Preliminary tests with mercury indicate that vapor cannot be reliably injected when the filament resistance is below 0.040 ohms.

TABLE A-II

	R = .1		R = .02	
	Mass within filament micrograms	Filament diameter mils	Mass within filament micrograms	Filament diameter mils
Cesium	.356	1.24	44.5	6.25
Mercury	46.3	3.36	5760.0	16.8

Filament diameter and mass of liquid metal contained. $z = \frac{\ell}{d} = 7$

Not only is the filament length over diameter ratio too large for manufacture by present techniques, but the surface tension of cesium is so low that very small stop holes would have to be used. Since the gaseous conductance goes as the fourth power of the tube diameter there is reason to believe that not enough gas could get through. Table A-III shows the surface tension and the stop hole sizes for the two liquids.

TABLE A-III

Metal	Surface Tension dynes/cm	Stop Hole Diam. mils	Scaled Conductance
Mercury	465	1.00	1.
Cesium	40	.085	$.548 \times 10^{-4}$

Clearly, cesium does not have a surface tension high enough to be compatible with the ELM concept. Some injection mechanism that does not require even the moderate backing pressures used here must be developed for its use.

Mercury seems to be ideally suited for this application because of its high density, resistivity, and surface tension. A capillary having a diameter .0025" to .003" with a length to diameter ratio of 7 can meet all the requirements discussed above.

APPENDIX B

Switching Circuits

The switching circuit originally used is shown on Fig. 5. It was composed of a 1 μf Hi-jul capacitor (Dearborn Electronic Lab) in series with a current transformer (for use in measuring the current) and a switching element. The switching function was performed by a silicon controlled rectifier and a silicon diode in anti-parallel (so that the discharge could ring). The silicon controlled rectifier was oriented so that the capacitor could be charged (up to about 100 volts) until the trigger pulse was applied.

The SCR (GE 2N685) was chosen so that it would have a minimal voltage drop ($\sim$ 1 volt at 100 amps) at the currents being drawn. The diode (1N1204A) was chosen on the same basis ($\sim$ .5 volts drop). It was expected that low loss switching could be accomplished in this way for even the billions of pulses needed in an actual mission.

Triggering of the SCR was initially provided by commercially available units. However, the requirement of six simultaneous ELM firings for the gun prompted the building of a self contained unit capable of simultaneous triggering of six SCR's.

A capability for single shot operation and repetitive operation between 2.5 pps and 250 pps was provided. In addition a separate output for oscilloscope triggering was supplied. The whole unit was housed in a box 8"x4"x5" and since it was powered by batteries could be isolated from the power lines.

Figure B-1 shows a trace of the trigger pulse as it fired an SCR.

The efficiency of the switching circuit was completely determined by the resistive losses within its components. If these losses were fixed they could be accounted for and the energy actually heating the ELM filament determined.

The two major external losses in the circuit were the energy storage capacitor and the SCR, while the leads contributed a much lesser amount.

1 V/cm

5 μ sec/cm

200 ma/cm

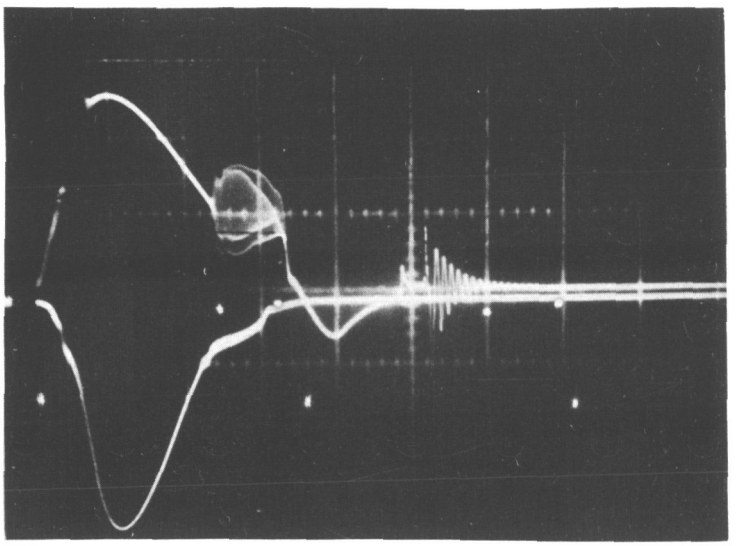

Fig. B-1. Trigger voltage (upper trace) and current (lower trace) as function of time as main discharge is switched.

The capacitor had a resistive impedance of approximately 0.080 ohms at the ringing frequency of the circuit. However, variations from 50 to 125 ohms were observed. The resistance of the SCR was very much a function of the current, but at peak currents of 100 amperes or more, it was of the order of 0.015 to 0.020 ohms. The resistance of the leads was about 0.005 ohms, and so the total for external components of the firing circuit was about 0.110 to 0.115 ohms. The resistance of a typical mercury filament (0.0025" diameter x 0.016" long) was approximately 0.140 ohms at ambient room temperatures and so initially only half of the energy was available to heat up the filament. However, as the temperature of the mercury filament increased as the heating pulse was applied, the resistance increased and so the division of energy dissipated in the external circuit components and the mercury becomes more favorable for vaporization. Analysing the current waveforms, an average resistance of about 0.400 ohms was computed, which agreed very well with the calculated value obtained by assuming a temperature increase to the critical temperature, 1463°C, and a constant coefficient of resistivity.[6] The parasitic resistive losses overall, accounted for a little more than 25% of the input energy.

Unfortunately, variations in the effective resistance of the circuit components could cause a significant change in the amount of energy being deposited in the ELM filament. This could lead to damage of the apertures (see section E).

Two solutions were conceived: to reduce the loss resistance to filament resistance ratio so that almost all the energy (>95%) ended up in the filament despite variations in the loss resistance, or to stabilize the loss resistance. Extensive testing of the last alternative was abandoned after tests showed considerable variation of circuit component characteristics over the ranges of parameters covered.

The means chosen to reduce the resistance ratio is shown on Fig. 6. The transformer coupling makes the reflected ELM filament impedance

17 times higher, reducing resistive losses to 1%. Transformer losses were also found to be a few percent and so the overall switching circuit efficiency was over 95%.

Another advantage of transformer coupling is the dc voltage isolation it affords. Any capacitive pickup in the ELM filament circuit from the high voltage is thereby further isolated from the SCR trigger.